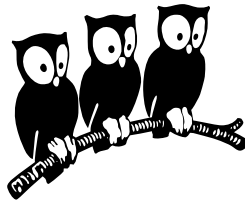# ÉCOLE NORMALE SUPÉRIEURE
Département de Physique
Laboratoire de Physique Statistique

THÈSE DE DOCTORAT DE
L'UNIVERSITÉ PIERRE ET MARIE CURIE (PARIS VI)

UFR DE PHYSIQUE

Spécialité : Physique Théorique

présentée par

Miguel TREJO

pour obtenir le titre de
Docteur de l'Université Pierre et Marie Curie (Paris VI)

Theoretical studies of fluid and elastic membranes

Soutenance prévue le 11 décembre 2009 devant le jury composé de :

Mme.	Martine BEN AMAR	Directrice
M.	Paolo GALATOLA	Rapporteur
M.	Gaetano NAPOLI	Rapporteur
M.	Alain ARNEODO	Examinateur
M.	Stéphane DOUADY	Examinateur
M.	Jean-François JOANNY .	Examinateur

INTRODUCTION

Typical soft matter systems exhibit complex behaviour at the microscopic level. However, at macroscopic length scales the relevant degrees of freedom are often purely geometrical. Classical differential geometry of curves and surfaces constitutes the most appropriate framework to study the interplay between physical properties and geometry. If one or two dimensions of the material are much smaller than the others, one can apply an effective description in terms of an elastic theory for low-dimensional continua. Representative examples are polymers such as DNA, biological fluid membranes, solid shells, elastic sheets, and growing soft thin tissues.

However, in some cases internal degrees of freedom, such as the concentration of molecules composing the material or the thickness variation due to structural mismatch between surface domains must be also considered in the description in order to characterize some physical properties in which these microscopic features deeply influence the physical and biological behavior of the material.

This thesis is focused on the study of fluid and elastic membranes (surfaces, interfaces), their physical and mathematical features and their possible ability to describe some properties of biological low-dimensional objects, like lipid vesicles (in the case of fluid surfaces), growing animal and vegetal tissues or other slender structures (in the case of elastic surfaces) or flexible confined sheets. To achieve our purpose we have used mainly theoretical techniques, but also numerics and experimental tools.

From the theoretical point of view, a common point on the description of fluid and elastic membranes is the use of variational methods to determine the shape of these low-dimensional objects. In our problems, it will always be possible to write a free energy incorporating their principal elastic features and consequently, their shapes can be obtained using a variational procedure. We discuss how this geometric characteristic may strongly influence several aspects of physical and mechanical properties of these biological objects.

This thesis is organized as follows. In Chap. 1 we describe the fundamental properties of natural and synthetic objects in which the theoretical framework of fluid and elastic surfaces may be applied. We review some previous results involving phase separation of the components of lipid vesicles, the growth of thin elastic structures like soft biological tissues or elastic plates and the confinement of low-dimensional elastic structures.

In Chap. 2 we introduce the theoretical framework that will be used to treat the elastic and mechanical properties of membranes during the thesis. For this purpose the differential geometry of surfaces and curves is the most appropriate formalism. The

principal energy contributions of fluid and elastic interfaces are presented and analyzed. Previous calculations will be generalized incorporating microscopic degrees of freedom in a continuous description. Formulations and results that are presented for fluid surfaces can be easily extended to elastic membranes.

In Chap. 3 we use this framework to present a revision of the usual description of inhomogeneous lipid vesicles, incorporating into the continuous formalism elastic microscopic degrees of freedom. The consequences of this modification is analyzed in the budding process occurring in a biphasic axisymmetric vesicle, through the behavior of the line tension and the stability of this process in the final shape of the vesicle.

In Chap. 4 we describe the geometry and elasticity of growing slender structures with constant Gaussian curvature. A Hamiltonian description of the evolution of a closed curved in three dimensional space describing a surface with this property is interpreted as a growth process in which the evolving curve is the boundary of the growing surface. This model is used to study isometric embeddings of the pseudosphere and examples of tissues that are observed in nature are analyzed.

In Chap. 5 the packing of flexible structures in confined geometries is studied using a simple experimental setup. A phase diagram describing the strength of confinement on the elastic sheets is described and the cascade of bifurcations leading to the preferred spiral structure that minimizes the pressure within the container are also presented. Numerical simulations confirm all the scenarios in the earliest stages of confinement.

CONTENTS

Chapter 1

PHYSICAL PROPERTIES OF FLUID AND ELASTIC MEMBRANES

In this chapter we briefly outline the principal features of the biological systems that will be considered in the course of this thesis. For this purpose we discuss and analyze some preliminary results involving elastic and fluid surfaces. First, the basic properties of cell membranes and inhomogeneous lipid vesicles will be described. Among them, fundamental processes such as phase separation, shape transformation, budding and fission occurring in fluid surfaces will be considered. Secondly, the mechanical and geometrical properties of biological soft tissues will be described. We present the consequences of growth processes for the shape of soft tissues.

1.1   Fluid surfaces

Fluid surfaces are characterized by the fact that they do not resist in plane deformations, that means, stretching may be neglected and their equilibrium shapes are totally determined by bending. Typical biological systems exhibiting this behaviour at large scale are cell membranes, lipid vesicles and amphiphilic monolayers. In this section we will describe their fundamental features, which will be useful in the rest of this thesis. We focus especially on lipid vesicles and their phenomenology.

1.1.1   The biological membrane

The biological membrane of living cells is a very complex structure made out mainly of a mixture of different lipid species such as cholesterol, sphingolipids, phospholipids, but also sugars and proteins. This structure is endowed with several interesting properties. For instance, it defines the only boundary that encloses the cells and it served as the boundary for intracellular organelles such as the mitochondria, the nucleus, the Golgi apparatus, the lysosome, etc. The membrane is able to interact with the environment and participates in active biological processes, such as the transport of lipids and proteins. Owing to its semi-permeability, it is a natural barrier for molecules and viruses that try to infect or to invade the cell. In view of the complexity of the real cellular membrane, it is difficult to study its *in vivo* or *in vitro* properties and for this reason

it may be more instructive to consider a simplified model system which can be easily controlled in the experiences: the lipid vesicle.
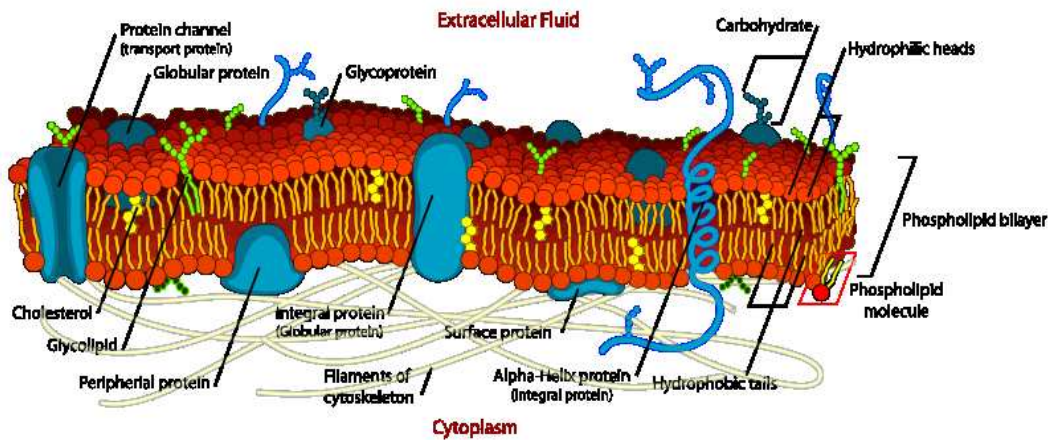
Fig. 1.1: A schematic representation of a cell membrane showing its typical biological components, such as lipid molecules, cholesterol, integral proteins and sugars. From Wikipedia

1.1.2 Lipid vesicles

Lipid vesicles are characterized by their size. Typical experimental systems in the literature are classified as: Small Unilamellar Vesicles SUV $(30-50[nm])$, Large Unilamellar Vesicles LUV $(50-500[nm])$, and Giant Unilamellar Vesicles GUV $(1-200[\mu m])$. The size of the lipid vesicle is directly related to the experimental process used to prepare it. Because of their properties and the diversity of shapes, GUV's constitute an interesting study subject. Their size and curvature are similar to those of living cells and their lipid bilayer exhibits the basic properties of biological membranes [89]. At mechanical equilibrium they adopt striking shapes which have been observed experimentally and explained both theoretically and numerically [18, 115, 116].

From a theoretical point of view, lipid vesicles are closed and semipermeable soft shells, which resist bending deformations but that are considered as fluid in their tangent plane. However, despite of their fluidity, they can exhibit lateral inhomogeneities due to micro-domain formation. These structures arise from a phase separation between the different types of lipids composing the membrane.

In recent experiments three families of lipids are used: *sphingolipids, phospholipids* and *cholesterol* [45, 117, 118]. Each of them has different structural, chemical and physical properties which determine the thermodynamic behavior of the vesicle. Cholesterol has a central role in membrane mechanics, participating in the membrane fluidity regulation. This is possible because it is a smaller molecule which inserts into the bilayer and modifies its fluidity locally, inducing domain segregation in the multi-component

membrane. Some important structures are called "rafts", which are domains enriched in cholesterol, sphingomyelin and certain membrane proteins.
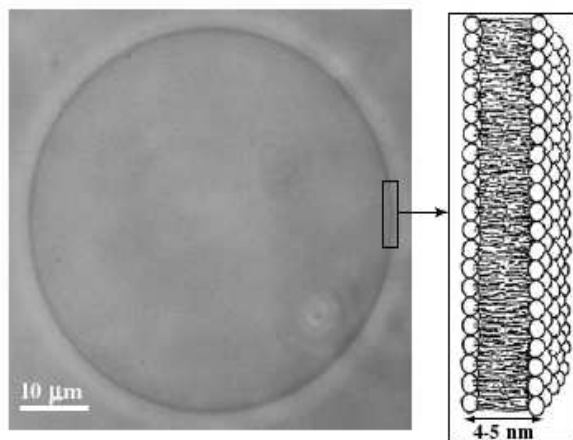
Fig. 1.2: A Giant Unilamellar Vesicle (GUV) observed using phase contrast microscopy. At right the scheme represents the lipid bilayer structure. Thickness is of the order of $4 - 5[nm]$. From [3].

In the next two sections we review some physical facts that determine morphological transitions of multi-component vesicles. In particular, we will focus on biphasic vesicles, where budding and fission process have been studied theoretically and observed experimentally and numerically.

1.1.3   Formation of lipid rafts

It is widely believed in the scientific community that lipid rafts are involved in several cell functions like signal transduction, lipid trafficking, cell migration, and protein displacements [121]. Although they have been observed experimentally in inhomogeneous lipid vesicles and their fabrication is standard in GUVs, a definitive model of lipid raft formation based on microscopic molecular interactions is still lacking. However, an approach involving mathematical models based on a microscopic theory of coagulation and fragmentation has been developed allowing to explain the raft formation in lipid bilayer membranes [111]. Although the term "raft" has been coined to denote lipid domains that are believed to be in cell membranes here we use the term to describe the lipid domains observed in GUVs.

From a mesoscopic point of view rafts can be interpreted as domains resulting from a thermodynamic phase separation of the lipid species. Typically this process triggers shape deformations in the multi-component membrane leaving striking and complex shapes [70, 129].

However, the typical small size of rafts has not been satisfactorily explained so far by means of a simple phase-separation process and new ingredients must be incorporated, as the exchange of lipids with the surrounding medium [53] or the membrane recycling

process [132]. Even more complete models incorporating coarse-grained molecular dynamics have been performed in order to explain the equilibrium phase separation in binary lipid mixtures at the liquid-gel phase coexistence [120]. Experimentally, the occurrence of phase separation has been confirmed in GUVs whose composition mimics those of cellular membranes [45, 135].

Rafts are more ordered and tightly packed than the surrounding membrane. They are called *Liquid ordered domains* (L_o). Classical surrounding membrane, that is less structured is typically called *Liquid disordered domain* (L_d). In spite of its more "dense" structure rafts conserve their fluidity. As the two coexisting phases are liquid, their elastic description is similar, but each of them has its own set of physical constants.

Rafts can also diffuse within the less dense L_d membrane showing a particle-like behaviour and giving rise to striking dynamics, recombining with each other to produce domains of larger sizes [141].

In experiments it has been shown that L_o domains can be extracted from the L_d domain. Such experiments use different methods as tubular deformation [6], osmotic shocks [15] or absorption of external molecules like proteins or detergents [124]. In all these processes line tension can drive the instability that produces the final shape transformation, at least in the first stages of budding. An increase of line tension tries to reduce the interface length between domains, favoring fission and budding [72]. The interesting subject is to reveal which are the physical factors taking part in line tension changes.
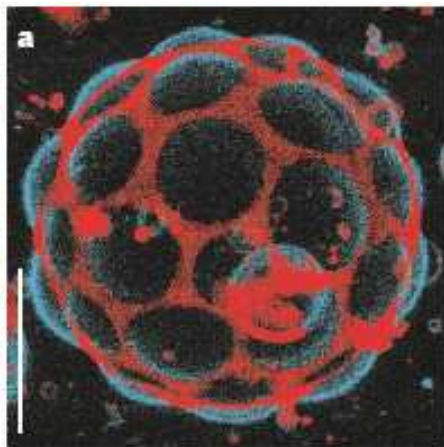
(a) Vesicle showing multiple raft formation. Hemispherical projection of image stack
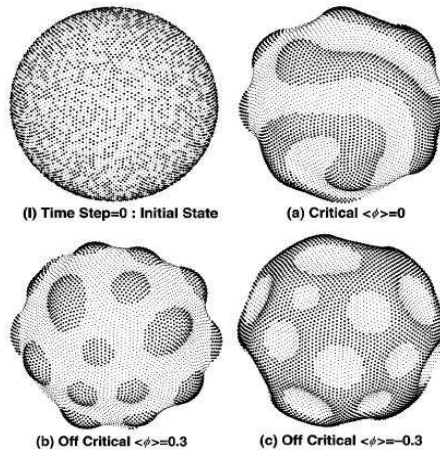
(b) Numerical simulations of phase transition driving shape deformation in a two-component membrane

Fig. 1.3: Images showing raft formation in a giant biphasic lipid vesicles using two-photon microscopy and numerical simulations. Images (a) and (b) from [15] and [129], respectively.

1.1.4 Budding and fission process

Budding is a shape transformation process occurring in homogeneous and inhomogeneous lipid vesicles: a portion of the membrane is bent slightly to form a small bud having the shape of a spherical cup. The resulting bud can either be separated from the larger vesicle in a multistep growing process which normally ends with the expulsion of the *daughter vesicle* or remains connected to it through a small membrane neck that resembles a catenoidal segment and is characterized by essentially zero mean curvature. This process can be triggered by different physical factors like the heating of the vesicle [48], the adsorption of proteins or detergent molecules at the interface between domains [124, 125] or by changing the osmotic pressure [48] which occurs at constant temperature.

By means of fluorescence microscopy of GUVs the domain formation and the subsequent budding process have been experimentally confirmed [15, 14, 13]. Ref. [15] also provides an evidence for the line tension of intramembrane domains.

The nucleated domains on the membrane may exhibit a dynamical behaviour, which has been studied numerically in [81] by means of Monte Carlo simulations on a discretized surface. Hydrodynamic effects have been considered numerically in [84] showing the formation of buds, vesiculation and the coalescence of caps and flat patches. The effects of line tension in domain formation has been also studied numerically in [137] by means of phase field models in multi-component vesicles and open membranes. Several of the experimental shapes induced by the budding process are reproduced by this simulation.

The shapes adopted by lipid membranes can be classified in two regimes. In the *high tension regime* they look very similar to those of fluid interfaces, and they are characterized by constant mean curvature. On the contrary, in the *low tension regime* the shape is governed by bending elasticity. The morphological transitions in this case involve the formation of a small neck between the small protrusion and the *mother vesicle*. The presence of a membrane tension acts to suppress the budding process.

Fission process is the later stage of budding and involves a striking topological change of the mother vesicle. To obtain a totally separated daughter vesicle, we need to destabilize the narrow neck produced during the budding transition. One option is to reduce the Gaussian rigidity of the membrane, or increase the line tension [37]. In this reference a model that couples the Gaussian curvature with the local lipid composition has been able to explain the neck destabilization. The components of lipids can reduce or increase the Gaussian rigidity and therefore enhance fission, or fusion process.

Having determined some physical and biological properties of real fluid surfaces, in the following section we will describe the main features of natural and synthetic elastic surfaces, such as biological tissues or elastic plates and shells.
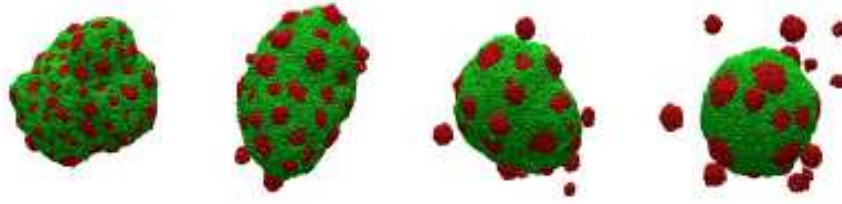
(a) Fission of small vesicles from phase separation
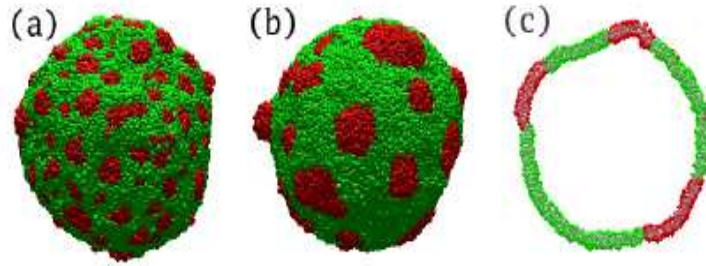
(b) Different stages of a numerical simulation of a budding process in a phase separating vesicle

Fig. 1.4: Numerical evidence of budding and fission process in a phase separating vesicle. From [84]

1.2   Elastic surfaces. Biological tissues and growth process

In-plane deformations of elastic surfaces are crucial in determining the geometric and mechanical properties of thin materials. An energy due to stretching must be added to the usual description in order to consider extension-compression deformations. Typical systems showing this feature are biological tissues and elastic plates and shells.

Biological tissues are conventionally classified into two categories: hard tissues (*e. g.* bones or teeth) and soft tissues (*e. g.* , skin, muscles arteries, etc). The major difference between hard and soft tissues lies in the magnitudes of the deformations that they can sustain. In this sense, the deformations of soft tissues require a nonlinear theory that allows for large deformations. In the following section we discuss some fundamental results in the growth process associated to biological tissues.

Both animal and vegetal tissues have the ability to grow and remodeling in response to internal and external loads. Growth is a process by which the shape of a body will change, either by mass rearrangement via bulk and surface diffusion, or by mass transfer from the surrounding environment. Then We can say that a growing deformable body is *an open system.* It means that the material particles are added or removed along the boundary by interchanging mass with the surrounding or with internal structure. In this sense in the growth process there is no correspondence between the initial and current configuration of a deformable body and then the classical continuum mechanics must be strongly modified to describe the properties of the growing body, even if this

description constitutes the most appropriate framework to determine the mechanical properties of soft tissues.

After the work of Skalak and Fung [59, 58, 122] soft tissues have been widely recognized and characterized as complex mechanical materials with nonlinear inhomogeneous and anisotropic behaviors.

It is necessary to distinguish different growth process, depending on the geometrical consequences that are produced in the growing structure. For instance, it can be restricted to specific locations such as *tip growth* which takes place in most microscopic filamentary systems, like the eukaryotic fungi or the prokaryotic actinomycetes. Deformations of teeth or horns and bones may be considered as *surface growth* in which accretion and deposition produce the principal mechanism of growth. Finally if the growth process occurs in the bulk of the material we will say that the growth is *volumetric*. Classical examples in which growth is a consequence of a physiological process are arteries, solid tumors and muscles.

(a) Deformations after the bifurcation produced by the instability of the growth process in an hyperelastic shell. From [7].

(b) The two first destabilized modes of a growing hyperelastic disc. A saddle shape and a symmetric shape. Comparison with the shape adopted by the *Acetabularia* algae. From [42].
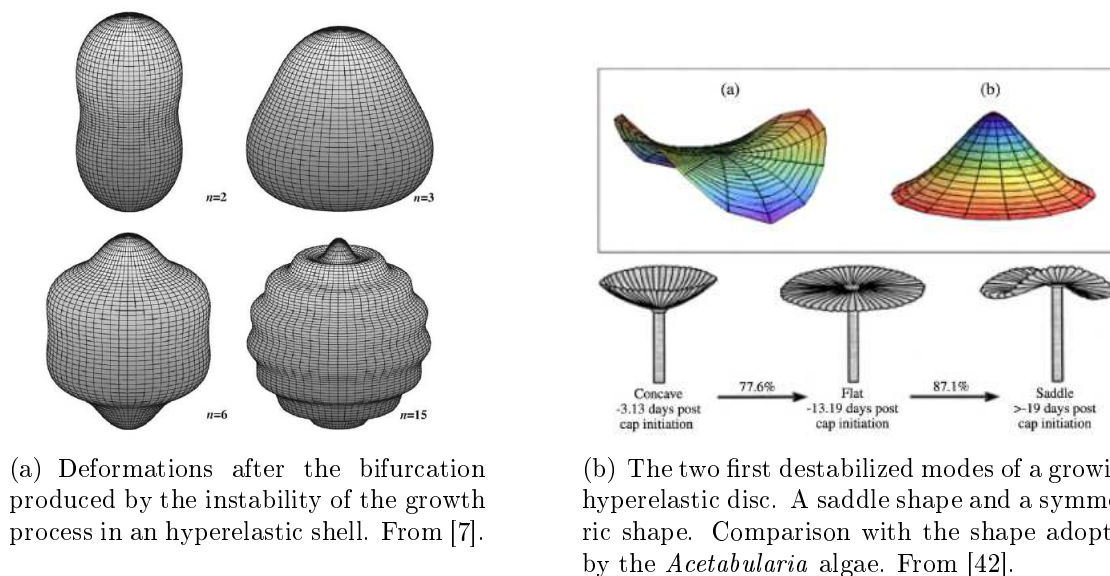
Fig. 1.5: Some shapes produced by instabilities in the growth process of thin hyperelastic structures.

Within the theory of *finite elasticity* [106] the framework for soft tissues accounting for volumetric growth has been established by Rodriguez et al [112]. The growth description is inspired by the elasto-plasticity itself: the deformation gradient (the geometric deformation tensor) can be decomposed as the product of a growth tensor (plasticity) describing the local addition of material and an elastic tensor that considers the elastic relaxation and reorganization of the body, ensuring its integrity (no cavitation) and compatibility (no overlap). From this fundamental framework several studies involving stress generation and compatibility have been performed, but the more important mechanical feature involving growth is the generation of *residual stress* [123].

In most tissues, stresses can limit the growth process. These stresses are, in turn, generated by the growth itself. They are crucial in some transcendental biological features of tissues, like regulation of growth in solid tumors. However, they are also important in morphogenesis and embryogenesis by generation of elastic instabilities, leading to shape transformations on the growing body [7, 63]. For instance, in Fig. 1.5(a) we show the typical shapes adopted by a growing body (a spherical hyperelastic shell) which undergoes an elastic instability due to anisotropic growth. The body is considered within the framework of the theory of finite elasticity as an hyperelastic material and the shape transformation is explained via incremental deformations. In any case, residual stresses are fundamental to determine when the intensity of anisotropic growth becomes important enough to destabilize the spherical shell shape.

Although in that case the stability properties have been studied in a thin body, the thickness of the shell has been used as a parameter determining the different regimes of the instability where mechanical and geometric effects both play a different role, determining the stability of thin and thick spherical objects under anisotropic growth.

In [43] a model of morphogenesis based on similar ideas has been developed. However, in this case, the dimensionality of the problem is reduced in order to characterize the growth of thin elastic structures. The behaviour of the plate is effectively described by a two dimensional elastic surface. The resulting model produces equilibrium equations that are of the Föppl-von Kármán type where growth acts as a source of mean and Gaussian curvature. This concept will be used in Chap. 4 when growing surfaces of constant Gaussian curvature will be studied.

The formulation introduced in [43] has been applied to the case of the anisotropic and homogeneous growth of an hyperelastic free disc [42]. In Fig. 1.5(b) we show two shapes adopted by the disc when growing planar disc is destabilized in its two first bending modes, in the small deformations regime. The saddle shape is produced by the most unstable mode, when growth is mainly circumferential. A symmetric shape occurs when radial growth dominates. These shapes can be compared with the change in shape experienced by a population of *Acetabularia* algae during their development. For these objects, the earliest stages of the development lead to a symmetric conical shape. Later circumferential growth predominates to produce the saddle shape.

The scenario is different when large deformations are allowed as a consequence of the growth process (see Fig 1.6). In this case the stretching contribution is bigger than bending energy and the general solution is a cone having zero Gaussian curvature, except at the tip, where bending effects are important. Bending energy is also used in this case to determine the preferred solution that has minimal energy. When radial growth dominates it is shown that singularities can be produced as a consequence of the growing process. The structure of this conical singularity appearing in growing sheets has been considered in [100]. They also describe the equilibrium states adopted by the cone which also exhibits a *surplus angle*. When this angle ϕ_e is positive the disc may fold into one of a discrete infinite number of states. All these states have a critical value of the surplus angle ϕ_e beyond which the surface touches itself. However the surfaces are stable before the self-contact and the ground state is characterized by the two fold

(a) The two modes of minimal energy far from the tip and their resultant shapes built out of paper. From [42].

(b) Surface shapes for $\phi_e = 2\pi$ with $n = 2, 3$ and 4. From [100].
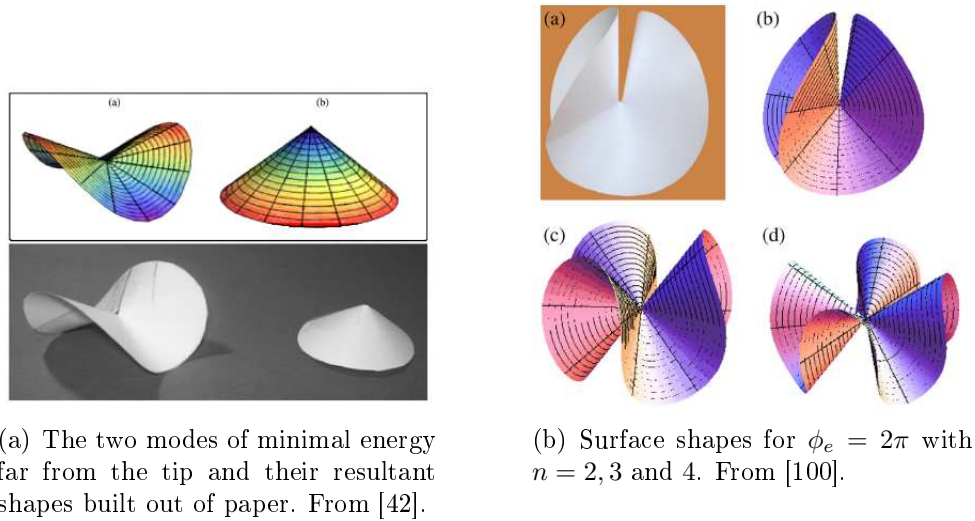
Fig. 1.6: Preferred shapes for the large deformation regime. In this case the geometry is characterized by zero Gaussian curvature in the whole surface except at the tip, where bending effects become important.

symmetry as it is depicted in Fig, 1.6(b) inset (a) and (b).

When ϕ_e grows, a successive series of shape transformations is allowed from $n = 2, 3, \ldots$, when the surface begins to be self-intersected. As the physical surface is not self-intersect the different regions come into contact and they experience forces that will deform the surface as in [21]. In this case the internal local pressure will appear and the spherical volume occupied by the cone is packed more and more densely. In this case the growth of the sheets is constrained by the volume occupied by the cone and the shape adopted by the surface is very intricate. In the following section we will discuss the characteristic of these structures constrained to grow into a given volume or surface. In Chap. 4 the growth of natural and synthetic structures as non-Euclidean plates or the shape of leaves and plants will be discussed, besides the role of stretching.

In the following Chapter we describe the theoretical framework that is needed to study fluid and elastic membranes.

Chapter 2

GEOMETRY, MECHANICS AND ELASTICITY OF SURFACES

In this Chapter we review the fundamental energetic properties of two dimensional elastic objects in a parametrization-free framework. We describe the elasticity of fluid interfaces, like lipid vesicles, for which bending deformations dominate. Typical energetic contributions that are used to obtain the equilibrium shape of these biological objects are analyzed in detail and their physical origins are explained. Then, to illustrate the formalism, two examples that will be useful in the following chapters are solved explicitly. Finally, we briefly describe the energetic and geometric properties of two-dimensional elastic slender objects, like plates and shells, in which the stretching contribution plays a fundamental role. Some previous results which have served as inspiration are outlined and the treatment of the elastic growth in this geometric framework is commented.

2.1   The Energetics of surfaces and interfaces

In most cases, at mesoscopic scales, the behavior of homogeneous elastic surfaces, like a lipid membrane, or elastic sheets is totally captured by its geometrical degrees of freedom. The previous statement is justified by the smallness of the elastic surface thickness $u \simeq 5 - 10[nm]$ if it is compared with the linear dimension of the membrane, $L_m \simeq \sqrt{A} \simeq 10[\mu m]$, where A is the membrane area.

However, in some problems involving inhomogeneous surfaces, the shape and the elastic behaviour of a membrane is not only determined by its geometric properties. Internal degree of freedom representing inhomogeneities on the surface and global or local constraint to the geometry may be added in the energetic description. All these contributions will influence the behavior and the final shape of the membrane, when it undergoes some external deformation. Changes in membrane shape are described by the variations of a total free energy which encodes its geometric and elastic properties. In what follows, the possible contributions to this free energy will be presented.

2.1.1   Description of a thin elastic object

There are two different approaches for determining the mechanical properties of a fluid membrane. One approach involves the concepts of mechanical deformations, moments and stresses. The other one describes the membrane in terms of an elastic free energy function. The former is considered as a microscopic approach in which the membrane appears as a possibly inhomogeneous thin layer with a force distribution in the transverse direction across the thickness. This point of view is similar to that considered in the classical elastic shell theory [52, 79]. The latter, the mesoscopic approach, corresponds to an effective two-dimensional description in which the membrane is considered as an infinitely thin surface, where the material properties are represented by the physical coefficients [90, 142]. It has been shown that both approaches are equivalent [24, 78, 91, 109].

In this thesis elastic membranes or elastic sheets or shells will be considered from a mesoscopic point of view. To deal with them mathematically we will adopt an effective two-dimensional surface description. Therefore, elastic and mechanical properties of membranes will be studied using the language of differential geometry of surfaces, which is briefly presented in App. A.

Before to proceed, we define the notation for the free energy and for the free energy density associated with it. The free energy contribution of a given surface will be denoted as $\mathcal{F}_{\rhd}$ and its corresponding free energy density is $\mathcal{H}_{\rhd}$. Thus, we have:

$$\mathcal{F}_{\rhd} := \int_{\Sigma} \mathrm{d}A \; \mathcal{H}_{\rhd} \;, \tag{2.1}$$

where Σ stands for the surface representing the fluid interface (usually, the neutral surface) and the symbol $\rhd$ denotes a specific free energy contribution, like bending elasticity or a global constraint fixing the volume, as we will see later.

2.1.2   Bending energy: The Canham-Helfrich model

Usually there are three types of deformations that allow us to describe the elastic properties of a surface. Any deformation occurring in the membrane will be expressed as a combination of these three elementary deformations. They are schematically depicted in Fig. 2.1.

Stretching

The *stretching* deforms the membrane in its own plane (tangentially). During this deformation the area of the surface is not preserved. The energy necessary to separate two lipid molecules is greater than the typical energy of the system, due to the hydrophilic nature of the molecules. Therefore as the area of each lipid does not change, the stretching deformation is, in most cases, neglected. The stretching energy depends

on the relative variation of the surface in a quadratic form:

$$\mathcal{F}_{\mathrm{st}}[\boldsymbol{X}] = \int_{\Sigma} \mathrm{d}A \frac{K_a}{2} \left(\frac{\Delta A}{A} \right)^2 , \tag{2.2}$$

where K_a is the compressibility modulus which is of order $0.2[J/m^2]$ for a lipid vesicle.

Pure Shear

On the other hand, as lipids can move freely on the surface, the membrane is considered as a two-dimensional incompressible viscous fluid and therefore the *shear* deformation does not contribute to the elastic free energy. This deformation becomes important in the case of crystalline or polymerized membranes, where the *shear modulus* is of order $6 \times 10^{-6}[J/m^2]$ [98]. In this case a free energy associated to a pure shear is obtained using the *Hooke law*:

$$\mathcal{F}_{\mathrm{sh}}[\boldsymbol{X}] = \int_{\Sigma} \mathrm{d}A \, \frac{1}{2}\mu(l^2 + l^{-2} - 2) , \tag{2.3}$$

where $l = (L_o + \Delta L)/L_o$ is the lateral expansion of the membrane.

Bending

The most important contribution to the elastic free energy at mesoscopical scales comes from the *bending* deformation. It implies a normal deformation with quasi-constant area of the surface. This deformation controls the shape assumed by the membrane in mechanical equilibrium.

It is possible to construct an elastic model that considers the geometric properties of the surface Σ, as the *mean extrinsic curvature H* and the *Gaussian curvature K_{G}*. Both curvatures are the invariants of the mixed curvature tensor K_a^b defined on Σ (see App. A). The mean extrinsic curvature is related to the trace of the curvature tensor according to:

$$K := g^{ab}K_{ab} := 2H , \tag{2.4}$$

and the Gaussian curvature is defined by: $K_{\mathrm{G}} = \mathrm{Det}(K_a^b)$. If we consider weak curvatures the lowest order in the expansion of these quantities produces the well-know *Canham-Helfrich* free energy [22, 68]:

$$\mathcal{F}_{\mathrm{CH}}[\boldsymbol{X}] = \int_{\Sigma} \mathrm{d}A \left[\frac{\kappa}{2}(K - K_o)^2 + \overline{\kappa}K_{\mathrm{G}} \right] , \tag{2.5}$$

where κ is the *bending rigidity* and $\overline{\kappa}$ is the *Gauss rigidity* or *saddle-splay modulus*. K_o is the *spontaneous curvature* which represents the possible asymmetry between the two leaflets composing the membrane. The free energy Eqn. (2.5) is also known as *Willmore functional* [139] when $K_o = 0$, and is used in shell theory to determine the elastic energy of *isometric immersions*. We return to this issue in Chapter 4.
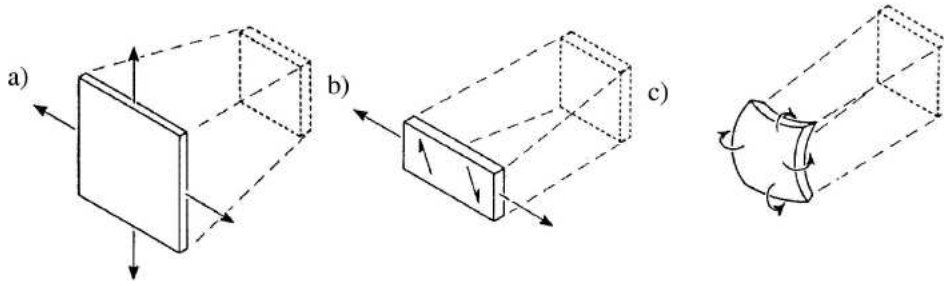
Fig. 2.1: Scheme representing the possible elementary deformations undergone by an elastic surface: a) Stretching; b) Shear; c) Bending. From [51].

The integral containing the Gaussian curvature is a topological invariant for homogeneous and closed surfaces according to the Gauss-Bonnet theorem (see App. A). This term will be only considered if a topological change takes place in the lipid membrane, as is the case of budding and fission processes or an open lipid membrane with and edge [27].

2.1.3   Surface tension energy

The surface tension energy is a combination of a stretching energy and an entropic effect due to the quasi-invisible fluctuations of the surface at different scales, mainly at scales smaller than the observation one. Fluctuations allow to define different areas of observation, which define different surface tensions [55]. Hereafter we denote $\sigma(x)$ the effective surface tension. Assuming that σ is a function of the coordinates we have:

$$\mathcal{F}_\sigma[\boldsymbol{X}] = \int_\Sigma \mathrm{d}A \; \sigma(x) \, , \qquad (2.6)$$

This term is incorporated into the Canham-Helfrich model to obtain the *Hamiltonian free-energy* of lipid vesicles:

$$\mathcal{F}_\mathrm{H}[\boldsymbol{X}] = \int_\Sigma \mathrm{d}A \left[\frac{\kappa}{2}(K - K_o)^2 + \overline{\kappa} K_\mathrm{G} + \sigma \right] \, . \qquad (2.7)$$

When the local surface tension $\sigma(x)$ is a constant, it can be interpreted as a minimization constraint imposing a fixed area in the lipid membrane. In this sense σ acts as a *Lagrange multiplier*. However, it can also be a function of the coordinates, imposing the local incompressibility condition. This constraint has been useful in several contexts, in particular in numerical simulations of a two-components lipid membrane that undergoes a phase separation and a shape transformation [129].

2.1.4   The Area-difference model

Typically in experiments a closed lipid membrane does not have a reservoir of lipid molecules and therefore the free energy minimization must be carried out at constant number of lipids. In this context two models exist: The *Bilayer coupled model* which imposes a constant number of lipids in each layer [127, 128] and the *Area-difference-elasticity model* (A.D.E) which allows the exchange of lipid molecules between the two monolayers [138, 134].

Consequently, the A.D.E model assumes that the area of each individual leaflet is not fixed, and then it can to stretch introducing an extra contribution to the Canham-Helfrich free energy. This contribution is reflected in a global area difference term: $(\Delta A - \Delta A_o)$, where $\Delta A = A^{out} - A^{in}$ is the area difference of the deflected membrane and $\Delta A_o = A_o^{out} - A_o^{in}$ is the area difference of the relaxed initial state:

$$\mathcal{F}_{\mathrm{ADE}}[\boldsymbol{X}] = \int_\Sigma \mathrm{d}A \left[\frac{\kappa}{2}(K - K_o)^2 \right] + \frac{\pi\overline{\kappa}}{2AD^2} \left(\Delta A - \Delta A_o \right) \ , \tag{2.8}$$

where $\overline{\kappa}$ is a *nonlocal bending rigidity*, D is the constant thickness of the membrane, and A is the area of the neutral surface Σ. This additional term is also known as the *nonlocal bending energy* in literature. The effect of stretching has been studied in [97, 126]. It has been able to explain the different shapes adopted by a lipid vesicle during its shape transitions, like budding and vesiculation. In the next chapter this free energy will be reviewed in order to consider the structural variations occurring at the joint between domains composing an inhomogeneous membrane which undergoes a phase separation of its lipid components. The free energy (2.8) must be minimized subject to different constraints, like fixed enclosed volume V or fixed total area A, adding new terms to the free energy (2.7).

2.1.5   Line tension energy

In some problems, the boundary of a lipid membrane may be in contact with a substrate, a fluid interface, or another elastic boundary, as in the case of biphasic vesicles. At the interface additional stresses and torques must be considered. They are transmitted along a *line of contact*, in which boundary conditions must be imposed.

The equilibrium configuration of an open membrane is obtained minimizing its total free energy, including edge effects. Simultaneously, the shape and the position of the boundary is locally adapted, minimizing the free energy. From a mathematical point of view a contact line is a curve $\mathcal{C}$ that represents the position of an interface that separates two different domains occurring at the membrane.

For a curve on Σ, we define a local orthonormal frame adapted to $\mathcal{C}$ (see App. A). When two or more domains are in contact a *line tension* tries to minimize the length of the contact line that separates. A free energy that takes into account this effect may

be expressed as:

$$\mathcal{F}_{\mathrm{L}}[\boldsymbol{Y}] = \oint_{\mathcal{C}} \mathrm{d}l\; \gamma\,, \tag{2.9}$$

where γ is the *line tension* (which can be a function of the coordinates). Here $\boldsymbol{Y} = \boldsymbol{X}(x^a(y))$ represents the embedding of the curve $\mathcal{C}$ defined in $\mathbb{R}^3$, $dl = \sqrt{h}\; dy$ is the infinitesimal length element, where $h = (\partial_y \boldsymbol{Y})^2$ is the induced metric on the curve. If we use the arc-length parametrization ($y = s$), then $h = 1$ and $\mathrm{d}l = \mathrm{d}s$.

The free energy (2.9) has been studied for a certain class of problems which involves the contact between interfaces, like lipid adhesion to different substrates [23, 44], the boundary conditions that must be satisfied in a lipid membrane with an edge [27] or the shape transformation in a lipid inhomogeneous vesicle which exhibits a phase separation between its components [72].

A nontrivial consequence that arises by adding a free energy term like Eqn. (2.9) is the emergence of discontinuities across the contact line of some of the geometrical properties defined on the surface, like Gaussian or perpendicular curvature, as we will see in Sec. 2.3.2 for a general situation.

Changes in line tension drives the shape transition observed in membranes [72]. These changes can appear when impurities modify the local curvature at the contact line, or if internal degrees of freedom are considered, as we will see in the next chapter. In what follows, we will discuss how they can be incorporated into the previous formalism.

2.1.6   Internal degrees of freedom

To describe some processes involving shape transformation in elastic membranes, like the interaction of protein inclusions, cell adhesion or phase separation of lipid components, the description presented so far is not enough. Sometimes the microscopic characteristics of the membrane are needed to describe these features satisfactorily. The surface can exhibit internal degrees of freedom, which can couple to the geometry.

Vector field. Tilt of lipid molecules

In their crystalline state the microscopical structure of a membrane is characterized by the *tilt* of the hydrocarbon chains with respect to the membrane plane. This is the case of the rippled ($P_{\beta'}$) phase which exhibits a long-range tilted order structure. However, even if the membrane is fluid, lipid tilt appears as a consequence of different biological effects, like protein inclusions, boundary conditions imposed on the membrane, or the hydrophobic mismatch at the joint between different domains composing the membrane.

The tilt variable is introduced to describe the fact that the average orientation $\boldsymbol{n}$ of lipids does not necessarily coincide with the unit normal $\boldsymbol{N}$ defined on Σ. In [67] it was shown that only the tangential part of this vector field is coupled with the geometry. We denote this tangential part as $\boldsymbol{m} = m^a \boldsymbol{e}_a$ which is not necessarily a unit vector. To account for the effect of a tilt variable an additional free energy term must be

considered:

$$\mathcal{F}_m[\boldsymbol{X}, m^a] = \int_\Sigma \mathrm{d}A f(m^a) \, , \tag{2.10}$$

where the *tilt energy density* $f(m^a)$ is given by:

$$
\begin{aligned}
f(m^a) = & a_1 \left(\nabla_a m^a \right) + a_2 \left(\nabla_a m^a \right) K + a_3 \left(\nabla_a m^a \right)^2 + a_4 \left(\nabla_b m^a K_a^b \right) + \dots \\
& + a_5 \left(\nabla_a m^b \nabla^a m_b \right) + a_6 (m^a m_a) \, ,
\end{aligned}
\tag{2.11}
$$

and the coefficients a_i are related each other. They are connected because tilt and bending deformations exert an equivalent strain on the membrane. On the other hand, additional terms can arise using symmetry arguments [104]. In [101] a representative example of a tilt free energy is introduced. It includes some terms that are considered in Eqn. (2.11). A free energy like this may be found in some references considering the effect of orientational order in surfaces [94, 101].

Scalar fields. Concentration and thickness

Internal degrees of freedom can be also incorporated through scalar fields depending on the coordinates. These scalar fields can couple to each other and also to the geometry. They represent, for instance, the local variation of lipid density [129, 4, 86], a local variation in some physical parameters describing the membrane which have been, so far, considered as constant, like the surface tension, the bending rigidity, the saddle-splay modulus, the spontaneous curvature, or the thickness of the membrane [54].

In some cases, it is sufficient to add to the geometrical free energy (2.7) a Ginzburg-Landau free energy term describing, for example, inhomogeneities on Σ:

$$\mathcal{F}_\phi[\boldsymbol{X}, \phi] = \int_\Sigma \mathrm{d}A \left[\frac{\xi}{2} \left(\nabla \phi \right)^2 + V(\phi) + \Lambda \phi K \right] \, , \tag{2.12}$$

where we have included a term that couple the scalar field ϕ with the extrinsic curvature by means of a coupling constant Λ.

A free energy of this type will be used in the next chapter to describe the thickness variation at the joint of a biphasic vesicle undergoing a phase separation. In this case, other coupling terms can be added accounting for impurities concentration. All these terms will be coupled to each other and with the geometrical large scale degrees of freedom. If the scalar field ϕ represents the concentration of adsorbed molecules, like proteins, it is necessary to add a chemical potential μ to assure an equilibrium concentration with the environment.

2.1.7 Global constraints: Fixing volume or pressure

In general lipid membranes live in an aqueous environment which is a source of stresses and torques acting on Σ. In the case of membranes composed by a lipid bilayer the hydrophobic nature of chains forces the edges of the membrane to merge and form a

closed vesicle. The volume of this closed vesicle may be fixed to a constant value V_o and consequently a free energy must be added to (2.7) to account for this constraint:

$$\mathcal{F}_{\mathrm{V}}[\boldsymbol{X}] = P(V - V_o) \, , \tag{2.13}$$

where P is the *global osmotic pressure* which can be viewed as a Lagrange multiplier enforcing the constraint of constant volume during the minimization process of the free energy. It is also possible to fix the global pressure difference between the two sides of the surface using the same expression for free energy. Indeed, both terms produce the same equilibrium equations. Note that the constraint (2.13) can also be expressed in the following form:

$$\mathcal{F}_{\mathrm{V}}[\boldsymbol{X}] = P \int_V \mathrm{d}V \, . \tag{2.14}$$

This expression can be cast in a different form using the Gauss divergence theorem and the fact that $\nabla \cdot \boldsymbol{X} = 3$ in $\mathbb{R}^3$:

$$\mathcal{F}_{\mathrm{V}}[\boldsymbol{X}] = \frac{P}{3} \int_\Sigma \mathrm{d}A \, (\boldsymbol{X} \cdot \boldsymbol{N}) \, . \tag{2.15}$$

Here the volume is expressed as an integral over $\Sigma := \partial V$. The total volume enclosed by the surface Σ is an invariant in $\mathbb{R}^3$. It is evident that the volume can be locally fixed by introducing a local pressure field, which can be expressed as a function of the coordinates. However, in this case the expression Eqn. (2.15) is not longer valid.

An interesting feature of this term is that it constitutes a source of *surface stress* which depends on the position of the surface $\boldsymbol{X}$, as we will see in Sec. 2.3.1.

2.1.8   *Local constraints: Tangential stresses*

So far we have considered free energies in which the minimization process is carried out imposing some global constraint, like fixed total area or fixed total enclosed volume. This procedure is performed with the help of Lagrange multipliers, which can be identified with physical parameters of the membrane, like the constant surface tension λ and the global pressure P, respectively.

Nevertheless, under determined conditions the deformations occurring in an elastic membrane or plate, may be solved using the previous framework and also incorporating *local constraint* acting on a geometric property, like the curvature or the metric [66]. Examples in which this formalism can be used include deformations, like patterns observed in paper sheets [8], or the depression of a circular sheet into a circular frame by the application of a point force to its center [33, 34, 35].

In the case of elastic materials the isometric bending deformations are such that they resist shear and stretching. As a consequence, the distance between points on the membrane remains fixed, and therefore the metric tensor is prescribed to some fixed

function $\overline{g}_{ab}$. In [66] a geometric functional is constructed to represent this constraint:

$$\mathcal{F}_{\mathrm{Loc}}[\boldsymbol{X}] = \int_{\Sigma} \mathrm{d}A \; S^{ab}(x) \, (g_{ab} - \overline{g}_{ab}) \; , \tag{2.16}$$

where $S^{ab}(x)$ is a set of Lagrange multipliers, defining a second rank symmetric tensor. A constraint may be imposed on different geometric functions. Let us consider the following functional:

$$\mathcal{F}_{\mathrm{C}}[\boldsymbol{X}] = \int_{\Sigma} \mathrm{d}A \; S_{ab}(x) g^{ab} \; , \tag{2.17}$$

i. e. we impose a set of constraints on the contravariant components of the metric tensor g^{ab}. The functional (2.17) may represent the gradient of some scalar field $\phi(x)$ defined on the surface if we choose the Lagrange multipliers S_{ab} in the following form:

$$S_{ab}(x) = \nabla_a \phi \nabla_b \phi \; , \tag{2.18}$$

This structure will be useful in Sec. 2.3.2 and in Chap. 3 to determine the equilibrium equations and the jump conditions at the interface between two domains composing a surface.

2.1.9 A general reparametrization invariant free energy

All the terms composing the total free energy and depending on geometrical properties of Σ alone may be considered in a general expression depending only on surface scalars which are constructed using the metric, the curvature tensor and its covariant derivatives [101]:

$$\mathcal{F}_{\mathrm{NL}}[\boldsymbol{X}] = \int_{\Sigma} dA \; \mathcal{H}_{NL}(g_{ab}, K_{ab}, \nabla_a K_{bc} \dots) \; , \tag{2.19}$$

This expression includes higher order terms in curvature elasticity, like K^4, $(\nabla_a K \nabla^a K)$, $\mathcal{R}^2$, etc. These terms appear in geometric models like the so-called egg-carton membrane [62] or in energies describing tubular structures [56]. They will not be considered in this thesis, and we will restrict ourselves to terms up to second order in the curvatures, like the Cahnam-Helfrich free energy.

On the other hand, it will be useful to introduce a free energy that couples a scalar function representing the possible inhomogeneities (changes in lipid concentration or structural degrees of freedom like thickness variation across the membrane) occurring on Σ with the geometrical properties. Then a general free energy describing an elastic fluid surface Σ with internal degree of freedom will be expressed by:

$$\mathcal{F}_{\Sigma}[\phi, \boldsymbol{X}] = \int_{\Sigma} \mathrm{d}A \; \mathcal{H}_{\Sigma}(\phi(x), g_{ab}, K_{ab}) \; . \tag{2.20}$$

The reparametrization invariance feature of this free energy will impose some consistency relations on the scalar field $\phi(x)$.

In this thesis we assume that the variations $\delta\phi$ and $\delta\boldsymbol{X}$ will be always independent of each other.

2.2   Surface mechanics

In the previous section we have presented the typical free energy terms that are used in the literature when the shape of a surface describing a membrane must be determined. Either using its geometrical properties, incorporating their internal degree of freedom or implementing global and local constraints we are able to describe the geometric properties of the surface by means of a minimization process that implies the variations of geometrical quantities.

Equilibrium of stresses and torques acting on the surface determine the shape adopted by the membrane when boundary conditions are specified. At the same time, if the shape is known, stresses and torques can be totally determined, because they are encoded in the geometry of the membrane.

Using the geometrical approach, there are two ways to determine the equilibrium shape equation. One approach use the variations of the geometric quantities ($\boldsymbol{e}_a$, $\boldsymbol{N}$, g_{ab}, g, K_{ab}, K, and $\mathcal{R}$) induced by an infinitesimal change in the embedding functions $\boldsymbol{X}$, [28, 29].

Otherwise one can consider the geometric quantities as independent variables and use Lagrange multipliers to enforce the structural relations between them. The former has been considered in [24, 142]. The latter can be found in [64, 101]. Obviously both approaches give the same results but, for the sake of simplicity, we briefly outline the latter.

2.2.1   The shape equation

In order to calculate the equilibrium shape equation of the surface we must determine how the free energy functional Eqn. (2.20) changes when an infinitesimal variation in the embedding function is performed, $\boldsymbol{X} \rightarrow \boldsymbol{X} + \delta\boldsymbol{X}$. This deformation may be decomposed into a tangential part and a normal part to Σ. It reads [24]:

$$\delta\boldsymbol{X} = \Phi^a \boldsymbol{e}_a + \Psi\boldsymbol{N} \,. \tag{2.21}$$

The response of the free energy surface may be also decomposed in two parts, a first part coming from tangential variations and the second one from normal variations. The entire expression including both contributions is given by:

$$\delta\mathcal{F}_\Sigma[\phi, \boldsymbol{X}] = \int_\Sigma \mathrm{d}A \, (\boldsymbol{E}_\Sigma \cdot \delta\boldsymbol{X}) + \int_\Sigma \mathrm{d}A \, \nabla_a Q_\Sigma^a \,, \tag{2.22}$$

where $\boldsymbol{E} = \mathcal{E}_\Sigma(\mathcal{H})\boldsymbol{N} + A_\Sigma^a \boldsymbol{e}_a$ is the bulk part of the variation and it corresponds to the Euler-Lagrange derivative (E-L) of $\mathcal{F}_\Sigma[\boldsymbol{X}]$ with respect to the embedding functions

$\boldsymbol{X}$ times the factor $g^{-1/2}$. As we will see in the course of this chapter the variations of all the possible contributions to the total free energy presented so far have the same structure as Eqn. (2.22) and therefore hereafter we drop the subscript Σ.

In this case the tangential part comes from the variation of the geometric functions including inhomogeneous terms, for instance coupling terms between a concentration function ϕ and the extrinsic geometry of the surfaces, or the local constraints reflected in the appearance of terms like $S^{ab}g_{ab}$, where $S^{ab}(x)$ is a symmetric tensor depending on the surface coordinates. The vanishing of Eqn. (2.22) dictates the equilibrium conditions which determine the shape adopted by the surface. It implies that $\boldsymbol{E} = \boldsymbol{0}$.

If the free energy only depends on the geometric properties of Σ, as in the case of Eqn. (2.19), then $A^a = 0$ is identically satisfied. The shape equation is only determined by the normal part of Eqn. (2.22). The equation $\mathcal{E} = 0$ corresponds to the so-called *Shape equation*, accounting for the equilibrium of normal forces, *i. e.*, it corresponds to the Euler-Lagrange functional derivative of $\mathcal{H}$ with respect to the normal deformation of the surface.

The last term in Eqn. (2.22) is a surface integral over a divergence corresponding to the *Noether charge* Q^a associated with $\delta\boldsymbol{X}$ [24]. Using the divergence theorem this term can be recast as a boundary integral. An expression for this term is obtained in [64] and reads:

$$Q^a = -\boldsymbol{f}^a \cdot \delta\boldsymbol{X} + \mathcal{H}^{ab}\boldsymbol{e}_b \cdot \delta\boldsymbol{N} \ , \tag{2.23}$$

where we have defined $\mathcal{H}^{ab} = \partial\mathcal{H}/\partial K_{ab}$. The expression of Q^a involves two contributions: one proportional to $\delta\boldsymbol{X}$ identified as the *surface stress tensor* $\boldsymbol{f}^a$, and the second proportional to $\delta\boldsymbol{N}$ which is related to the partial derivatives with respect to the curvature tensor K_{ab}. Here, we will consider free energies like Eqn. (2.20) since the inhomogeneities can easily be incorporated in this geometrical framework.

Noether's theorem states that every *continuous symmetry* (a translational or rotational invariance) of a free energy implies a *conserved current* (the stress and torque tensors), when the equilibrium equations are satisfied. In the next section we exploit the consequences of this theorem to obtain the explicit expressions for the stress and torque tensor as function of the geometrical properties on Σ.

2.2.2 Surface stress tensor

So far we have considered arbitrary deformations of the embedding functions $\boldsymbol{X}$. If the boundary of the membrane is infinitesimally translated by a constant vector $\delta\boldsymbol{X} = \boldsymbol{a}$ then we have $\Psi = \boldsymbol{a} \cdot \boldsymbol{N}$, and also $\Phi_a = \boldsymbol{a} \cdot \boldsymbol{e}_a$. If we insert these expressions in Eqn. (2.22) we obtain:

$$\delta\mathcal{F}_{\mathrm{T}}[\boldsymbol{X}] = -\boldsymbol{a} \cdot \int_{\Sigma} dA\{\mathcal{E}(\mathcal{H})\boldsymbol{N} + A^a\boldsymbol{e}_a + \nabla_a\boldsymbol{f}^a\} \ . \tag{2.24}$$

This translation leaves the free energy invariant. The current Q^a is a linear operator acting on Φ_a and Ψ [24]. It can be expressed as $Q^a = \boldsymbol{a}\cdot\boldsymbol{f}^a$, where the vector $\boldsymbol{f}^a$ describes

the non-vanishing components of the *stress tensor* on the surface. This denomination comes from its similarity with the three-dimensional stress tensor arising in the classical elastic theory [83]. Even if no external forces are acting on Σ, the vector $\boldsymbol{f}^a$ exactly represents the stresses in the surface.

The integral (2.24) must be equal to zero since the vector $\boldsymbol{a}$ can be arbitrarily chosen. As the surface Σ is also arbitrary, the integrand must vanish at every point of Σ. Thus we have:

$$\nabla_a \boldsymbol{f}^a = \mathcal{E}(\mathcal{H})\boldsymbol{N} + A^a \boldsymbol{e}_a \, . \tag{2.25}$$

Note that in the absence of external sources of stress, the equilibrium equation can be written as a conservation law [24]:

$$\nabla_a \boldsymbol{f}^a = 0 \, . \tag{2.26}$$

The vector $\boldsymbol{f}^a$ may be decomposed into its tangential and normal components, which defines the tensors f^{ab} and f^a as follows:

$$\boldsymbol{f}^a = f^{ab}\boldsymbol{e}_b + f^a \boldsymbol{N} \, . \tag{2.27}$$

Using the Gauss-Weingarten equations (see App. A.1.3) the surface projections of (2.25) are given by:

$$\nabla_a f^a - K_{ab} f^{ab} \;=\; \mathcal{E}(\mathcal{H}) \, , \tag{2.28a}$$
$$\nabla_a f^{ab} + K_a^b f^a \;=\; A^a \, . \tag{2.28b}$$

The normal projection (2.28a) is the shape equation, which vanishes at equilibrium. The tangential projection is a consistency equation on the stress components, which indicates the reparametrization invariance of $\mathcal{F}_{\mathrm{T}}$. When inhomogeneities or local constraints are considered the tangent vector A^a may be cast as a divergence of a tensor $\nabla_b M^{ab}$. At equilibrium this implies that the tensor M^{ab} is itself conserved [66].

The method described in [64, 101] using auxiliary variables allows us to readily identify the terms occurring in the normal and tangential components of the stress tensor $\boldsymbol{f}^a$ as well as the conservation laws associated with it. By means of an elimination processes of the Lagrange multipliers we obtain an explicit expression for f^{ab} and f^a in terms of the original geometrical variables:

$$f^{ab} \;=\; T^{ab} - \mathcal{H}^{ac} K_c^b \, , \tag{2.29a}$$
$$f^a \;=\; -\nabla_b \mathcal{H}^{ab} \, , \tag{2.29b}$$

where the contravariant tensors T^{ab} and $\mathcal{H}^{ab}$ are defined by:

$$T^{ab} \quad := \quad -\frac{2}{\sqrt{g}}\,\frac{\delta(\sqrt{g}\mathcal{H})}{\delta g_{ab}} \tag{2.30a}$$

$$\mathcal{H}^{ab} \quad := \quad \frac{\delta\mathcal{H}}{\delta K_{ab}} \tag{2.30b}$$

In these expressions the functional derivatives must be replaced by the partial one if $\mathcal{H}$ does not depend on covariant derivatives of K_{ab}. Note also that $\mathcal{H}$ may be either $\mathcal{H}_\Sigma$ or $\mathcal{H}_{\mathrm{NL}}$ or any other of the contribution so far presented and the Eqns. (2.30) remain valid.

2.2.3   Surface torque tensor

Let us now explain how to obtain the torque tensor. We assume that the membrane Σ undergoes a constant infinitesimal rotation $\boldsymbol{b}$ on its boundary: $\delta\boldsymbol{X} = \boldsymbol{b} \times \boldsymbol{X}$. In this case we have $\Phi = \boldsymbol{b} \cdot (\boldsymbol{X} \times \boldsymbol{N})$ and $\Psi_a = \boldsymbol{b} \cdot (\boldsymbol{X} \times \boldsymbol{e}_a)$. Note that the normal vector changes according to $\delta\boldsymbol{N} = \boldsymbol{b} \times \boldsymbol{N}$. As in the case of infinitesimal translations, we insert these expressions in Eqn. (2.22) to obtain:

$$\delta\mathcal{F}_{\mathrm{T}}[\boldsymbol{X}] = -\boldsymbol{b} \cdot \int_\Sigma dA\{\mathcal{E}(\mathcal{H})(\boldsymbol{X} \times \boldsymbol{N}) + A^a(\boldsymbol{X} \times \boldsymbol{e}_a) + \nabla_a\boldsymbol{\tau}^a\}\ . \tag{2.31}$$

In this case $Q^a = -\boldsymbol{b} \cdot \boldsymbol{\tau}^a$, where $\boldsymbol{\tau}^a$ is identified as the covariant conserved *torque tensor* acting on Σ. It reads:

$$\boldsymbol{\tau}^a \quad = \quad \boldsymbol{X} \times \boldsymbol{f}^a + \boldsymbol{s}^a\ , \tag{2.32a}$$

$$\boldsymbol{s}^a \quad = \quad \mathcal{H}^{ab}\,(\boldsymbol{e}_b \times \boldsymbol{N})\ . \tag{2.32b}$$

The first term in Eqn. (2.32a) is a contribution due to the couple of the stress tensor $\boldsymbol{f}^a$ about the origin. The latter term is an intrinsic contribution coming from curvature terms and is given by the Eqn. (2.30b). Note that $\boldsymbol{s}^a$ has always tangential components on Σ.

Neither s^a nor the couple due to $\boldsymbol{f}^a$ alone is conserved. As in the case of the stress tensor, the integrand in Eqn. (2.22) vanishes pointwise on Σ ($\boldsymbol{b}$ is and arbitrary infinitesimal angle) and then:

$$\nabla_a\boldsymbol{\tau}^{\boldsymbol{a}} = \boldsymbol{X} \times \boldsymbol{E}\ , \tag{2.33}$$

which in equilibrium $\boldsymbol{E} = 0$. The Noether theorem requires that the divergence of $\boldsymbol{\tau}^a$ vanishes identically on Σ:

$$\nabla_a\boldsymbol{\tau}^a = 0\ . \tag{2.34}$$

As an immediate consequence of Eqns. (2.32a), (2.25) and (2.34) we have the relation:

$$\nabla_a\boldsymbol{s}^a = \boldsymbol{f}^a \times \boldsymbol{e}_a\ . \tag{2.35}$$

As mentioned before the tensor $\boldsymbol{s}^a$ has only tangential components.

$$\boldsymbol{s}^a = S^{ab} g_{bc} \varepsilon^{dc} \boldsymbol{e}_d \ , \tag{2.36}$$

where ε^{cd} is the totally antisymmetric tensor $\varepsilon^{11} = -\varepsilon^{22} = g^{-1/2}$ and $\varepsilon^{12} = \varepsilon^{21} = 0$ (see App. A).

To obtain the expressions for stress and torque tensor it was not required to assume that the Euler-Lagrange equation was satisfied on Σ. The only properties that have been used so far are the translational, rotational and reparametrization invariance of the free energy $\mathcal{F}$.

Another interesting feature of the stress and torque tensors is that they only depend on geometric properties of Σ when the membrane is not inhomogeneous or locally constrained. Otherwise, there are contributions coming from internal degrees of freedom or local constraints imposed on Σ. In both cases the knowledge of solutions of the shape equation allows us to determine in principle, the forces and torques acting on the surface.

The specific form of the shape equation $\mathcal{E} = 0$, the tangential vector $A^a = 0$ and the stress and torque tensors $\boldsymbol{f}^a$, $\boldsymbol{\tau}^a$, depend on the specific choice of the free energy (2.20). In the next section we will present two useful examples that can analyzed using the previous formalism.

2.3   Some useful examples

In this section we illustrate through two examples the formalism introduced previously to describe the mechanical and energetic properties of surfaces. These specific examples will be useful in the next chapters. The first one shows how to incorporate a global constraint in the minimization process of the free energy as an effective surface stress. Some concepts and calculations of this example will be borrowed in Chap. 4. The second example concerns the jump conditions at a contact line which separates two domains in a *general inhomogeneous surface*. The analysis presented in this sections is again general and includes possible inhomogeneities of the surface, local constraints and tangential variations.

2.3.1   Example 1: Global pressure difference as a source of surface stress

Let us consider a fluid surface described by a free energy like Eqn. (2.20) which encloses a fixed volume V. With this constraint, the total free energy depends not only on the local geometry but also on a term implementing the constraint, which has been explained in Sec. 2.1.7. Then, the total free energy of this system is expressed by:

$$\mathcal{F}_{\mathrm{T}}[\phi, \boldsymbol{X}] = \mathcal{F}_{\Sigma}[\phi, \boldsymbol{X}] + \mathcal{F}_{\mathrm{V}}[\boldsymbol{X}] \ , \tag{2.37}$$

The variation of the free energy $\mathcal{F}_{\Sigma}[\phi, \boldsymbol{X}]$ given by Eqn. (2.20) may be carried out using the formalism introduced in Sec. 2.2. The general structure of this variation has

been already expressed in Eqn. (2.22). The normal part of the bulk term is:

$$\mathcal{E}_\Sigma(\mathcal{H}) = K\mathcal{H}_\Sigma - (K^2 - \mathcal{R})\left(\frac{\partial \mathcal{H}_\Sigma}{\partial K}\right) - \mathcal{R}K\left(\frac{\partial \mathcal{H}_\Sigma}{\partial \mathcal{R}}\right)$$
$$- g^{ab}\nabla_a\nabla_b\left(\frac{\partial \mathcal{H}_\Sigma}{\partial K}\right) - 2L^{ab}\nabla_a\nabla_b\left(\frac{\partial \mathcal{H}_\Sigma}{\partial \mathcal{R}}\right) , \tag{2.38}$$

where the fourth term on the *r.h.s* of the previous equation is the *Laplace-Beltrami* operator defined on Σ and the latter term is a gradient operator in which L^{ab} is a contravariant tensor that appears when the variation of the Gaussian curvature term is performed: $L^{ab} = Kg^{ab} - K^{ab}$. This tensor has a nice property in two dimensions: $\nabla_a L^{ab} = 0$.

The remaining terms are functions of both the mean and scalar curvature of Σ. For the tangential part of the bulk term we have:

$$A_\Sigma^a = -\left(\frac{\partial \mathcal{H}_\Sigma}{\partial \phi}\right)\nabla^a\phi , \tag{2.39}$$

whose contribution is different from zero, because of the scalar field appearing in $\mathcal{H}_\Sigma$. The boundary term Q_Σ^a is given by Eqn. (2.23) which in turn depends on Eqn. (2.29) and Eqn. (2.30b). Here we give the expression of these three tensors. The tangential component f_Σ^{ab} of the stress tensor reads:

$$f_\Sigma^{ab} = -g^{ab}\mathcal{H}_\Sigma + K^{ab}\left(\frac{\partial \mathcal{H}_\Sigma}{\partial K}\right) + g^{ab}\mathcal{R}\left(\frac{\partial \mathcal{H}_\Sigma}{\partial \mathcal{R}}\right) , \tag{2.40}$$

the normal component f_Σ^a of the stress tensor $\boldsymbol{f}_\Sigma^a$ is given by:

$$f_\Sigma^a = -\nabla^a\left(\frac{\partial \mathcal{H}_\Sigma}{\partial K}\right) - 2L^{ab}\nabla_b\left(\frac{\partial \mathcal{H}_\Sigma}{\partial \mathcal{R}}\right) . \tag{2.41}$$

Finally the tangential components of the intrinsic torque tensor $\mathcal{H}_\Sigma^{ab}$ is expressed as:

$$\mathcal{H}_\Sigma^{ab} = g^{ab}\left(\frac{\partial \mathcal{H}_\Sigma}{\partial K}\right) + 2L^{ab}\left(\frac{\partial \mathcal{H}_\Sigma}{\partial \mathcal{R}}\right) . \tag{2.42}$$

As the surface Σ must be closed (although this is not absolutely necessary), the boundary terms produced by the variation of the free energy $\mathcal{F}_V[\boldsymbol{X}]$ does not contribute to the total boundary term. On the other hand, it is possible to show that its total variation leaves a normal term proportional to P. Hence in equilibrium conditions the normal Euler-Lagrange derivative of (2.37) must be equal to the constant Laplace pressure P. Consequently the shape equation for a fluid surface constrained to remain with a fixed volume during its deformation is $\mathcal{E}_\Sigma(\mathcal{H}) = P$.

The formalism used to describe the geometrical properties of the shape, the stress and the torque tensors so far has been quite general and only uses invariance prop-

erties of $\mathcal{H}_\Sigma$ and therefore it may represent different physical fluid surfaces, like lipid membranes or soap films. However in some problems addressed in this thesis it will be necessary to specify the free energy density function $\mathcal{H}_\Sigma$.

For instance, if we suppose that the fluid surface is an homogeneous membrane and we add a constant surface tension contribution fixing the area of the surface during the deformation we obtain the case of the Helfrich free energy, described by Eqn. (2.7). For this case the shape equation is:

$$\mathcal{E}_{\mathrm{H}}(\mathcal{H}) = -\kappa \nabla^2 K + \frac{1}{2}\kappa(K - K_o)[(K - K_o)K - 2K_{ab}K^{ab}] + \lambda K \; , \qquad (2.43)$$

where $\sigma = \lambda$ is a constant imposing the global constraint. Using the conservation law (2.26) the equilibrium condition $\mathcal{E}_{\mathrm{H}}(\mathcal{H}) = P$ is expressed as the surface divergence of the stress tensor which in this case is equal to the pressure times the normal vector:

$$\nabla_a \boldsymbol{f}^a = P\boldsymbol{N} \; . \qquad (2.44)$$

The stress tensor $\boldsymbol{f}^a$ is calculated using Eqns. (2.29) and (2.30) which have been written in a general form in Eqns. (2.40), (2.41) and (2.42). If we specialize for the lipid membrane, the stress tensor is given by:

$$\boldsymbol{f}^a = \{\kappa(K - K_o)\left[K^{ab} - \frac{1}{2}(K - K_o)g^{ab}\right] - \lambda g^{ab}\}\boldsymbol{e}_b - \kappa(\nabla^a K)\boldsymbol{N} \; , \qquad (2.45)$$

and the torque tensor reads:

$$\boldsymbol{\tau}^a = \boldsymbol{X} \times \boldsymbol{f}^a + \{\kappa(K - K_o)g^{ab} + \overline{\kappa}L^{ab}\}(\boldsymbol{e}_b \times \boldsymbol{N}) \; , \qquad (2.46)$$

Now we discuss an interesting feature of the volume term $\mathcal{F}_{\mathrm{V}}[\boldsymbol{X}]$ which has been previously addressed in [65]. In Sec. 2.1.7 we have seen that the volume integral of a closed surface is expressed as a surface integral in which the integrand is dependent on the position $\boldsymbol{X}$. If the surface is not closed we need to analyze the behaviour of the volume under variation of the open surface patch. This corresponds to the volume of the cone with the apex at the origin of the reference system and the basis consisting in the surface patch.

The first variation of this surface patch with respect to the infinitesimal changes of the embedding functions $\delta\boldsymbol{X}$ is:

$$\delta\mathcal{F}_{\mathrm{V}}[\boldsymbol{X}] = \int_\Sigma \mathrm{d}A \; P(\boldsymbol{N} \cdot \delta\boldsymbol{X}) - \frac{P}{3}\int_\Sigma \mathrm{d}A \; \nabla_a(\boldsymbol{f}_v^a \cdot \delta\boldsymbol{X}) \; , \qquad (2.47)$$

where the tensor $\boldsymbol{f}_v^a$ has been introduced in [65]:

$$\boldsymbol{f}_v^a = (\boldsymbol{X} \cdot \boldsymbol{e}^a)\boldsymbol{N} - (\boldsymbol{X} \cdot \boldsymbol{N})\boldsymbol{e}^a = \boldsymbol{X} \times (\boldsymbol{N} \times \boldsymbol{e}^a) \; . \qquad (2.48)$$

The surface divergence of this stress-like object is proportional to the normal vector:

$$\nabla_a \boldsymbol{f}_v^a = 2\boldsymbol{N} \ . \tag{2.49}$$

If we use this latter relation in Eqn. (2.44) a new *effective stress tensor* can be defined as follows:

$$
\begin{aligned}
\boldsymbol{f}_{\mathrm{e}}^a &= \boldsymbol{f}^a - \frac{P}{2}\boldsymbol{f}_v^a \ , \tag{2.50a} \\
\nabla_a \boldsymbol{f}_{\mathrm{e}}^a &= 0 \ , \tag{2.50b}
\end{aligned}
$$

where Eqn. (2.50b) means that $\boldsymbol{f}_e^a$ is a divergence-free tensor, unlike the geometrical tensor $\boldsymbol{f}^a$ (see Eqn. (2.44)).

A consequence of this structure is that the volume constraint can be treated like another surface constraint. Some striking features appearing with this equivalence are discussed in [65]. For instance, the effective tensor is not translationally invariant because of its explicit dependence on $\boldsymbol{X}$. However, the additional stress appearing due to a constant translation, does not contribute to the external force on a surface patch. This additional term can be cast in the following form:

$$\boldsymbol{f}_n^a = \varepsilon^{ab}\nabla_b \boldsymbol{J} \ , \tag{2.51}$$

where $\boldsymbol{J}$ is a vector potential on Σ and ε^{ab} is the two-dimensional anti-symmetric Levi-Civita tensor. It is obvious that the previous expression is also a divergence-free stress tensor, and therefore the additional term, arising from the translation of $\boldsymbol{f}_e^a$, is a *null stress* [65].

2.3.2   Example 2: Contact line variation between surface domains

As a second example we derive the equilibrium equations and the boundary conditions on the phase boundary between two coexisting domains composing a closed surface Σ. The domains can, for example, originate from a phase separation that occurs on the surface. The total surface is then separated in two regions, Σ_1 and Σ_2, which meet in a curve $\mathcal{C}$ on Σ (see Fig. 2.2). This curve defines the phase boundary. The free energy describing the surface Σ will be composed by different contributions, which need not be given explicitly. All results are parametrization-free and do not depend on the possible symmetries of the system.

As mentioned earlier, a line tension energy appears in several contexts. Some problems dealing with the geometric properties of surfaces at contact lines, as the adhesion of a fluid surface to a rigid or a deformable substrate [23, 44], or the lipid membrane with a free edge [27] have been studied before, showing the appearance of discontinuities in certain geometrical properties across the contact line. For instance, in the case of vesicle adhesion to a rigid substrate, the normal projection of the curvature tensor on $\mathcal{C}$ exhibits a discontinuity in equilibrium.

The problem treated here has been addressed before in the specific case of a biphasic lipid membrane in which phase separation takes place [19, 72]. In these references it has been shown that geometric quantities exist whose changes are discontinuous across the contact line: the balance of forces and torques includes a complicated relation between the curvatures and the contact line properties, like its geodesic or normal curvature.

However, as was pointed out in [44] in more general cases the specific form of the free energy density $\mathcal{H}$ determines and restricts the numeber of quantities that must be discontinuous, due to the integrability requirement for the total free energy.

Hereafter the label $i \in \{1, 2\}$ denotes the quantities belonging to each domain. The typical Einstein's summation rules for the repeated index is not valid for the label i. We assume that each phase is described by a free energy density $\mathcal{H}_\Sigma^{(i)}(\phi_i, K_i, \mathcal{R}_i)$ which depends on the geometrical properties of Σ_i and on a possible internal degree of freedom that will be represented by a scalar field $\phi_i(x)$ (see Eqn. (2.20)). We will also consider a possible set of local Lagrange multipliers $S_{ab}^{(i)}(x)$ imposing some constraint on the components of the contravariant metric $g^{(i)ab}$ (Eqn. (2.18)). Finally the total free energy of the system is completed by adding the three following terms: *i*) a line tension energy term like Eqn. (2.9) accounting for the contact energy between domains, *ii*) a volume free energy term like Eqn. (2.14) if the volume enclosed by the domains remains constant during the deformation of Σ, *iii*) and a surface tension energy term like Eqn. (2.6), which locally fixes the area of the surface in each domain. Then, the total free energy that describes the biphasic closed surface is:

$$\mathcal{F}_\mathrm{T}[\phi, \boldsymbol{X}] = \sum_{i=1,2} \left(\mathcal{F}_\Sigma^{(i)}[\phi, \boldsymbol{X}] + \mathcal{F}_\mathrm{C}^{(i)}[\boldsymbol{X}] + \mathcal{F}_\sigma^{(i)}[\boldsymbol{X}] \right) - \mathcal{F}_\mathrm{V}[\boldsymbol{X}] + \mathcal{F}_\mathrm{L}[\boldsymbol{X}] \,, \qquad (2.52)$$

The minimization of this functional must be carried out with respect to the variations of the functions $\boldsymbol{X}_i$, $\phi_i(x)$ and $\boldsymbol{Y}(y)$. The latter vector represents the embedding functions of the regular curve $\mathcal{C}$ and y is a parameter along the contour. We first perform the variation with respect to the embedding functions $\boldsymbol{X}$ and $\boldsymbol{Y}$. The response of Eqn. (2.52) with respect to an infinitesimal variation $\delta \boldsymbol{X}$, like that of Eqn. (2.21) can be written as:

$$\delta \mathcal{F}_\mathrm{T}[\phi, \boldsymbol{X}] = \sum_{i=1,2} \{ \int_{\Sigma_i} \mathrm{d}A^{(i)} \, (\boldsymbol{E}^{(i)} \cdot \delta \boldsymbol{X}_i) + \int_{\Sigma_i} \mathrm{d}A^{(i)} \, \nabla_a Q^{(i)a} \} \,, \qquad (2.53)$$

where $\boldsymbol{E}^{(i)} = \mathcal{E}^{(i)} \boldsymbol{N}_i + A^{(i)a} \boldsymbol{e}_a^{(i)}$. The latter term in the previous equation can be cast as a boundary integral on a closed curve. This term will determine the boundary conditions at the interface between both domains:

$$\int_{\Sigma_i} \mathrm{d}A^{(i)} \nabla_a Q^{(i)a} = \oint_\mathcal{C} \mathrm{d}l \, l_a Q^{(i)a} \,, \qquad (2.54)$$

where l_a are the covariant components of the vector $\boldsymbol{l}$. It is the outward normal to $\mathcal{C}$ and therefore it points out of the surface Σ_2 in this case (see Fig. (2.2)).
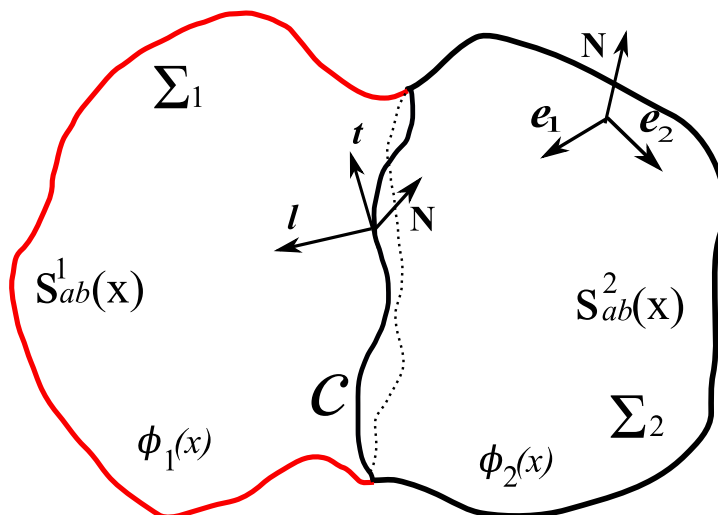
Fig. 2.2: Scheme representing a surface Σ composed by two phases, Σ_1 and Σ_2 which meet in a contact line $\mathcal{C}$. The geometry of this curve on Σ is also depicted. The geometrical properties of both domains can be decomposed in this tangential basis $\{\boldsymbol{t}, \boldsymbol{l}\}$. Note that the unit vector $\boldsymbol{l}$ is the outward normal to $\mathcal{C}$ and points out of the surface Σ_2. ϕ_i and $S_{ab}^{(i)}$ denote possible internal degrees of freedom occurring at each domain.

Now we will outline the variation of each term composing Eqn. (2.52). We start with the line tension energy (2.9). The variation of the surface on the curve can be decomposed with respect to $\{\boldsymbol{t}, \boldsymbol{l}, \boldsymbol{N}\}$, the basis adapted to both embeddings $\boldsymbol{X}$ and $\boldsymbol{Y}$. It reads:

$$\delta \boldsymbol{Y} = \Phi_t \boldsymbol{t} + \Phi_l \boldsymbol{l} + \Psi \boldsymbol{N} \ , \tag{2.55}$$

where $\Phi_t = \Phi^a t_a$ and $\Phi_l = \Phi^a l_a$ and here we have used the relation $\boldsymbol{e}_a = t_a \boldsymbol{t} + l_a \boldsymbol{l}$. Normally the first term in Eqn. (2.55) is omitted because if the line tension γ is a constant it can be expressed as a divergence term over the closed curve and therefore it can be associated with a reparametrization of the boundary. Here we consider the most general variation and a variable line tension $\gamma(y)$.

The geometric properties of the surfaces Σ_i can be decomposed in this basis (see App. A.2.2). Using these definitions the variation of the contact line free energy reads:

$$\delta \mathcal{F}_{\mathrm{L}}[\boldsymbol{Y}] = [\gamma(y)\boldsymbol{t} \cdot \delta \boldsymbol{Y}(y)]_{y_i}^{y_f} - \oint_{\mathcal{C}} \mathrm{d}l \ \left\{ \frac{1}{\sqrt{h}} \left(\frac{d\gamma}{dy} \right) \boldsymbol{t} + \gamma \kappa_g \boldsymbol{l} + \gamma \kappa_n \boldsymbol{N} \right\} \cdot \delta \boldsymbol{Y} \ , \tag{2.56}$$

where $\mathrm{d}l = \sqrt{h} \, \mathrm{d}y$ is the line element on $\mathcal{C}$ which is parametrized by y (y is not necessarily the arc-length parameter s). In Eqn. (2.56) the first term is zero because the curve is closed and thus $y_i = y_f$. The term $\kappa_g(y)$ is the *geodesic curvature* of the curve and $\kappa_n(y)$ is its *normal curvature*. The metric of the curve is given by h (see App. A.2 for more details).

Now we perform the variation of the free energy (2.17) which is related to the set

of constraints S_{ab}:

$$\delta\mathcal{F}_{\mathrm{C}}[\boldsymbol{X}] = \int_{\Sigma} \mathrm{d}A \left\{ \mathcal{E}_{\mathrm{C}} \boldsymbol{N} + A_{\mathrm{C}}^{a} \boldsymbol{e}_{a} \right\} \cdot \delta\boldsymbol{X} + \int_{\Sigma} \mathrm{d}A \, \nabla_{a} Q_{\mathrm{C}}^{a} \, , \qquad (2.57)$$

where each term of the previous expression is written as:

$$\mathcal{E}_{\mathrm{C}} = K S_{ab} g^{ab} - 2 K^{ab} S_{ab} \, , \qquad (2.58\mathrm{a})$$

$$A_{\mathrm{C}}^{a} = 2 \nabla_{b} S^{ba} - \nabla^{a} \left(g^{bc} S_{bc} \right) \, , \qquad (2.58\mathrm{b})$$

$$Q_{\mathrm{C}}^{a} = - \left(2 S^{ab} - g^{ab} g^{cd} S_{cd} \right) \left(\boldsymbol{e}_{b} \cdot \delta\boldsymbol{X} \right) \, . \qquad (2.58\mathrm{c})$$

On the other hand, the variation of the surface tension term (2.6) verifies:

$$\delta\mathcal{F}_{\sigma}[\boldsymbol{X}] = \int_{\Sigma} \mathrm{d}A \{ \sigma(x) K \boldsymbol{N} - (\nabla^{a}\sigma) \boldsymbol{e}_{a} \} \cdot \delta\boldsymbol{X} + \int_{\Sigma} \mathrm{d}A \nabla_{a} [g^{ab} \sigma(x) (\boldsymbol{e}_{b} \cdot \delta\boldsymbol{X})] \, , \quad (2.59)$$

where we have suppressed the label i in Eqns. (2.57) and (2.59), for simplicity.

Finally note that in Sec. 2.3.1 the variations of the global pressure difference term $\mathcal{F}_{\mathrm{V}}[\boldsymbol{X}]$ and the elastic free energy term $\mathcal{F}_{\Sigma}^{(i)}[\phi, \boldsymbol{X}]$ have already been calculated. The boundary term corresponding to the pressure energy is given by the second part of Eqn. (2.47) but, as the total surface is closed, this term does not contribute to the total boundary conditions. Even if this additional term is taken into account it vanishes identically because the stress tensor $\boldsymbol{f}_{v}^{a}$ consists of quantities that are continuous at the interface (like $\boldsymbol{X}$, $\boldsymbol{e}_{a}$ and $\boldsymbol{N}$).

Following the structure of the Eqn. (2.53) the final result comes from the variations of each free energy contribution. Collecting all these terms the normal part of the bulk term $\mathcal{E}_{\mathrm{T}}(\mathcal{H})$ reads:

$$S_{ab}^{(i)} g^{ab(i)} K_{i} + \sigma^{(i)} K_{i} + K_{i} \mathcal{H}_{\Sigma}^{(i)} - 2 K^{ab(i)} S_{ab}^{(i)} - (K_{i}^{2} - \mathcal{R}_{i}) \left(\frac{\partial \mathcal{H}_{\Sigma}^{(i)}}{\partial K_{i}} \right) -$$
$$\mathcal{R}_{i} K_{i} \left(\frac{\partial \mathcal{H}_{\Sigma}^{(i)}}{\partial \mathcal{R}_{i}} \right) - g^{(i)ab} \nabla_{a} \nabla_{b} \left(\frac{\partial \mathcal{H}_{\Sigma}^{(i)}}{\partial K_{i}} \right) - 2 L^{(i)ab} \nabla_{a} \nabla_{b} \left(\frac{\partial \mathcal{H}_{\Sigma}^{(i)}}{\partial \mathcal{R}_{i}} \right) - P = 0 \, . \qquad (2.60)$$

The Eqn. (2.60) corresponds to the shape equation that must be satisfied in each domain. The tangential part of the bulk term $A^{(i)a}$ imposes a relation between the local surface tension $\sigma^{(i)}(x)$ and the scalar field $\phi_{i}(x)$ in each domain. It is given by:

$$- \left(\frac{\partial \mathcal{H}_{\Sigma}^{(i)}}{\partial \phi_{i}} \right) \nabla^{a} \phi_{i} - \nabla^{a} \sigma^{(i)} + 2 \nabla_{b} S^{(i)ab} - \nabla^{a} \left(g^{(i)bc} S_{bc}^{(i)} \right) = 0 \, . \qquad (2.61)$$

If $\sigma^{(i)} = \lambda_{i}$ is constant, $\phi_{i} = 0$ and $S_{ab}^{(i)} = 0$ we obtain a purely geometric case.

The typical jump conditions at the interface between domains have been obtained in [72] for the case of an axisymmetric closed vesicle composed of two phases. These

conditions will be modified by the addition of a scalar field and its spatial variations, which represents some internal degree of freedom on the surface. Now we will obtain the jump conditions at $\mathcal{C}$ that must be satisfied by Eqn. (2.52) in a parametrization-free way. They will also be independent of any possible symmetry of the surface Σ (like translational or rotational symmetries).

From now on we introduce the following notation for the partial derivatives of the free energy density $\mathcal{H}_\Sigma^{(i)}(\phi, K, \mathcal{R})$ with respect to its arguments:

$$\mathcal{G}_g^{(i)} = \frac{\partial \mathcal{H}_\Sigma^{(i)}}{\partial g} \,, \qquad g(x) \in \{\phi, K, \mathcal{R}\} \,, \tag{2.62}$$

At equilibrium the total free energy must be stationary with respect to the variations of the contact line and the embedding functions $\boldsymbol{X}$. Therefore the E-L equations must be satisfied and the second part of the condition Eqn. (2.53) can be written as follows:

$$
\begin{aligned}
\delta \mathcal{F}_\mathrm{T}[\phi, \boldsymbol{X}] &= \oint_\mathcal{C} \mathrm{d}l \, \left[l_a Q_\mathrm{T}^{(2)a} + m_a Q_\mathrm{T}^{(1)a} - \left\{ \frac{1}{\sqrt{h}} \left(\frac{d\gamma}{dy} \right) \boldsymbol{t} + \gamma \kappa_g \boldsymbol{l} + \gamma \kappa_n \boldsymbol{N} \right\} \cdot \delta \boldsymbol{X} \right] \,, \\
&= \oint_\mathcal{C} \mathrm{d}l \, \Delta \mathcal{I}_\mathrm{T}[\phi, \boldsymbol{X}] \,,
\end{aligned}
\tag{2.63}
$$

where $m_a = -l_a$ are the covariant components of the vector $\boldsymbol{m} = -\boldsymbol{l}$, which is normal to $\mathcal{C}$, tangent to Σ and pointing out to Σ_1. The term $\mathcal{I}_\mathrm{T}[\phi, \boldsymbol{X}]$ encodes the independent variations that contribute to the total contact line variation. It corresponds to the sum of the variation of the line tension free energy and the boundary variation of the total elastic free energy of each domain composing the biphasic surface. It has the following structure:

$$\Delta \mathcal{I}_\mathrm{T}[\phi, \boldsymbol{X}] = \Delta \mathcal{S}_t(\boldsymbol{t} \cdot \delta \boldsymbol{X}) + \Delta \mathcal{S}_l(\boldsymbol{l} \cdot \delta \boldsymbol{X}) + \Delta \mathcal{S}_\mathrm{N}(\boldsymbol{N} \cdot \delta \boldsymbol{X}) + \Delta \mathcal{T}_t(\boldsymbol{l} \cdot \delta \boldsymbol{N}) \,, \tag{2.64}$$

Now we determine each contribution. Before we proceed we introduce the following notations:

$$
\begin{aligned}
\Delta \mathcal{G}_K &= \frac{\partial \mathcal{H}_\Sigma^{(2)}}{\partial K_2} - \frac{\partial \mathcal{H}_\Sigma^{(1)}}{\partial K_1} \,, \tag{2.65a} \\
\Delta \mathcal{G}_\mathcal{R} &= \frac{\partial \mathcal{H}_\Sigma^{(2)}}{\partial \mathcal{R}_2} - \frac{\partial \mathcal{H}_\Sigma^{(1)}}{\partial \mathcal{R}_1} \,, \tag{2.65b} \\
\Delta S_{ab} &= S_{ab}^{(2)} - S_{ab}^{(1)} \,. \tag{2.65c}
\end{aligned}
$$

Thus the first term in the expression (2.64) is given by:

$$\Delta \mathcal{S}_t[\boldsymbol{X}] = \tau_g \Delta \mathcal{G}_K - 2\kappa_n \tau_g \Delta \mathcal{G}_\mathcal{R} - 2l^a t^b \Delta S_{ab} - \frac{1}{\sqrt{h}} \left(\frac{d\gamma}{dy} \right) \,, \tag{2.66}$$

where τ_g is the *geodesic torsion* of $\mathcal{C}$. It is continuous across the boundary. This

relation represents the equilibrium of the tangential forces acting in the direction $\boldsymbol{t}$. It can also be identified with the translation $(\boldsymbol{t} \cdot \delta \boldsymbol{X})$ of the contact line. Normally this term is discarded because it is related to a reparametrization of the boundary curve $\mathcal{C}$. It occurs when the free energy depends only on geometric properties of the surface Σ and when the line tension is not a constant. Here it will be considered due to the internal degrees of freedom and the constraint imposed on the surfaces Σ_i. As we will see in the next chapter this expression is identically zero in the axisymmetric case because $\tau_g = 0$ and the line tension γ is constrained to be a constant. Note that if γ is not a constant the balance between both domains would break and lipids molecules could migrate from one domain to another along the boundary.

The second term in Eqn. (2.64) is associated to the tangential translation described by $(\boldsymbol{l} \cdot \delta \boldsymbol{X})$. It reads:

$$\Delta \mathcal{S}_l[\boldsymbol{X}] = \mathcal{H}_{\mathrm{T}}^{(2)} - \mathcal{H}_{\mathrm{T}}^{(1)} - K_{2\perp} \mathcal{G}_{K_2}^{(2)} + K_{1\perp} \mathcal{G}_{K_1}^{(1)} - \mathcal{R}_2 \mathcal{G}_{\mathcal{R}_2}^{(2)} \\ + \mathcal{R}_1 \mathcal{G}_{\mathcal{R}_1}^{(1)} - 2\tau_g^2 \Delta \mathcal{G}_K - 2l^a l^b \Delta S_{ab} - \gamma \kappa_g \; , \tag{2.67}$$

where the term $K_{i\perp} = l^a l^b K_{ab}^{(i)}$ is the projection of the curvature tensor onto the tangential basis (see App. A.2). The equation (2.67) represents the balance of the tangential forces acting in the direction $\boldsymbol{l}$.

The third term in Eqn. (2.64) is related to the perpendicular translation $(\boldsymbol{N} \cdot \delta \boldsymbol{X})$. It is given by:

$$\Delta \mathcal{S}_{\mathrm{N}}[\boldsymbol{X}] = \nabla_\perp \Delta \mathcal{G}_K - 2\kappa_n \nabla_\perp \Delta \mathcal{G}_{\mathcal{R}} + 2\tau_g \nabla_\parallel \Delta \mathcal{G}_{\mathcal{R}} + 2\nabla_\parallel \left[\tau_g \Delta \mathcal{G}_{\mathcal{R}} \right] - \gamma \kappa_n \; . \tag{2.68}$$

were τ_g and κ_n will always be considered as continuous quantities across the boundary, unlike the perpendicular curvature term $K_{i\perp}$ which is discontinuous. We have used here the two directional surface derivatives introduced in App. (A.2.2), $\nabla_\perp$ and $\nabla_\parallel$. The equation (2.68) expresses the balance of normal forces acting across the surface Σ on $\mathcal{C}$.

Finally the fourth term in Eqn. (2.64) is given by:

$$\Delta \mathcal{T}_{\mathrm{t}}[\boldsymbol{X}] = \Delta \mathcal{G}_K - 2\kappa_n \Delta \mathcal{G}_{\mathcal{R}} \; . \tag{2.69}$$

This term is associated with a rotation around the contact line $\mathcal{C}$ and originates from the variation $(\boldsymbol{l} \cdot \delta \boldsymbol{N})$. It expresses the balance of torques acting in the tangential direction $\boldsymbol{t}$.

The vanishing of the terms (2.66), (2.67), (2.68), and (2.69) give us the *jump conditions* at the interface. In their derivation it has been assumed that τ_g, κ_g, κ_n are continuous at the boundary, however the normal curvature in the direction $\boldsymbol{l}$, namely $K_\perp$, is not continuous.

The boundary conditions derived here do not depend neither on the parametrization nor on the possible symmetries of the closed surface Σ. They allow us to explore the relation between the elastic coefficients of each domain and the line tension of the

boundary connecting both phases. In Chapter 3 we will study this problem in the axisymmetric case, when a phase separation takes place in a biphasic lipid vesicle, followed by a budding process which deforms the vesicle.

2.4 Two-dimensional elasticity of elastic plates and shells

So far, the discussion has been focused to deal with fluid surfaces and its energetic properties. For instance, a fluid membrane is an isotropic continuum which cannot resists in-plain shear strain. Accordingly, its main elastic and geometric features are described (at mesoscopical scales) by a bending free energy Eqn. (2.5) which depends only on the invariants constructed from the curvature tensor K_{ab}, namely, the mean and Gaussian curvature.

Otherwise, plates and shells are slender elastic bodies which are able to endure both bending and in-plane strain. In this section we briefly review the energetic and elastic properties of these structures. For this purpose, differential geometry of surfaces is the most appropriate formalism.

In most cases the elastic energies describing these thin structures are based on the well established three dimensional nonlinear elastic theory of bodies [106]. The dimensional reduction of this theory is carried out using various assumptions, such as small deformations, small deflections, and parallel stress to the midsurface. As a result, an effective two-dimensional elastic energy results which allows to describe the geometrical and elastic properties of these thin bodies by means of their mid-surface configuration.

This theoretical background will be useful in Chapter 5, where an experimental setup is presented which allows us to study the packing of thin elastic cylindrical sheets, and also in Chapter 4, when the elastic behavior of non-Euclidean growing sheets will be considered.

2.4.1 Elastic plates

Here we use the term *plate* to denote a thin elastic body of constant thickness h, which is planar in its rest state and bears no structural variation across its thin dimension.

During the past decades the properties of elastic plates have been intensively studied experimental, numerical and theoretically. From a theoretical point of view some typical features like crumpling, buckling or cracking have been well understood using the nonlinear *Föppl-von Karman equations* (FvK) [60, 136]. These equations come from the minimization of an elastic free energy which is the sum of bending and stretching terms [83]. The bending energy, which is cubic in h, considers the curvature of the deformed plate and accounts for the out-plane deformations. On the other hand, the stretching energy is proportional to h and describes the in-plane deformations:

$$\mathcal{F}_{FvK}[\xi] = \mathcal{F}_b[\xi] + \mathcal{F}_{st}[\xi] \, , \tag{2.70}$$

$$\mathcal{F}_b[\xi] \;=\; \frac{1}{2}\kappa_o \int_{\mathcal{D}} \{(\triangle\xi)^2 - 2(1-\nu)[\xi,\xi]\}\; \mathrm{d}x\mathrm{d}y \;, \tag{2.71a}$$

$$\mathcal{F}_{st}[\xi] \;=\; \frac{h}{2} \int_{\mathcal{D}} \sigma_{ab}u_{ab}\; \mathrm{d}x\mathrm{d}y \;, \tag{2.71b}$$

$$\kappa_o \;=\; \frac{Eh^3}{12(1-\nu^2)} \;, \tag{2.71c}$$

where κ_o is the bending modulus, E is the Young modulus and ν is the Poisson ratio. In the stretching energy term u_{ab} is the two dimensional *strain tensor* and σ_{ab} corresponds to the *stress tensor*. Both tensor and the bracket $[\cdot,\cdot]$ used Eqn. (2.71a) are defined by:

$$u_{ab} \;=\; \frac{1}{2}\left(\frac{\partial u_a}{\partial x_b} + \frac{\partial u_b}{\partial x_a} + \frac{\partial \xi}{\partial x_a}\frac{\partial \xi}{\partial x_b} \right) \;, \tag{2.72a}$$

$$\sigma_{ab} \;=\; \frac{E}{1-\nu}[(1-\nu)u_{ab} + \nu u_{cc}\delta_{ab}] \;, \tag{2.72b}$$

$$[f,g] \;=\; \frac{1}{2}\frac{\partial^2 f}{\partial x^2}\frac{\partial^2 g}{\partial y^2} + \frac{1}{2}\frac{\partial^2 f}{\partial y^2}\frac{\partial^2 g}{\partial x^2} - \frac{\partial^2 f}{\partial x\partial y}\frac{\partial^2 g}{\partial x\partial y} \;, \tag{2.72c}$$

where u_a stand for the components of the *displacement vector* ($a,b \in \{1,2\}$). The elastic energy (2.70) is obtained by means of a dimensional reduction process using the *Kirchhoff-Love* assumptions [92], whose validity is widely disputed. However, the FvK equations have been rigorously derived from three-dimensional elasticity using an asymptotic expansion method [38], were the thickness h is the expansion parameter.

The equations arising from the minimization of Eqn. (2.70) are highly nonlinear and its resolution is a very hard task. However, some progress has been achieved in the case of singularities that arise when an elastic sheets is submitted to a punctual load. For instance in [8] the geometry of a *d-cone* is studied in detail (a d-cone is a solution of FvK equations) some scaling relations are obtained for the core size of the d-cone in [33]. From an experimental point of view, the mechanical stability, shape and energy of this conical singularity have been characterized in [35, 36].

2.4.2   Elastic shells

A shell is a two-dimensional structure whose initial rest configuration is not planar. This is because it exhibits a structural variation across its thin dimension. Here we describe the *Koiter shell theory* which, as in the case of elastic plates, comes from the $3D$ nonlinear elastic theory. By means of a dimensional reduction process, a free energy that accounts for bending and stretching deformations of the shell is derived. This elastic energy is obtained, assuming that both stresses and strains are parallel to

the deformed mid-surface Σ during the deformation. This free energy reads [75, 39]:

$$\mathcal{F}_K[\boldsymbol{u}] = \frac{h^3}{24} \int_{\overline{\Sigma}} \mathrm{d}\overline{A} \; \mathcal{A}^{abcd} b_{ab}(\boldsymbol{u}) b_{cd}(\boldsymbol{u}) + \frac{h}{2} \int_{\overline{\Sigma}} \mathrm{d}\overline{A} \; \mathcal{A}^{abcd} \varepsilon_{ab}(\boldsymbol{u}) \varepsilon_{cd}(\boldsymbol{u}) \; , \qquad (2.73)$$

where $\boldsymbol{u}$ corresponds to the *displacement vector* $\boldsymbol{u} = \boldsymbol{X} - \overline{\boldsymbol{X}}$, $\mathrm{d}\overline{A} = \sqrt{\overline{g}} \mathrm{d}\overline{x}^1 \mathrm{d}\overline{x}^2$ is the infinitesimal area element on $\overline{\Sigma}$, the initial rest configuration. Hereafter, the bar denotes quantities associated with the initial configuration. The raising and lowering of indices is only defined with respect to the reference metric $\overline{g}_{ab}$, even for tensors defined in the current deformed state. $\mathcal{A}^{abcd}$ stand for the contravariant components of the *elastic tensor* whose structure is imposed by the assumption of spatial isotropy. $b_{ab}(\boldsymbol{u})$ are the covariant components of the *mixed curvature tensor* which accounts the changes in the curvature tensor associated with the displacement vector. ε^{ab} correspond to the covariant components of the *strain tensor* evaluated at the midsurface, accounting for changes in the metric tensor with respect to the displacement vector. All these quantities are expressed by:

$$\mathcal{A}^{abcd} = \frac{E}{1+\nu} \left(\frac{\nu}{1-\nu} \overline{g}^{ab} \overline{g}^{cd} + \overline{g}^{ac} \overline{g}^{bd} \right) \; , \qquad (2.74\text{a})$$

$$b_{ab}(\boldsymbol{u}) = K_{ab}(\boldsymbol{u}) - \overline{K}_{ab} \; , \qquad (2.74\text{b})$$

$$\varepsilon_{ab}(\boldsymbol{u}) = \frac{1}{2}(g_{ab}(\boldsymbol{u}) - \overline{g}_{ab}) \; , \qquad (2.74\text{c})$$

where again E is the Young modulus and ν is the Poisson ratio of the shell.

The elastic response of shells and plates under different deformations is quite different. This is a consequence of the underlying geometry of the initial rest configuration. Thus, whereas a plate can almost always be bend weakly without stretching, this is not possible for elastic shells, for which stretching and bending occur simultaneously. In general surfaces with positive Gaussian curvature ($K_G > 0$) exhibit localized patterns deformation (like points or curves), in which the stretching energy is highly concentrated. These patterns connect regions in which the surface is isometric, that means, the measure of lengths is preserved during the deformation. This striking behavior has also been observed in the case of *developable surfaces* i.e, surfaces with zero Gaussian curvature ($K_G = 0$). An example is the crumpling of paper [8]. Otherwise, surfaces with negative Gaussian curvature ($K_G < 0$) display a very different behavior showing a nonlocal concentration of stretching during their deformations [133].

In the next chapters we will use the formalism introduced in this chapter to solve problems that involve fluid surfaces that resist stretching, but that incorporate internal degrees of freedom and elastic growing surfaces, in which stretching is crucial to determine the energetic properties and the energy concentration.

Chapter 3

LINE TENSION AND BUDDING OF BIPHASIC VESICLES

Inhomogeneities in the cell membrane give rise to localized interactions at the interface between domains in a two-component vesicle. The corresponding energy is expressed as a line tension between the two phases. In this chapter we will study the conditions under which this line tension can destabilize the domains when budding occurs in inhomogeneous vesicles. The consequences of the adsorption of impurities will also be examined, our scope being the extension of the Helfrich model to elastic deformations and chemical interactions arising at microscopic scales.

3.1   Introduction

As we have seen in Sec 1.1 the membrane of lipid vesicles constitutes a simplified system in which some basic characteristics of the real cell membrane can be studied. Among them, we have mentioned the formation of ordered domains (sometimes called *rafts* or liquid ordered domains) which have been experimentally observed in a ternary mixture of lipids in GUVs. They are essentially composed of cholesterol and sphingolipids (or phospholipids).

Domain formation is a consequence of a phase separation occurring in the lipid vesicles. This can be triggered by various external physical factors, like temperature changes or osmotic pressure changes. It has been shown that this phase separation can trigger a shape transformation of the vesicle, leaving as a result its budding and possibly the fission of the ordered domain.

Most of the experiments suggest that budding and fission in lipid vesicles can be explained by the physical properties of the membrane. As a consequence the budding process has been studied theoretically in several works [87, 88, 71, 72] in which the generic mechanism that predicts the domain formation is governed principally by the line tension of the domain boundaries. This mechanism is also modulated by the spontaneous curvature and the bending rigidity of each membrane domain. The influence of the size of the buds during the budding has also been studied. Line tension tries to reduce the length of the interface between domains and therefore favors the formation of buds. It is thus important to understand which factors allow the variation of the line tension between domains in a biphasic vesicle. This is the matter of study of this

chapter

3.2   Properties of the contact line between domains. Line tension

We now focus on the contact line between domains composing a biphasic vesicle. When two or more domains are in contact a free energy proportional to the length of the domain boundary must be added in order to take into account the energetic cost of possible changes for the interface length.

Line tension is a quantity that depends not only on chemical properties of the lipid species composing both domains but also depends on the mechanical state of each domain. At length scales comparable to the membrane thickness the interface exhibits structural variations which come from short-scale elastic degrees of freedom, like the matching of thicknesses [61, 85] or the tilt of lipid molecules [82].

Typically liquid-ordered domains are thicker than the surrounding membrane. An abrupt step between domains would expose the lipid tails to the surrounding water which is prohibited because of their hydrophobicity. This induces a distortion which implies the tilt of the lipid molecules. As a consequence there is an energy associated with the elastic deformations of both domains at the interface (see fig 3.1(a)). This structural difference induces a line tension energy, subject of study of this chapter.

In the unrealistic case of the step junction the energy per unit length of such a mismatch has been estimated in [87] (see Fig. 3.1(a)). When the height mismatch is $\sim 0.5 - 1[nN]$ (*i.e* 10 % of the total height), the line tension energy is $\sim 10[pN]$. Now if the surface is deformed at the interface these values are much smaller. In [82] it has been estimated to be of order $\sim 1[pN]$. In this case the principal contribution comes from the elastic deformation of lipids in the narrow region of the contact line (see 3.1(b)). The thicker raft decreases its thickness and the thinner domain increases it. The consequence is a reduction of the boundary energy.

Line tension has been experimentally deduced in [14, 15] from the shape of biphasic vesicles using typical values for the osmotic pressure and the elastic constants. The estimated values are $\sim 0.5[pN]$ which is in favour of a dilute interface.

Several factors may influence the effective line tension variation between domains. For example, in ref [2] the effect of lateral surface tension on the interfacial energy is studied. It has been shown in the case of height mismatch that the application of lateral tension produces an increase of the line tension which depends on the values of the spontaneous curvatures of each domain. Height mismatch is determined not only by lipid compositions but also by the mechanical conditions at equilibrium. In this chapter we study the consequences of mechanical distortions due to the height mismatch between phases. We show that they modify the line tension.

In all the references cited so far, the slope of the neutral surface membrane has been considered as continuous at the interface. This assumption is not realistic in all situations, because monolayers that compose the cell membrane can exhibit a very pro-
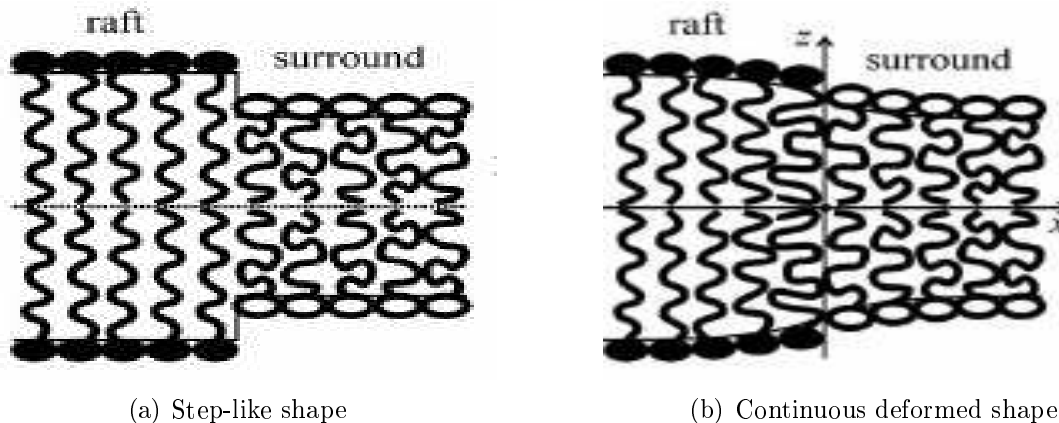
(a) Step-like shape

(b) Continuous deformed shape

Fig. 3.1: Structure of domains shapes at the interface. Image extracted from [2]

nounced asymmetry. This asymmetry (besides the structural difference between lipids composing both domains) modifies the energetic properties and destabilizes the domains in budding and fission processes. Note that cells exhibit asymmetry between monolayers contrary to vesicles whose monolayers are symmetric so this effect is important.

If the membrane has monolayers which strongly differ, the usual description involving Helfrich elasticity must be modified. The mesoscopic description is no longer valid at scales comparable to a few times the membrane thickness ($\simeq 10nm$). In the neighborhood of the joint between membrane domains there are elastic degrees of freedom which are excited. These short-scale internal properties are related to the height mismatch between the domains [54] and the tilt of lipid molecules [67, 82].

In the next section we will see how to take into account the structural variation at the interface between domains modifying the usual Helfrich elasticity which describes the equilibrium properties of the membrane. The thickness of the bilayer will be introduced as a variable representing the height mismatch.

3.3   Modifying Helfrich elasticity

The aim of this section is to show how we can take into account the structure at the interface from a macroscopic (continuous) point of view. The coupling between internal degrees of freedom, represented by the thickness variation across the neutral surface and the macroscopic degrees of freedom related to the surface geometry (like mean and Gaussian curvatures) will be deduced using only arguments of elastic and geometric nature. Deductions will be performed from first principles, considering the elastic deformations associated to the different structure of each lipid molecule, and referring it to the neutral surface.

Furthermore the deductions will be performed without taking into account the parametrization or the possible symmetries of the biphasic vesicle. Later we will specialize our findings to the case of a closed biphasic axisymmetric vesicle.
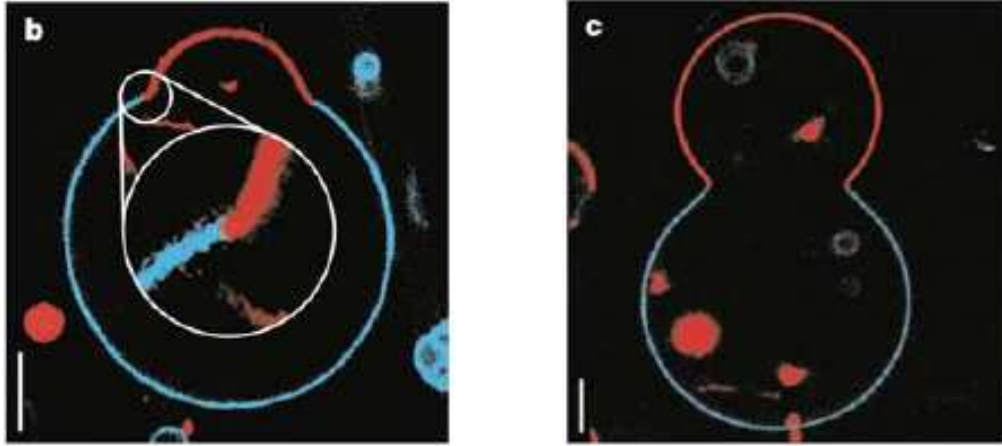
(a) Structural thickness variation at the interface in a GUV when budding occurs. The inset is the neck region which has been enlarged.

(b) Another stage of budding in a biphasic vesicle. Peanut shape.

Fig. 3.2: Equatorial section showing two fluid phases coexisting in a GUV. Images extracted from [15].
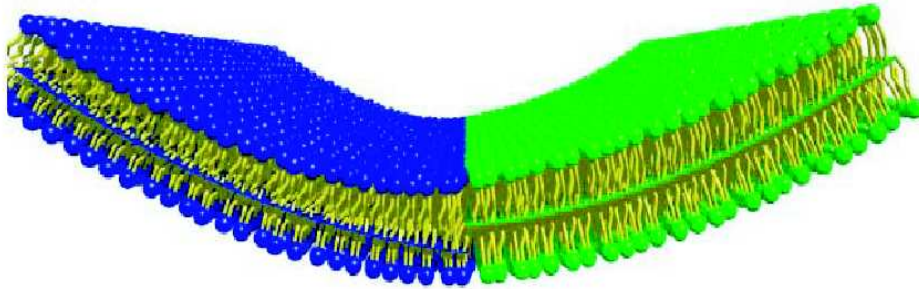
Fig. 3.3: Scheme representing the structural height mismatch at the interface between two different lipid domains. Extrapolated neutral surfaces do not agree at the joint, In contrast to the usual Helfrich description. Courtesy of J. B. Fournier.

Unlike Chap. 2 during the course of this chapter we will use the mean curvature H and the Gaussian curvature K_{G} instead of the trace of the extrinsic curvature tensor K and the scalar curvature $\mathcal{R}$, respectively. We note that they are simply connected by the relation $K = 2H$ and $\mathcal{R} = 2K_{\mathrm{G}}$.

3.3.1   Coupling between thickness and curvature

The membrane of the biphasic vesicle will be considered as an anisotropic elastic continuum composed of two phases, each denoted by the label $\{i = 1, 2\}$. Both phases

will be described by the same type of elasticity and they will only differ in the value of physical coefficients, like Gaussian or bending stiffness. Hence in this section we will suppress this label. In turn, each phase consists of two lipid monolayers (from now each denoted by the label $\{I = \pm\}$). This elastic continuum can undergo different types of elastic deformations, such as stretching and bending.

We suppose that the coupling terms arise from two contributions. A first contribution is related to a non-homogeneous bending energy which can be characterized by a two-dimensional gradient of the thickness, $\nabla_a u$, occurring in the total free energy. A second term comes from a *local area-difference elasticity* between both lipid monolayers that compose each membrane domain.

From Fig. 3.4 we see that the hydrophilic (outer or inner) surface is a dividing surface situated at the region of contact between the lipid heads and water. To describe the thickness variation at the interface we assume that the normal distance between the neutral surface Σ and the hydrophilic surfaces $\Sigma^{(+)}$ (resp. $\Sigma^{(-)}$) of the outer (resp. inner) leaflet is a function of the coordinates defined on Σ (see Fig. 3.4 for definitions). We will denote this distance as $\eta^{(+)}$ (resp. $\eta^{(-)}$). In this way, the thickness of the bilayer is defined as $u(x) = \eta^{(-)}(x) + \eta^{(+)}(x)$.

The choice of the neutral surface as reference surface is convenient because stretching and bending are independent when they are defined with respect to Σ. As a consequence the area of the neutral surface does not change during the deformation of bending.

The stretching and bending terms that we will consider here for each phase are then expressed by:

$$\mathcal{F}[\boldsymbol{X}^{(\pm)}] \;\; = \;\; \oint_{\Sigma^{(+)}} dA^{(+)} f^{(+)} + \oint_{\Sigma^{(-)}} dA^{(-)} f^{(-)} \, , \tag{3.1a}$$

$$f^{(I)}(A^{(I)}, H^{(I)}) \;\; = \;\; \frac{\mathcal{K}^{(I)}}{2} \left(A^{(I)} - A_o^{(I)}\right)^2 + \frac{\kappa^{(I)}}{2} \left(2H^{(I)} - H_s^{(I)}\right)^2 \, , \tag{3.1b}$$

where $A^{(I)}$ is the surface area of each side (inner and outer), $A_o^{(I)}$ is the preferred area of each monolayer, $H^{(I)}$ is the mean curvature, $\kappa^{(I)}$ is the bending stiffness and $\mathcal{K}^{(I)}$ is the area-stretching elasticity coefficient. Note that in the expressions (3.1a) and (3.1b) we have again removed the label i.

The infinitesimal area element $dA^{(I)}$ (resp. inner and outer) is related to dA which is defined on the neutral surface, by means of an expansion to leading orders (see App. B):

$$dA^{(I)} = dA \left(1 \pm 2H\eta^{(I)} + K_{\mathrm{G}}\eta^{(I)2} + \frac{1}{2}\nabla^a \eta^{(I)} \nabla_a \eta^{(I)} + \dots\right) \, . \tag{3.2}$$

Introducing these relations in (3.1a) we obtain the free energy density (see App. B for a detailed derivation) at dominant order in u for each phase:

$$f_h = \frac{1}{2}\kappa(2H - H_s)^2 + \overline{\kappa} K_{\mathrm{G}} + 2\Lambda H u + u^2 K_{\mathrm{G}}\delta + \lambda \, , \tag{3.3}$$

where the coefficients κ, $\overline{\kappa}$, Λ, δ and λ depend on the microscopic coefficients $A_o^{(I)}$, $\kappa^{(I)}$, $H_s^{(I)}$ and $\mathcal{K}^{(I)}$ characterizing each monolayer.

Thickness variations become important at the joint between domains. We consider these contributions including a term in the free energy where inhomogeneities in curvature induce changes in the (inner and outer) hydrophilic surface.

Thickness variation and bending deformation in the bilayer give an increase of the area of both hydrophilic (inner and outer) surfaces. We will assume that the change of free energy per molecule arising from the extension of the hydrophilic surfaces is simply proportional to this extension and therefore [77]:

$$f_{nh}^{(I)} = \xi^{(I)} \Delta A_{nh}^{(I)} \, , \tag{3.4}$$

where $A_{nh}^{(I)}$ is the area of each hydrophilic surface and $\xi^{(I)}$ is a coefficient having the dimensions of a surface tension. Then, at the lowest order, we derive the following expression (see App. B):

$$f_{nh}^{(I)} = \frac{1}{2} a \xi^{(I)} (1 - H\eta^{(I)} - K_G \eta^{(I)2} - ...)(\nabla \eta^{(I)})^2 \simeq \frac{1}{2} a \xi^{(I)} (\nabla \eta^{(I)})^2 \, . \tag{3.5}$$

Note that using the definition (3.4) we have isolated the contribution of inhomogeneous bending from the homogeneous one.

The Helfrich model does not consider mean or Gaussian curvature gradients. However it is possible to generate scalars in the free energy density which depend on derivatives of the surface curvature [62] in order to prevent the occurrence of infinitely sharp curvature changes. Then, we have:

$$\mathcal{H}_{nh} = \frac{1}{2} \kappa_{nh} (\nabla_a H)(\nabla^a H) \, . \tag{3.6}$$

Note that the importance of this term depends on whether or not the curvature changes significantly on length scales comparable to l_g, a characteristic length which is given by: $l_{gr} := \sqrt{\kappa_{gr}/\kappa}$. A similar inhomogeneous bending term has been also used to determine the persistence length in a surfactant monolayer [77].

So far, we have established the coupling terms and the thickness variation contribution to the free energy. Finally, there is a cost to pay when the distance between the two leaflets varies from a_o given by the chemical interactions between lipids. To take into account this effect to leading order we assume an harmonic-like energy:

$$f_{ch}^{(i)} = \frac{1}{2} B_i (u_i(x) - a_{oi})^2 \, . \tag{3.7}$$

Note that the energy density (3.7) is already written for the entire bilayer of a given phase (although a similar expression must be valid for each monolayer). For the rest of the contributing terms the energy of the bilayer of each phase is simply the sum of each monolayer contribution, redefining the respective coefficients.
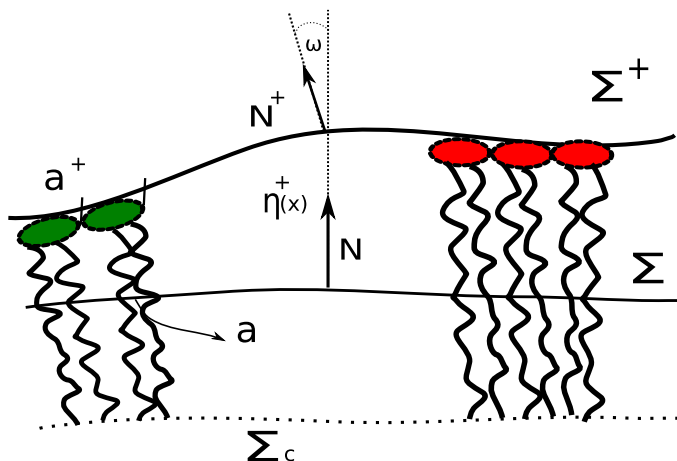
Fig. 3.4: Schematic representation of a monolayer with inhomogeneous curvature. The neutral surface is denoted as Σ, and the hydrophilic surface is Σ^+. Their normal vectors are $\boldsymbol{N}$ and $\boldsymbol{N}^+$ respectively. Note that in this case, the schema depicts the external leaflet of the bilayer. Σ_c is a region denoting the position of the base of the hydrocarbon chains. The area per lipid molecule on the hydrophilic surface is a^+, and its area on the neutral surface is a. The normal distance between the Σ and Σ^+ at a given point x is denoted by $\eta^+(x)$. Note that as a consequence of the non-homogeneous bending the normal vectors $\boldsymbol{N}$ and $\boldsymbol{N}^+$ are not parallel, exhibiting a nonzero angle ω. The generalization to the inner monolayer is obvious.

3.3.2   Total free energy of the biphasic vesicle

Considering all the contributions introduced in the previous section, the total free energy of the system can be expressed as:

$$\mathcal{F}_{\mathrm{T}}[u(x), \boldsymbol{X}] = \sum_{i=1,2} \int_{\Sigma_i} \mathrm{d}A \; (f^{(i)} + f_{nh}^{(i)} + f_{ch}^{(i)}) - P \int_{V(\Sigma)} \mathrm{d}V + \int_{\mathcal{C}} \gamma dl \; , \qquad (3.8)$$

where the label $\{i = 1, 2\}$ denotes each phase. The previous expression is equivalent to:

$$\mathcal{F}_{\mathrm{T}}[u(x), \boldsymbol{X}] = \sum_{i=1,2} \int_{\Sigma_i} \mathrm{d}A \; (f_1^{(i)} + f_2^{(i)} + f_3^{(i)}) - P \int_{V(\Sigma)} \mathrm{d}V + \int_{\mathcal{C}} \gamma dl \; , \qquad (3.9)$$

where the terms $f_\alpha^{(i)}$, with $\alpha \in \{1, 2, 3\}$, represent the different contributions to the free energy in each domain. First, we have the classical description given by the Helfrich model accounting for the large scale elastic deformations:

$$f_1^{(i)} = \frac{1}{2}\kappa_i(2H_i - H_{si})^2 + \overline{\kappa}_i K_{\mathrm{G}i} + \lambda_i \; , \qquad (3.10)$$

in which λ_i stands for the constraint of constant global area during the deforma-

tion. In addition, we have a *structural* free energy density accounting for the inner deformations of the membrane. They are described by the thickness function $u(x)$ and its variation along the neutral surface Σ:

$$f_2^{(i)} = \frac{1}{2}B_i(u_i - a_{oi})^2 + \frac{1}{2}\xi_i g^{ab}\nabla_a u_i \nabla_b u_i \ . \tag{3.11}$$

Note that in the previous equation the free energy density is expressed as a function of u_i and not as a function of $\eta^{(\pm)}$. The total free energy associated with inhomogeneous bending is the sum of each monolayer contribution, given by the term (B.24). As is shown in App. B the definition of the neutral surface Σ allow us to express a condition between $\eta^{(+)}$, $\eta^{(-)}$ (see Eqn. (B.6)). This relation and the definition $u = \eta^{(+)} + \eta^{(-)}$ imply that both $\eta^{(+)}$ and $\eta^{(-)}$ are proportional to u and therefore the gradient term in Eqn. (3.11) is expressed as a function of u.

Although the thickness variation occurs at length-scales of order of a few nanometers, we keep a continuous description for the possible elastic deformations of the membrane, including stretching and non-homogeneous bending. Finally we have a third contribution that takes into account the interaction between the thickness variations and the large scale elasticity. It is given by the term:

$$f_3^{(i)} = 2\Lambda_i H_i u_i + \delta_i u_i^2 K_{\mathrm{G}i} \ , \tag{3.12}$$

which couples $u(x)$ with the geometrical description of the membrane, represented by its mean and Gaussian curvatures. The volume integral in (3.9) expresses the constraint of constant volume during the deformation (which is enforced by a Lagrange multiplier P). The last term is a line tension free energy accounting for the microscopic interactions at the contact line $\mathcal{C}$ between both domains (which arise *e. g.* from van der Waals forces between lipid molecules).

In summary we have a two-components lipid vesicle where each phase is described by a large scale free energy given by the Helfrich model and a structural microscopic free energy accounting for the internal deformations and expressed by the thickness variation of the membrane. The model is completed adding a line tension energy and a global pressure difference energy, which stands for the constant volume condition.

Note that this problem has already been addressed in Sec. 2.3.2, but the exact energetic properties of the biphasic surface have not been specified. In order to relate both sections and take advantage of the results obtained in Sec. 2.3.2, we can identify the terms composing the total free energy given by Eqn. (2.52) with the terms present in Eqn. (3.9).

Thereby, the term $\mathcal{H}_\Sigma$ given in Eqn. (2.20) reads:

$$\mathcal{H}_\Sigma^{(i)}[u_i(x), H_i, K_{\mathrm{G}i}] = \frac{1}{2}\kappa_i(2H_i - H_{si})^2 + \overline{\kappa}_i K_{\mathrm{G}i} + 2\Lambda_i H_i u_i + \delta_i u_i^2 K_{\mathrm{G}i} \ , \tag{3.13}$$

where we have identified the scalar field $\phi(x)$ as the thickness function $u(x)$ and, as mentioned earlier, the macroscopic elastic description is given by the Helfrich model.

For the term related to the surface tension $\mathcal{H}_\sigma$ (see Eqn. (2.6)) we write:

$$\mathcal{H}_\sigma^{(i)}[u_i(x)] = \lambda_i + \frac{1}{2}B_i(u_i - a_{oi})^2 \; , \tag{3.14}$$

where the local surface tension term $\sigma_i(x)$ can be identified as the sum of the constant surface tension λ_i (imposing the constraint of local surface area Σ_i during the deformation) and the term that stands for the chemical interaction between lipids.

Finally the term associated with the local constraints $\mathcal{H}_C$ (see Eqn. (2.17)) is given by:

$$\mathcal{H}_C^{(i)}[\nabla_a u_i(x)] = \frac{1}{2}\xi_i g_i^{ab}\nabla_a u_i \nabla_b u_i \; , \tag{3.15}$$

where again we have identified $\phi(x)$ with $u(x)$. In this case we have interpreted the square of the thickness gradient as the components of the constraints tensor S_{ab} (see Eqn. (2.18)):

$$S_{ab}^{(i)} = \frac{1}{2}\xi_i \nabla_a u_i \nabla_b u_i \; . \tag{3.16}$$

We also define the total free energy per unit of area as:

$$\mathcal{H}_T^{(i)} = \mathcal{H}_\Sigma^{(i)} + \mathcal{H}_C^{(i)} + \mathcal{H}_\sigma^{(i)} \; . \tag{3.17}$$

Having identified each term composing the free energy (3.9) and their relation with the free energy given by Eqn.(2.52) in the next section we will derive the Euler-Lagrange equations for each domain and the jump conditions at the contact line between them in the case of a biphasic vesicle. We will focus specifically in the axisymmetric case which has been observed in several experimental situations [14, 15, 117, 124].

3.4   Equilibrium equations, boundary conditions and jump conditions

3.4.1   Equilibrium equations

To obtain the Euler-Lagrange equations, we must calculate the variation of (3.9) with respect to the variation of both, the position vector $\delta \boldsymbol{X}(x^\alpha)$, and the thickness field $\delta u(x^\alpha)$. Here it will be assumed that both variations are independent from each other. This is possible because both have different physical origins. Thickness variation arises from the excitation of elastic internal degrees of freedom, like the tilt of lipid tails [67] or the different chemical composition of lipid molecules in each domain. On the other hand $\delta \boldsymbol{X}$ is a geometrical elastic variation associated with a macroscopic degree of freedom and it can appear as a consequence of an external deformation.

The variations with respect to $\delta \boldsymbol{X}$ have already been studied in Sec. 2.3.2. Here we only adapt these results to the case of a biphasic elastic membrane with internal degree of freedom. Accordingly, the equations (2.60) and (2.61) corresponding to the

equilibrium of normal and tangential forces respectively, read:

$$-\frac{1}{2}\nabla_s^2\mathcal{G}_H - \overline{\nabla}_s^2\mathcal{G}_{K_G} - \left(2H^2 - K_G\right)\mathcal{G}_H - 2HK_G\mathcal{G}_{K_G} + 2H\mathcal{H}_T - \xi K^{ab}\nabla_a u\nabla_b u = P \; ,$$

$$(3.18a)$$

$$\left(\xi\nabla_s^2 u - \mathcal{G}_u\right)\nabla^a u = 0 \; , \tag{3.18b}$$

where ∇_s^2 is the *Laplace-Beltrami* operator defined on Σ, $\overline{\nabla}_s^2$ is a differential operator acting over scalar fields defined on Σ. It is defined by:

$$\overline{\nabla}_s^2\phi = K\nabla_s^2\phi - K^{ab}\nabla_a\nabla_b\phi \; , \tag{3.19}$$

As in Sec. 2.3.2 we denote $\mathcal{G}_g$ the partial derivatives of the free energy density $\mathcal{H}_\Sigma(u, K, K_G)$ with respect to its arguments:

$$\mathcal{G}_g = \frac{\partial\mathcal{H}_\Sigma(u, H, K_G)}{\partial g} \; , \qquad g(x) \in \{u(x), H(x), K_G(x)\}. \tag{3.20}$$

For the case of the biphasic vesicle we have:

$$\mathcal{G}_H = 2\kappa(2H - H_s) + 2\Lambda u \; , \tag{3.21a}$$

$$\mathcal{G}_{K_G} = \overline{\kappa} + u^2\delta \; , \tag{3.21b}$$

$$\mathcal{G}_u = 2\Lambda H + 2\delta K_G u \; . \tag{3.21c}$$

The equation (3.18a) corresponds to the equilibrium of normal forces on the surfaces and (3.18b) represents the equilibrium of tangential forces acting on each phase of the surface. The E-L equation corresponding to the variations of thickness reads:

$$-\xi\nabla_s^2 u + 2\Lambda H + 2\delta u K_G + B\left(u - a_0\right) = 0 \; . \tag{3.22}$$

Finally, the current Q_u^a associated with the variations δu is given by:

$$Q_u^a = g^{ab}\partial_b u, \tag{3.23}$$

and therefore the equilibrium of forces associated with this variation at the contact line is:

$$\Delta\mathscr{F}_u = \nabla_\perp\left(u_2 - u_1\right) \; , \tag{3.24}$$

where $\nabla_\perp$ is the surface derivative in the direction $\boldsymbol{l}$ (see App. A.2)

3.4.2   Boundary conditions at the interface

At the joint three continuity equations must be satisfied:

$$\boldsymbol{X}_2^{(\pm)}\,|_\mathcal{C} = \boldsymbol{X}_1^{(\pm)}\,|_\mathcal{C} \; , \qquad \boldsymbol{X}_i^{(\pm)} = \boldsymbol{X}_i \pm \eta_i^{(\pm)}(x)\boldsymbol{N}_i \; . \tag{3.25}$$

$$\nabla_a \boldsymbol{X}_2 \mid_{\mathcal{C}} = \nabla_a \boldsymbol{X}_1 \mid_{\mathcal{C}} , \qquad a \in \{1, 2\} , \tag{3.26}$$

The two first relations indicate that the polar head of each monolayer at the hydrophilic surface must match at the contact line. As before, the symbols ($\pm$) represent the outer and inner hydrophilic surfaces, respectively. The third condition is necessary to assure the finiteness of the total free energy, because they depend on the square of the mean curvature, $2H = (\nabla^a \nabla_a \boldsymbol{X}) \cdot \boldsymbol{N}$.

3.4.3   Jump conditions at the interface

The jump conditions that have been obtained in Sec. 2.3.2 can be expressed for the case of the biphasic vesicle. In equilibrium they entail the balance of the forces and torques acting at the contact line $\mathcal{C}$ in different directions. In order to determine the these conditions we need to specialize the expressions given by Eqns. (2.65) along with other useful expressions using the free energies (3.13), (3.14) and (3.15). Thus we have:

$$\Delta \mathcal{G}_K = \Delta \kappa K_{\parallel} + \kappa_2 K_{2\perp} - \kappa_1 K_{1\perp} - \Delta K_o + \Lambda \Delta u , \tag{3.27a}$$

$$\Delta \mathcal{G}_{\mathcal{R}} = \frac{\Delta \overline{\kappa}}{2} + \frac{\delta}{2}(u_2^2 - u_1^2) , \tag{3.27b}$$

$$l^a t^b \Delta S_{ab} = \frac{\xi}{2} \left[\nabla_{\parallel} u_2 \nabla_{\perp} u_2 - \nabla_{\parallel} u_1 \nabla_{\perp} u_1 \right] , \tag{3.27c}$$

$$l^a l^b \Delta S_{ab} = \frac{\xi}{2} \left[(\nabla_{\perp} u_2)^2 - (\nabla_{\perp} u_1)^2 \right] , \tag{3.27d}$$

$$\Delta \mathcal{H}_C = \frac{\xi}{2} \left[(\nabla_{\perp} u_2)^2 - (\nabla_{\perp} u_1)^2 + (\nabla_{\parallel} u_2)^2 - (\nabla_{\parallel} u_1)^2 \right] , \tag{3.28}$$

$$\Delta \mathcal{H}_C = \Delta \lambda + \frac{B}{2} \left[(u_2 - a_{o2})^2 - (u_1 - a_{o1})^2 \right] \tag{3.29}$$

where we have supposed by simplicity that the coefficients (Λ, δ, B and ξ) have the same value in both domains. We have also defined the following quantities: $\Delta \kappa = \kappa_2 - \kappa_1$, $\Delta \lambda = \lambda_2 - \lambda_1$, $\Delta \overline{\kappa} = \overline{\kappa}_2 - \overline{\kappa}_1$, $\Delta u = u_2 - u_1$ and $\Delta K_o = \kappa_2 H_{s2} - \kappa_1 H_{s1}$. Also note that $K_{\parallel} = K_{1\parallel} = K_{2\parallel} = -\kappa_n$ and $K_{\perp\parallel} = K_{2\perp\parallel} = K_{1\perp\parallel} = \tau_g$ *i. e.*, these quantities are continuous across the boundary line. From now on we assume that the line tension is a constant.

With these expressions we can determine the jump conditions at the interface of the biphasic vesicle They are parametrization-free and independent on symmetries. However, we are interested in axisymmetric deformations of this system and therefore by simplicity we will express the conditions in this symmetry.

3.5   The axisymmetric biphasic vesicle

Now focusing on closed axisymmetric biphasic vesicles (see Fig. 3.5), we define cylindrical coordinates (r, φ, z) where z represents the height, φ is the revolution angle and r is the distance between the symmetry axis z and the surface of revolution Σ of the biphasic vesicle. The geometric relation between the coordinate and the tangent angle over the surface is $r'(z) = \cot \psi(r)$, where $r'(z)$ denotes the derivative with respect to z. The coordinates on the surface are $x^1 = \varphi$, $x^2 = z$. A point of the surface is represented by:

$$\boldsymbol{X}(\varphi, z) = r(z)\widehat{\boldsymbol{r}} + z\widehat{\boldsymbol{z}} \,, \tag{3.30}$$

$\widehat{r}$ and $\widehat{z}$ being unit vectors.

In this parametrization, the mean and Gaussian curvatures are only functions of z:

$$H(z) = \frac{1}{2}\left(c_1(z) + c_2(z)\right) = \frac{1 + r'^2 - rr''}{2r\left(1 + r'^2\right)^{3/2}} \,, \tag{3.31}$$

$$K_{\mathrm{G}}(z) = c_1(z)c_2(z) = -\frac{r''}{r\left(1 + r'^2\right)^2} \,. \tag{3.32}$$

3.5.1   Equilibrium equations. Axisymmetric case.

If we insert all the previous expressions in (3.18a) and (3.22) we find two equations for the variables $r(z)$ and $u(z)$:

$$
\begin{aligned}
&2\kappa\nabla_s^2 H + \Lambda\nabla_s^2 u + 2u\delta\overline{\nabla}_s^2 K_{\mathrm{G}} + \kappa(2H + H_s)(2H^2 - 2K_{\mathrm{G}} - HH_s) - P \\
&- 2\lambda H - 2\Lambda u K_{\mathrm{G}} - BH(u - a_o)^2 + \xi K^{ab}\partial_a u\partial_b u - \xi H g^{ab}\partial_a u\partial_b u = 0 \,,
\end{aligned} \tag{3.33}
$$

$$2\Lambda H + B(u - a_o) + 2\delta K_{\mathrm{G}} u + \frac{\xi r'u'}{r\left(1 + r'^2\right)^2} + \frac{\xi r'^3 u'}{r\left(1 + r'^2\right)^2} - \frac{\xi r'u'r''}{\left(1 + r'^2\right)^2} + \frac{\xi u''}{\left(1 + r'^2\right)^2} + \frac{\xi r'^2 u''}{\left(1 + r'^2\right)^2} = 0 \,. \tag{3.34}$$

The former equation represents the classical *shape equation* modified by the presence of a scalar field $u(z)$. The latter is the Euler-Lagrange equation associated to thickness variation. Replacing in (3.33) the expressions of ∇^2, $\overline{\nabla}^2$, K^{ab} and g^{ab} in axisymmetric geometry it is possible to obtain a fourth order equation for the shape variable r, coupled with u. Note that in the case $u = a_o$ the equation (3.33) becomes the classical shape equation.

3.5.2   Boundary conditions at the interface. Axisymmetric case.

As mentioned before, we will consider the schematic configuration depicted in Fig. 3.5. We assume that the liquid ordered phase is located in the region $0 \leq z \leq -p$ and will be labeled with the subscript 1. The liquid disordered domain is located in the region $-p \leq z \leq -D$ (where we suppose that $p, D > 0$) and will be labeled by the subscript
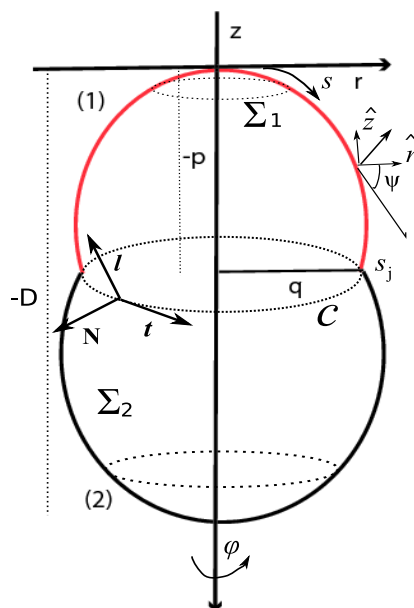
Fig. 3.5: Schematic parametrization of a biphasic vesicle. Before the axisymmetric deformation showed here, we have supposed that the initial configuration was a sphere of radius R_o. Phases labeled with (1) and (2) correspond to a liquid ordered domain (L_o) and liquid disordered domain (L_d), respectively.

2. The interface between them is then located at the point ($z^j = -p, r^j = q$). At this point the arc-length variable s, which is measured with respect to the north pole at domain 1 (from the origin of the coordinate system $\boldsymbol{O}$), is given by s_j.

Using the parametrization, we deduce from Eqn. 3.25 the three following conditions:

$$r_2 \mid_{z=-p} \ = \ r_1 \mid_{z=-p} , \tag{3.35a}$$

$$u_2 \mid_{z=-p} \ = \ u_1 \mid_{z=-p} , \tag{3.35b}$$

$$\partial_z r_2 \mid_{z=-p} \ = \ \partial_z r_1 \mid_{z=-p} . \tag{3.35c}$$

The two first equations represent the continuity of both r and u separately. The latter is a slope continuity equation which is imposed in order to avoid an infinite curvature energy, since the free energy density is proportional to the square of the mean curvature H. Then at this "microscopic" level there is no contact angle.

3.5.3 Jump conditions at the interface. Axisymmetric case

The jump conditions which have been previously obtained in a general way must be specialized to the case of an axisymmetric biphasic vesicle. The condition (2.66) is identically satisfied because $\tau_g = 0$ in the axisymmetric case. The term proportional to the thickness gradient is also zero and the line tension is a constant. The conditions (2.67), (2.68), and (2.69) are the only ones that give us relations between the physical parameters at the interface: The equilibrium of tangential forces in the direction $\boldsymbol{l}$ may be expressed as:

$$
\begin{aligned}
\frac{\kappa_2}{2}[\dot{\psi}(s+\epsilon)] - \frac{\kappa_1}{2}[\dot{\psi}(s-\epsilon)] =& \frac{\kappa_2}{2}\left(\frac{\sin\psi}{q} - H_{s2}\right) - \frac{\kappa_1}{2}\left(\frac{\sin\psi}{q} - H_{s1}\right) \\
&+ \Delta\lambda - \gamma\frac{\cos\psi}{q} + \Lambda\frac{\sin\psi}{q}\Delta u - \frac{\xi}{2}\left[\dot{u}_1 - \dot{u}_2\right] \\
&+ \frac{B}{2}\left[(u_2 - a_{o2})^2 - (u_1 - a_{o1})^2\right] ,
\end{aligned}
\tag{3.36}
$$

where q (see Fig. 3.5) is the radius of the contact line. The equilibrium of normal forces is:

$$
\begin{aligned}
\kappa_2\ddot{\psi}(s+\epsilon) - \kappa_1\ddot{\psi}(s-\epsilon) =& \left[(2\Delta\kappa + \Delta\overline{\kappa})\frac{\cos\psi}{q} + \gamma\right]\frac{\sin\psi}{q} - \frac{\cos\psi}{q}\Delta K_o \\
&+ \Lambda(\dot{u}_2 - \dot{u}_1) + \frac{\sin\psi}{q}\delta(u_2\dot{u}_2 - u_1\dot{u}_1) ,
\end{aligned}
\tag{3.37}
$$

and finally the tangential torques:

$$
\kappa_2\dot{\psi}(s+\epsilon) - \kappa_1\dot{\psi}(s-\epsilon) = -(\Delta\kappa + \Delta\overline{\kappa})\frac{\sin\psi}{q} + \Delta K_o + \Lambda(u_2 - u_1) + \delta\frac{\sin\psi}{q}(u_2^2 - u_1^2) .
\tag{3.38}
$$

This three conditions have been previously obtained in [72] in the case of an axisymmetric biphasic vesicle. However, in this reference they did not include the internal degrees of freedom. The jump condition (3.36), (3.37) and (3.38) are thus more general. Note also that in order to compare these conditions with the conditions obtained in [72] we have expressed them in the arc-length parametrization (see Fig. 3.5). However in this chapter our calculation are performed using the height z as relevant curvilinear coordinate.

Finally, to complete the conditions we add the force related to thickness variations, Eqn. (3.24):

$$
\xi(\dot{u}_2 - \dot{u}_1) = 0 .
\tag{3.39}
$$

3.6 Structure at the joint and boundary layer analysis

The equations (3.33) and (3.34) are difficult to treat exactly, but we can perform an asymptotic analysis assuming that the narrow region around the interface between the domains is comparable with the typical thickness size ($\approx 5[nm]$). In this section we will derive an asymptotic expression for the shape function $r(z)$ and for the thickness $u(z)$ in this region whose extension is very small compared to the size of the vesicle.

This region exhibits a boundary layer that is characterized by a rapid change in mean and Gaussian curvatures. In addition, away from the narrow part of the joint these curvatures become uniform, as the thickness which takes its equilibrium value u_o. At the lowest-order analysis in the outer region we suppose that the shape is given by two spherical cups, joined by a narrow neck.

The analytical method used in this section is standard and can be found in [16]. For instance, it has been used in [41] in the case of a two coexisting fluid phases in (GUV) dominated by surface tension. They perform a boundary layer analysis in the small but non-zero bending stiffness limit when it is compared with the surface tension but without thickness variation at the interface. In another context in [17] a boundary layer analysis has been performed in order to derive an analytical expression for the shape of a closed vesicle induced by the presence of an inclusion.

We introduce now dimensionless parameters necessary for our asymptotic analysis. The width of the joint is given by the interplay between slope correlations and the spring energy associated with the thickness variation. From Eqn. (3.11) the size is of order $l_j = \sqrt{\xi/B}$. For distances large compared to l_j the width of the bilayer does not vary anymore. We define our small dimensionless parameter as:

$$\varepsilon = \frac{1}{R_o}\sqrt{\frac{\xi}{B}}\,, \tag{3.40}$$

where R_o is the radius of the initial spherical vesicle. Hereafter we choose R_o as the length unit. This choice gives $\varepsilon \simeq 10^{-3}$ and therefore we can perform a regular perturbation expansion in the small parameter ε.

We must compare the order of magnitude of the physical parameters with respect to ε. Since we assume that the joint length scale is of the order of thickness, $B = \nu/\varepsilon^2$ and $a_{oi} = \varepsilon a_i$. Moreover, assuming that the mechanical energy Eqn. (3.12) is equivalent to the chemical one, Eqn. (3.11) gives the scaling: $\Lambda = \chi/\varepsilon$.

For the sake of simplicity we assume that $B_1 = B_2 \equiv B$, $\xi_1 = \xi_2 \equiv \xi$, $\Lambda_1 = \Lambda_2 \equiv \Lambda$, and we keep $\kappa_1 \neq \kappa_2$, $\overline{\kappa}_1 \neq \overline{\kappa}_2$, $H_{s1} \neq H_{s2}$ $a_1 \neq a_2$, and $\lambda_1 \neq \lambda_2$.

3.6.1 Outer layer: Long-scale behaviour

By definition the outer layer is the region away from the interface. Here the membrane has constant mean curvature H_o . Then we can perform a regular perturbation expansion of the variables $r(z)$, $u(z)$, $H(z)$ and $K(z)$ in the small parameter ε. Hereafter all

the calculations will be carried out in the (L_o) phase, which has been denoted with the subscript 1. For the sake of simplicity it will be suppressed. Generalization to the (L_d) domain is straightforward. We have:

$$
\begin{align}
r(z) &= r^{(0)}(z) + \varepsilon r^{(1)}(z) + \varepsilon^2 r^{(2)}(z) + \dots , \tag{3.41a} \\
u(z) &= \varepsilon u^{(1)}(z) + \varepsilon^2 u^{(2)}(z) + \dots , \tag{3.41b} \\
H(z) &= H^{(0)}(z) + \varepsilon H^{(1)}(z) + \varepsilon^2 H^{(2)}(z) + \dots , \tag{3.41c} \\
K_G(z) &= K_G{}^{(0)}(z) + \varepsilon K_G{}^{(1)}(z) + \varepsilon^2 K_G{}^{(2)}(z) + \dots , \tag{3.41d} \\
\lambda &= \lambda^{(0)} + \varepsilon \lambda^{(1)} + \varepsilon^2 \lambda^{(2)} + \dots . \tag{3.41e}
\end{align}
$$

Hereafter, the superscript (i) denotes the order of the expansion and the subscript appearing in functions or physical parameters (1 and 2) denotes the different domains. At the lowest order the constraint of constant curvature is satisfied by the spherical cup solution. The north pole is chosen as the origin of the coordinate systems ($z = 0$, $r = 0$, see Fig. (3.5)). Then we have:

$$
r^{(0)}(z) = \sqrt{R_1^2 - (z + R_1)^2} , \tag{3.42}
$$

$$
H^{(0)}(z) = \frac{1}{R_1} , \qquad K_G{}^{(0)}(z) = \frac{1}{R_1^2} , \tag{3.43}
$$

at order ε, the mean curvature remains constant $H^{(1)}(z) = \Gamma_1$ which gives an equation for $r^{(1)}(z)$:

$$
-\frac{4z^2 R_1 \left(3r'^{(1)} + zr''^{(1)}\right) + z^3 \left(4r'^{(1)} + zr''^{(1)}\right) + R_1^2 \left(r^{(1)} + 4z\left(2r'^{(1)} + zr''^{(1)}\right)\right)}{2R_1^3\sqrt{-z\left(z + 2R_1\right)}} = \Gamma_1 , \tag{3.44}
$$

with Γ_1 an undetermined constant. By the choice of the origin of the coordinate system we have $-2R_1 \leq z \leq 0$. The previous relation can be solved to obtain:

$$
r^{(1)}(z) = \frac{c_1\left(z + R_1\right)}{\sqrt{z}R_1\sqrt{z + 2R_1}} + \frac{c_2\left(-1 + \frac{(-\log(-z) + \log(z + 2R_1))(z + R_1)}{2R_1}\right)}{\sqrt{z}\sqrt{z + 2R_1}} + \frac{zR_1^2\Gamma_1}{\sqrt{-z\left(z + 2R_1\right)}} . \tag{3.45}
$$

To satisfy the boundary conditions at the north pole $r(0) = 0$ and $r'(0) \to \infty$, it is necessary to set $c_1 = 0$ and $c_2 = 0$. Finally, the solutions for the shape function and for the thickness at first order ε are given by:

$$
r^{(1)}(z) = \frac{zR_1^2\Gamma_1}{\sqrt{-z\left(z + 2R_1\right)}} , \qquad u^{(1)}(z) = \frac{-2\chi + a_1\nu R_1}{\nu R_1} . \tag{3.46}
$$

The remaining parameters must satisfy some relations at order ε. For the pressure

and the mean curvature Γ_1 we have:

$$\Gamma_1 \;=\; \frac{2\left(-\nu^2 \lambda^{(1)} R_1^4\right)}{\nu^2 R_1^4 \left(R_1 \kappa_1 H_{\mathrm{s}1}^2 - 4\kappa_1 H_{\mathrm{s}1} - 4a_1 \chi + 2R_1 \lambda^{(0)}\right)} \;, \tag{3.47a}$$

where $H_{\mathrm{s}1}$ is the spontaneous curvature of the domain 1, $\lambda^{(0)}$ and $\lambda^{(1)}$ are the zero and first order of the surface tension expansion, defined by Eqn. (3.41e).

3.6.2 Inner layer: Detailed structure of the interface

At the joint we assume that the distance from the symmetry axis is of order one, that is $r = q$. It means that we do not consider the ultimate stages of budding and fission, when this distance goes to zero. The fission period requires new physical interactions between lipids and is not considered here. At the joint, both curvatures change rapidly. We scale variable and coordinates by ε in the following way:

$$z = -p + \varepsilon x \;, \qquad r(z) = q + \varepsilon \zeta(x) \;, \qquad u(z) = \varepsilon \eta(x) \;, \tag{3.48}$$

which gives for the curvatures:

$$H(z) = \frac{1}{\varepsilon} h(x) \;, \qquad K_{\mathrm{G}}(z) = \frac{1}{\varepsilon} k(x) \;, \tag{3.49}$$

Obviously the curvatures are large. Each new variable admits a regular perturbation expansion in the small parameter ε given by:

$$\begin{aligned}
\zeta(x) &= \zeta^{(0)}(x) + \varepsilon \zeta^{(1)}(x) + \varepsilon^2 \zeta^{(2)}(x) + \dots \;, & \text{(3.50a)} \\
h(x) &= h^{(0)}(x) + \varepsilon h^{(1)}(x) + \varepsilon^2 h^{(2)}(x) + \dots \;, & \text{(3.50b)} \\
k(x) &= k^{(0)}(x) + \varepsilon k^{(1)}(x) + \varepsilon^2 k^{(2)}(x) + \dots \;, & \text{(3.50c)} \\
\eta(x) &= \eta^{(0)}(x) + \varepsilon \eta^{(1)}(x) + \varepsilon^2 \eta^{(2)}(x) + \dots \;, & \text{(3.50d)} \\
\psi(x) &= \psi^{(0)}(x) + \varepsilon \psi^{(1)}(x) + \varepsilon^2 \psi^{(2)}(x) + \dots \;, & \text{(3.50e)}
\end{aligned}$$

By definition the relation between the rescaled mean curvature h and the rescaled shape function ζ is:

$$h^{(0)}(x) = -\frac{\zeta''^{(0)}}{2\left(1 + \zeta'^{(0)2}\right)^{3/2}} \;, \tag{3.51}$$

which implies Eqn. (3.50e). Once the perturbation expansions are introduced in Eqn. (3.33) and Eqn. (3.34), we find relations which need to be satisfied at each order. At $\mathcal{O}(\varepsilon)$:

$$\zeta^{(0)}(x) = d_1 + b_1 x \;, \qquad h^{(0)}(x) = 0 \;, \qquad k^{(0)}(x) = 0 \;. \tag{3.52}$$

At the next order ε we obtain a pair of coupled equations for the variables $h^{(1)}$ et $\eta^{(0)}$

$$\eta''^{(0)}(x) + l_1 h''^{(1)}(x) + l_2 \eta^{(0)}(x) + l_3 = 0 \;, \tag{3.53a}$$

$$h^{''(1)}(x) - l_o \eta^{''(0)}(x) = 0 \ , \tag{3.53b}$$

where all the coefficients l_k depend on the physical parameters characterizing of each domain like bending stiffness modulus and coupling constants.

They also depend on the unknown constant b_1 which will be obtained by the analysis. The solutions of the previous system are trivial:

$$\eta^{(o)}(x) \ = \ e^{-x\sqrt{\gamma_1}}C_5 + e^{x\sqrt{\gamma_1}}C_6 + xC_7 + C_8 \ , \tag{3.54a}$$

$$h^{(1)}(x) \ = \ e^{-x\sqrt{\gamma_1}}C_1 + e^{x\sqrt{\gamma_1}}C_2 + xC_3 + C_4 \ , \tag{3.54b}$$

$$\gamma_1 \ = \ \frac{(b_1^2 + 1)(\nu\kappa_1 - \chi^2)}{\xi\kappa_1} \ , \tag{3.54c}$$

where the constants $\{C_i\}$ are integration constants that we need to determine. The expansion of the mean curvature at $\mathcal{O}(\varepsilon)$ allows us to calculate the rescaled shape function $\zeta^{(1)}(x)$ at order ε. It reads:

$$\zeta^{(1)}(x) = V_1 + W_1 x + \alpha_1 x^2 + \beta_1 x^3 - \frac{2(b_1^2 + 1)^{3/2}}{\gamma_1}(C_1 e^{x\sqrt{\gamma_1}} + C_2 e^{-x\sqrt{\gamma_1}}) \ , \tag{3.55}$$

where the coefficients α_1 and β_1 are given by:

$$\alpha_1 \ = \ -\frac{(b_1^2 + 1)\left(2q\sqrt{b_1^2 + 1}C_4 - 1\right)}{2q} \ , \tag{3.56a}$$

$$\beta_1 \ = \ -\frac{1}{3}(1 + b_1^2)^{\frac{3}{2}}C_3 = 0 \ . \tag{3.56b}$$

If we consider the domain (1), we must choose: $C_2 = 0$, $C_3 = 0$, $C_6 = 0$ and $C_7 = 0$ for reasons of convergence. The matching between the inner and outer layers will provide the constants V_1, W_1 and C_1, but before we treat the second domain.

3.6.3   Inner and outer layer for the domain 2

Following the same procedure we deduce the inner and outer layer in the liquid disordered domain 2. The outer layer is given by:

$$r_2(z) \ = \ \sqrt{R_2^2 - (D + z - R_2)^2} - \varepsilon\left(\frac{(D + z)R_2^2\Gamma_2}{\sqrt{(-D - z)(D + z - 2R_2)}}\right) + \dots \tag{3.57a}$$

$$u_2(z) \ = \ \varepsilon\left(\frac{-2\chi + \nu a_2 R_2}{\nu R_2}\right) + \dots \tag{3.57b}$$

where D is the distance from the origin $\mathbf{O}$ of the coordinate system to the south pole of the spherical cup solution (see Fig.(3.5)). At order zero the spherical cup has a different radius R_2. The constant Γ_2 corresponds to the value of the mean curvature

at order ε, which is related to the coefficients of the surface tension expansion in the domain 2 by the following relation:

$$\Gamma_2 \;=\; \frac{-2\left(\nu^2 \lambda_2^{(1)} R_2^4\right)}{\nu^2 R_2^4 \left(R_2 \kappa_2 H_{s2}^2 - 4\kappa_2 H_{s2} - 4\chi a_2 + 2R_2 \lambda_2^{(0)}\right)} \;. \tag{3.58}$$

The inner layer solution at the order zero in ε is given by the following terms:

$$\zeta_2^{(0)}(x) = d_2 + b_2 x \;, \qquad h_2^{(0)}(x) = 0 \;, \qquad k_2^{(0)}(x) = 0 \;, \tag{3.59}$$

and at the order ε we have:

$$h_2^{(1)}(x) \;=\; e^{x\sqrt{\gamma_2}} D_2 + D_4 \;, \tag{3.60a}$$

$$\eta_2^{(0)}(x) \;=\; e^{x\sqrt{\gamma_2}} D_6 + D_8 \;, \tag{3.60b}$$

$$\gamma_2 \;=\; \frac{\left(b_2^2 + 1\right)\left(\nu\kappa_2 - \chi^2\right)}{\xi\kappa_2} \;, \tag{3.60c}$$

here, like in the case of the domain 1, we have canceled some coefficients for reasons of convergence. Finally at the order ε^2 we derive.

$$\zeta_2^{(1)} = V_2 + W_2 x + \alpha_2 x^2 + \beta_2 x^3 - \frac{2\left(b_2^2 + 1\right)^{3/2}}{\gamma_2} D_2 e^{-x\sqrt{\gamma_2}} \;. \tag{3.61}$$

We need also to determinate V_2 and W_2. So far, all the solutions involve integration constants that have to be determined. To do this we use the equations obtained from asymptotic matching of outer and inner solution and the jump conditions at the interface and the boundary conditions.

As the pressure is homogeneous in each domain, the mechanical equilibrium imposes the equality of P_1 and P_2, which gives:

$$\frac{-R_1\kappa_1 H_{s1}^2 + 2\kappa_1 H_{s1} + 2\chi a_1 - 2R_1 \lambda_1^{(0)}}{R_1^2} = \frac{-R_2\kappa_2 H_{s2}^2 + 2\kappa_2 H_{s2} + 2\chi a_2 - 2R_2 \lambda_2^{(0)}}{R_2^2} \;. \tag{3.62}$$

As a consequence we obtain a relation between $\lambda_1^{(0)}$ and $\lambda_2^{(0)}$, *i. e.* the surface tensions at order zero in ε as function of the physical parameters.

3.6.4 Asymptotic matching for the boundary layer

In the previous sections we have determined solutions valid in different parts of the surface; the boundary layer (the region around the interface between the domains) and away from the boundary layer. These solutions must agree in an intermediate region [16]. Therefore it is useful to find their asymptotic behaviour.

In the inner region at the interface, we let x go to $\to \infty$ in domain (1) and $x \to -\infty$

in domain 2 and we keep only calculations of $\mathcal{O}(0)$, $\mathcal{O}(\varepsilon)$ and $\mathcal{O}(\varepsilon x)$. In the outer layer we substitute $z = -p + \varepsilon x$ in the solutions and we expand the solutions in powers of ε. Finally the corresponding terms resulting at order $\mathcal{O}(0)$, $\mathcal{O}(\varepsilon)$ and $\mathcal{O}(\varepsilon x)$ are balanced after taking their respective limits. Note that the matching of the thickness function at orders zero and ε is trivial.

The asymptotic matching of the mean curvature H between both region is immediately satisfied at order ε^{-1}. At order zero it allows us to derive:

$$C_4 = \frac{1}{R_1} \,, \qquad D_4 = \frac{1}{R_2} \,. \tag{3.63}$$

At order ε it gives the following relations:

$$q_1 \;=\; \sqrt{-p\left(p - 2R_1\right)} \,, \tag{3.64a}$$

$$q_2 \;=\; \sqrt{\left(p - D\right)\left(D - p - 2R_2\right)} \,, \tag{3.64b}$$

and finally at order εx it reads:

$$d_1 \;=\; -\frac{pR_1^2\Gamma_1}{q_1} \,, \tag{3.65a}$$

$$d_2 \;=\; -\frac{(D - p)R_2^2\Gamma_2}{q_2} \,, \tag{3.65b}$$

with p and D the distances defined in Fig.(3.5) and Γ_i the constant mean curvatures at order ε at each domain.

In summary, at this stage we have calculated solutions for the shape function, the mean curvature and the Gaussian curvature up to order ε and the thickness function up to order ε^2 in the inner and outer layers for both the (L_o) and (L_d) domains. By means of an asymptotic matching analysis we have related some known physical parameters like p, D, R_i with some of the unknown integration constants which appear during the calculation. So far we have not determined all these constants because we have not considered yet the mechanical equilibrium, which provides the jump condition at the interface between the domains. In the next section we will see how the usual jump conditions at the interface, which has been established in [72] and that are valid for constant thickness vesicles, are modified by the joint structure.

3.6.5   Jump conditions at the interface up to order ε

Forces and torques acting at the interface which have been previously calculated in Sec. 3.5.3 must be equilibrated at any order. The balance of tangential force in the direction $\boldsymbol{l}$ at order $\mathcal{O}(1)$ gives us:

$$A_1 + A_2C_1^2 = B_1 + B_2D_2^2 \,. \tag{3.66}$$

The coefficients $\{A_i, B_i\}$ are complicated functions of the physical parameters of the

problem. At lowest order the tangential force in the direction of $\boldsymbol{l}$ can not be calculated, because it depends on unknown functions like $\zeta_i^{(2)}$ or $\eta_i^{(1)}$. There is no contribution of the normal force at order $\mathcal{O}(\varepsilon^{-1})$ and at order one it cannot be determined.

The balance of the force associated with the thickness variation at order $\mathcal{O}(\varepsilon^2)$ is given by:

$$A_3 C_1 = B_3 D_2 \ . \tag{3.67}$$

The tangential torque in the direction of $\boldsymbol{t}$ at order zero reads:

$$A_4 = B_4 \ . \tag{3.68}$$

The balance of the normal component of the torque at order zero is:

$$-\frac{2\chi^2}{\nu R_2^2} + \frac{a_2\chi}{R_2} - \frac{H_{s2}\kappa_2}{R_2} + \frac{2\kappa_2}{R_2^2} + \frac{\overline{\kappa}_2}{R_2^2} = -\frac{2\chi^2}{\nu R_1^2} + \frac{a_1\chi}{R_1} - \frac{H_{s1}\kappa_1}{R_1} + \frac{2\kappa_1}{R_1^2} + \frac{\overline{\kappa}_1}{R_1^2} \ . \tag{3.69}$$

Note that in this case the coupling with thickness introduces a modification in the usual expression obtained in [72]. This change is due to the terms in χ and a_i. As a result the components of the moment tensor in each domain will be modified. Finally balancing the moment at order ε we find a relation between C_1 and D_2.

$$\frac{q_1^2 \sqrt{\gamma_1}\kappa_1}{R_1} C_1 = -\frac{q_2^2 \sqrt{\gamma_2}\kappa_2}{R_2} D_2 \ , \tag{3.70}$$

3.6.6   Boundary conditions at the interface up to order ε^2

The boundary conditions discussed in Sec. 3.6.1 must be valid at each order in ε. At the order zero we have:

$$q_1 = q_2 \equiv q \ , \tag{3.71}$$

where q is a known parameter (see Fig.(3.5)). The condition (3.35a) at order ε allows us to deduce:

$$d_1 = d_2 \ , \tag{3.72a}$$
$$b_1 = b_2 \ , \tag{3.72b}$$

At this order neither a contact angle nor a height mismatch exist. Finally at order ε^2:

$$V_1 - \frac{2C_1 R_1^3}{\gamma_1 q^3} = V_2 - \frac{2D_2 R_2^3}{\gamma_2 q^3} \ , \tag{3.73a}$$

$$-\frac{2\chi}{\nu R_1} + a_1 - \frac{2C_1\kappa_1}{\chi} = -\frac{2\chi}{\nu R_2} + a_2 - \frac{2D_2\kappa_2}{\chi} \ , \tag{3.73b}$$

$$\frac{2C_1 R_1^3}{\sqrt{\gamma_1} q^3} + W_1 = \frac{2D_2 R_2^3}{\sqrt{\gamma_2} q^3} + W_2 \ . \tag{3.73c}$$

Now, using (3.73b) and (3.70) it is possible to calculate the integration constants C_1 and D_2 as functions of all the known physical parameters, which gives:

$$C_1 = \frac{\chi q_2^2 \left(R_1 \left(2\chi + \nu \left(a_1 - a_2\right) R_2\right) - 2\chi R_2\right) \sqrt{\gamma_2}}{2\nu R_2 \left(R_2 \sqrt{\gamma_1} q_1^2 + q_2^2 R_1 \sqrt{\gamma_2}\right) \kappa_1} \ , \tag{3.74}$$

$$D_2 = \frac{\chi \left(2\chi R_2 + R_1 \left(\nu \left(a_2 - a_1\right) R_2 - 2\chi\right)\right) \sqrt{\gamma_1}}{2\nu R_1 \left(R_2 \sqrt{\gamma_1} + R_1 \sqrt{\gamma_2}\right) \kappa_2} \ . \tag{3.75}$$

So far we have been able to determine the integration constants $\{b_i, d_i\}$ as a function of the geometric parameters of the problem, like p, D, Q, R_i (see Fig.(3.5)). This allows us to express the coefficients $\{\alpha_i, \gamma_i\}$ which appear in the solutions of the inner region. The rest of the relations are used to find the value of the remaining unknown parameters, like Γ_i, the constant mean curvatures of each domain at order ε.

3.7   Contact angle and height mismatch

With all the constants at hand it is possible to determine a contact angle and a height mismatch if we extrapolate the large-scale solutions up to the interface $\mathcal{C}$. The height mismatch defined as $h = V_1 - V_2$ is found using Eqn.(3.73a) and Eqn.(3.73c). We note that h is non-zero at order ε^2, thus it is a small parameter.

Solving for the height mismatch we find:

$$h = -\frac{2 \left(D_2 R_2^3 \gamma_1 - C_1 R_1^3 \gamma_2\right)}{q^3 \gamma_1 \gamma_2} \ . \tag{3.76}$$

The polar hydrophilic heads that composes the external and the internal surfaces of each monolayer ($\pm$, respectively) must be matched at the interface. This thickness matching induces a *non-zero contact angle* expressed as the difference of the slope in the extrapolated large-scale solutions at the interface. In our notation, this slope difference is $\theta_d = W_1 - V_1$. It is given by:

$$\theta_d = \frac{\chi\{R_1 \left(2\chi + \nu a_1 R_2 - \nu a_2 R_2\right) - 2\chi R_2\} \left(q_1^5 R_2^4 \gamma_1 \kappa_1 - q_2^5 R_1^4 \gamma_2 \kappa_2\right)}{\nu q_1^3 q_2^3 R_1 R_2 \sqrt{\gamma_1} \left(R_2 \sqrt{\gamma_1} q_1^2 + q_2^2 R_1 \sqrt{\gamma_2}\right) \sqrt{\gamma_2} \kappa_1 \kappa_2} \ . \tag{3.77}$$

This angle depends on the values of both mean curvatures at large-scale $H_i^{(0)}$. Note that θ_d is proportional to χ, the scaled coupling constant between thickness and mean curvature. If this constant is zero there is no contact angle. It is noteworthy that for $a_1 = a_2$ the contact angle is not zero, because curvatures at large scale in the outer layer are constant and non-zero and therefore $C_1 \neq 0$ in this case. The thickness equilibrium value is modified by this constant. In order to have a zero contact angle the equilibrium

thickness u_{oi} must be shifted with respect to a_i:

$$u_{oi} = \frac{-2\chi + a_i \nu R_i}{\nu R_i} \, . \tag{3.78}$$

Then, if $u_{o1} = u_{o2}$ the contact angle is zero because $C_1 = 0$ and $D_2 = 0$. If we take typical values for the membrane parameters (discussed for example in [54]) we obtain $\theta_d \sim 15.8\,°$.

3.7.1 Energy of the equilibrium configuration up to order ε

So far, we have solutions of the problem at each order in ε which are valid in different regions. We need to form a *composite solution,* uniformly valid in the entire vesicle. To obtain the composite solution we use the following relation, explained in [16]:

$$\text{Composite Solution} = \text{Inner solution} + \text{Outer solution} - \text{Matching} \tag{3.79}$$

This solution must be replaced in the total free energy (3.8) and its corrections at each order of ε must be calculated. Remember that we are able to obtain all the integration constants up to order ε for both, the thickness and the shape function. Solutions at order ε^2 are only known for the thickness variable. Corrections of the free energy induced by the thickness variations are better understood subtracting the entire composite solution and the *macroscopic solution* (that is the solution omitting the thickness contribution). This comparison at each order leaves an effective term representing a *line tension energy.* Taking the reference line tension $\gamma_r = 0$ and replacing the composite solution in the total free energy up to order ε, it may be expressed in the following form:

$$\mathcal{F}_T = \mathcal{F}_o + \varepsilon\gamma_o(\theta) \, , \tag{3.80}$$

where $\mathcal{F}_o$ is the total free energy calculated only using the macroscopic part of the solution, and γ_o is the effective line tension:

$$\gamma_o(\theta) = \frac{R_1 \left(R_1 \left(2\chi + \nu \left(a_1 - a_2 \right) R_2 \right) - 2\chi R_2 \right)^2 \gamma_2 q_2^4}{4\nu R_2^2 \sqrt{\gamma_1} \left(R_2 \sqrt{\gamma_1} q_1^2 + q_2^2 R_1 \sqrt{\gamma_2} \right)^2} + \frac{\nu D_2^2 R_2 \kappa_2^2}{\chi^2 \sqrt{\gamma_2}} \, , \tag{3.81}$$

which is finally expressed as a function of the *contact angle*:

$$\gamma_o(\theta) = A + B\theta + C\theta^2 \, , \tag{3.82}$$

where the coefficients A, B, and C depend on the physical parameters of the problem:

$$A = \frac{\nu C_1^2 \left(R_1 R_2^5 \sqrt{\gamma_1} \kappa_1^2 q_1^6 + q_2^6 R_1^6 \sqrt{\gamma_2} \kappa_2^2 \right)}{\chi^2 q_1^6 R_2^5 \gamma_1} \, , \tag{3.83}$$

$$B = \frac{\nu C_1 q_2^6 R_1^3 \sqrt{\gamma_2} \kappa_2^2}{\chi^2 q_1^3 R_2^5 \sqrt{\gamma_1}} \, , \tag{3.84}$$

$$C = \frac{\nu q_2^6 \sqrt{\gamma_2} \kappa_2^2}{4 \chi^2 R_2^5} \ . \tag{3.85}$$

Then at order ε the line tension is a parabolic function of the contact angle. This behavior is depicted in Fig.(3.6), for typical values used in experiments [14, 15] which have been also discussed in [54].
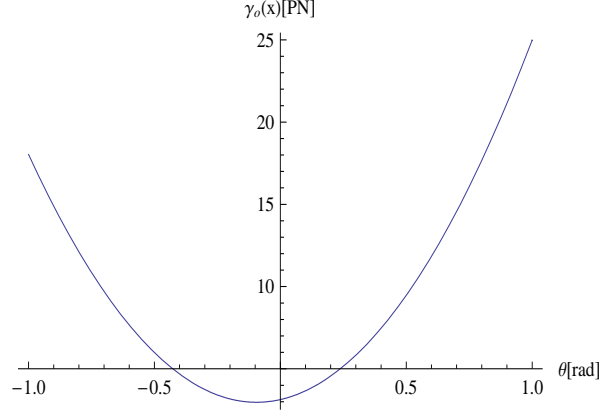

Fig. 3.6: Effective line tension γ_o as a function of the contact angle θ for typical values: $\kappa_2 = 20 K_B T$, $\kappa_1 = 5\kappa_2$, $H_{s1} = (50nm)^{-1}$, $H_{s2} = 0.003 H_{s1}$, $\nu = 4 \times 10^{15} Jm^{-4}$, $a_1 = 7nm$, $a_2 = 5nm$, $\xi = 10^{-1} Jm^{-2}$, $\chi = 1, 2 \times 10^{-2} Jm^{-2}$

3.7.2   Discussion

Here we have shown that the short-scale degrees of freedom excited at the interface between domains that compose a biphasic membrane give rise to a discontinuity in the membrane slope at the joint. These degrees of freedom have been represented by means of an elastic structural thickness variable. The discontinuity is taken into account introducing an effective line tension γ_o, that is a quadratic function of this contact angle. Since the term $\mathcal{F}_o$ in equation (3.80) is given (at each order in ε) only by the macroscopic part of the elastic model we state that the microscopic thickness mismatch coupled to the mean curvature keeps the large scale description of the bilayer represented by the usual Helfrich model of elasticity with a modification only at the interface by an anisotropic line tension energy which depends on the boundary conditions.

A trivial analysis can be performed. Note that the value θ^* for which $\gamma_o(\theta^*) = \gamma_{min}$ is different from zero. Also, if the angle θ is zero, the value of the line tension γ_o is different to zero. When $u_{o1} = u_{o2}$ the line tension is proportional to the square of the contact angle, because $A = 0$ and $B = 0$ in this approximation. If we fix the value of the contact angle, γ_o is proportional to the square of the thickness difference (the "renormalized" thickness difference) because the integration constant C_1 is proportional to $\Delta = u_{o1} - u_{o2}$.

As a consequence a modification in the boundary conditions is important for the

structure of the junction and may be responsible for mechanical instabilities as it has been shown for tubes [6] for example.

Finally note that the solutions at order ε, given by the functions $\zeta^{(1)}$ and $\eta^{(0)}$ (see Eqns. (3.54) and (3.55)) have the same analytical structure as those that have been obtained in [54] in the case of two membrane domains with high spontaneous curvature. This is not surprising since our analysis of the joint structure is local. Moreover we have solved the model that includes the curvature properties of a closed biphasic vesicle and then there is not need to introduce artificial boundary forces and torques in the bilayer (because the vesicle is self-sustained and has not boundaries). In this sense our calculation is more general and also allows us to incorporate relevant physical parameters which have been neglected in [54] as Gaussian stiffness and surface tension. Therefore, our system is more suitable to be related with experimental situations carried out in axisymmetric biphasic vesicles [15].

Another interesting effect which has been omitted in [54] is the adsorption of dilute impurities which normally accumulate in the joint. As we will see in the next section they enhance the local spontaneous curvature of the bilayer and thus the local coupling constant modifying the contact angle structure and the line tension between domains.

3.8 Adsorption of impurities and proteins

Addition of impurities or proteins in vesicles has been widely studied experimentally [124], theoretically [4] and numerically [10] for homogeneous and inhomogeneous vesicles. For example, in [4] the first stages of the elastic instability produced by the budding process in an inhomogeneous vesicle are explained using a linear stability analysis. The driving force of vesicle deformation may come from the adsorption of molecules. However, their analysis refers to a bulk effect, assuming that impurities are distributed everywhere on the membrane. Proteins have the preference to accumulate in regions of high curvature, like the interface between domains in separation, in order to relax some of the microscopic distortions.

Here we want to study the inclusion of proteins with concentration $\phi(x^a)$ in the joint region. We guess that they have a direct influence on the line tension, yet modified by the thickness matching at the joint, as it has been shown before. Proteins are adsorbed in both phases, but with a different affinity. They are localized in the outer surface (+) and we assume that they do not cross the bilayer, as is more or less established for PLA_2 proteins [124].

The conical shape of proteins modifies the geometry of the bilayer and induces a local curvature in the membrane. This local distortion can be represented by a density energy that couples the local concentration and the local mean curvature [86]:

$$f_{int} = \Lambda_c \phi(x)\overline{H}(x) , \qquad (3.86)$$

where the sign of the coupling coefficient Λ_c is given by the shape of the adsorbed proteins. The function $\overline{H}(x^a)$ is the mean curvature of the external surface (which

is physically represented by the hydrophilic polar heads of the lipid molecules). This curvature and the mean curvature of the neutral surface $H(x^a)$ are related by the following expression:

$$\overline{H}(x) = H(x) + \frac{1}{2}\nabla_s^2 u + (2H^2 - K_\mathrm{G})u + \ldots \tag{3.87}$$

This relation has been calculated up to dominant order in u, ϕ and H. Replacing this expression in the coupling free energy term (3.86) we obtain:

$$f_{int} = f_4^{(i)} + f_5^{(i)} + f_6^{(i)} \ , \tag{3.88}$$

where each term depends on the geometric properties of the neutral surface:

$$f_4^{(i)} = \frac{1}{2}\Lambda_{ci}\phi_i(x)\nabla_s^2 u_i \ , \tag{3.89a}$$

$$f_5^{(i)} = \mu_i\phi_i + \frac{1}{2}\alpha_i(\phi_i - \phi_o i)^2 + \frac{1}{2}\beta_i(\nabla\phi_i)^2 \ , \tag{3.89b}$$

$$f_6^{(i)} = \Lambda_{ci}\phi_i H_i \ , \tag{3.89c}$$

where the subscript $(i = 1, 2)$ represents each domain. The term $f_5^{(i)}$ is a Landau type model that represents the energy needed to adsorb proteins on the surface nearby the optimal equilibrium concentration ϕ_{oi}. Such a model has been employed in [4]. It implies that there is an optimal concentration of proteins in each phase and an energetic cost to pay for any change or inhomogeneity in the repartition measured by $\nabla_a\phi$. The constant μ_i is the chemical potential of the proteins, which can be interpreted as a Lagrange multiplier fixing the number of molecules in each phase. This model assumes that the proteins do not interact chemically with the lipids of the membrane. Consequently, the adsorption process is a pure physical effect in our model. The new terms must be added to (3.8) in order to obtain, by means of a variational process, a set of three coupled equations corresponding to the variations of $\delta \boldsymbol{X}(x)$, $\delta u(x)$, $\delta\phi(x)$. They are given respectively by:

$$\frac{1}{2}\nabla_s^2\mathcal{G}_H + \overline{\nabla}_s^2\mathcal{G}_{K_\mathrm{G}} + (2H^2 - K_\mathrm{G})\mathcal{G}_H + 2HK\mathcal{G}_{K_\mathrm{G}} - 2H\mathcal{H}_\mathrm{T}+$$
$$+\xi K^{ab}\nabla_a u\nabla_b u + \beta_i K^{ab}\nabla_a\phi\nabla_b\phi + \Lambda_{ci}\phi K^{ab}\nabla_a\nabla_\beta u = P \ , \tag{3.90a}$$

$$\xi\nabla_s^2 u + \frac{1}{2}\Lambda_{ci}\nabla_s^2\phi + B(u - a_{oi}) + 2\Lambda H + 2\delta u K_\mathrm{G} = 0 \ , \tag{3.90b}$$

$$-\beta_i\nabla_s^2\phi + \mu_i + \alpha_i(\phi - \phi_{oi}) + \frac{1}{2}\Lambda_{ci}\nabla_s^2 u + \Lambda_{ci}H = 0 \ . \tag{3.90c}$$

The three previous equations will allow us to determine if the adsorption of proteins or another type of impurities (reflected in the change of the coupling constant Λ_{ci}) is able to change the contact angle (and therefore the effective line tension) and finally to enable

the instability of domain separation, increasing the value of γ_o. Obviously this analysis is very similar to the previous one and therefore we will not repeat all the details. We again perform a boundary layer analysis in the narrow region of the interface. Regular expansions will be performed using the same parameter ε. It is helpful to scale the physical parameters associated with protein concentration adsorption and we choose:

$$\mu_i = \frac{m_i}{\varepsilon} , \qquad \phi_{oi} = \varepsilon\varphi_i , \tag{3.91}$$

$$\alpha_i = \frac{\rho_i}{\varepsilon^2} , \qquad \Lambda_{c_1} = \chi_a , \qquad \Lambda_{c_2} = \chi_b . \tag{3.92}$$

As before, we write the solutions in the liquid ordered domain (1) and then we generalize the solution to domain (2). At large scales, the outer layer solutions for the variables $r(z)$ and $u(z)$ are the same that have been calculated for the case without impurities. Here we only give the solution for the concentration $\phi(z)$:

$$\phi_1(z) = \varepsilon\left(\frac{\rho_1\varphi_1 - m_1}{\rho_1}\right) + \mathcal{O}(\varepsilon^2) , \tag{3.93}$$

which is a constant at order ε. The inner layer solutions for the shape function and the thickness are again the same as before if the same scaling is performed. For the concentration we consider the scaling $\phi(z) = \varepsilon\Phi(x)$. At order zero we must solve the following three equations for the variables $h_1^{(1)}$, $\eta_1^{(0)}$ and $\Phi_1^{(0)}$ respectively:

$$2\kappa_1 h_1^{(1)''}(x) + \chi\eta_1^{(0)''}(x) = 0 , \tag{3.94a}$$

$$-\nu a_1 + 2\chi h_1^{(1)}(x) + \nu\eta_1^{(0)}(x) - \frac{\xi\eta_1^{(0)''}(x)}{b_1^2 + 1} + \frac{\chi_a\Phi_1^{(0)''}(x)}{2\left(b_1^2 + 1\right)} = 0 , \tag{3.94b}$$

$$m_1 - \rho_1\varphi_1 + \rho_1\Phi_1^{(0)}(x) + \frac{\chi_a\eta_1^{(0)''}(x)}{2\left(b_1^2 + 1\right)} - \frac{\beta_1\Phi_1^{(0)''}(x)}{b_1^2 + 1} = 0 . \tag{3.94c}$$

After the asymptotic matching between inner and outer layers we find the relations between physical parameters, which will be used as input parameters, and also the unknown integration constants. In this way the solutions of the previous equations are:

$$h_1^{(1)}(x) \;=\; e^{-x\sqrt{\gamma_1}}C_1 + C_4 , \tag{3.95a}$$

$$\eta_1^{(0)}(x) \;=\; \frac{\nu a_1 - 2\chi C_4}{\nu} - \frac{2e^{-x\sqrt{\gamma_1}}C_1\kappa_1}{\chi} , \tag{3.95b}$$

$$\Phi_1^{(0)}(x) \;=\; \frac{\rho_1\varphi_1 - m_1}{\rho_1} - \frac{e^{-x\sqrt{\gamma_1}}C_1\gamma_1\kappa_1\chi_a}{\chi\left(-\rho_1 b_1^2 + \beta_1\gamma_1 - \rho_1\right)} , \tag{3.95c}$$

where $C_4 = 1/R_1$. The jump conditions, imposed at each order in ε, are almost the same, except the stress associated to the thickness, which must be modified by the

presence of impurities:

$$F_u(x) \mid_{x=0} = \frac{q_1^2 \sqrt{\gamma_1} \kappa_1 \left(\gamma_1 \chi_a^2 q_1^2 - 4\xi \beta_1 \gamma_1 q_1^2 + 4\xi R_1^2 \rho_1 \right)}{2\chi R_1 \left(R_1^2 \rho_1 - q_1^2 \beta_1 \gamma_1 \right)} C_1 \ . \tag{3.96}$$

There is also a stress related to the variation of the total free energy with respect to the concentration Φ and a torque related to the thickness and coupled with the impurities concentration. These two terms allow us to establish consistency relations between the different physical parameters of each domain (α_i, β_i, μ_i, etc).

We need to calculate C_1 and D_2 which will now depend on β_i, ρ_i, χ_a and χ_b. Then, as in the previous analysis, it is possible to derive an expression for the contact angle between membrane domains and also for the thickness mismatch θ_c and h_c.

On the other hand, we can verify directly from these expressions that if we take the limit $\chi_{a,b} \to 0$ we recover the previous results (3.74) and (3.75). We have a similar situation for the coefficients γ_1 and γ_2 in this limit.

We note that we know the solutions of $r(z)$, $u(z)$ and $\phi(z)$ up to order ε, in the inner, outer and the entire region, where composite solutions are valid. The effect of protein concentration at the joint can be analyzed graphically, using the difference in the adsorption affinity of both domains. This fact is accounted for by considering the coupling constants χ_a and χ_b as variables.

Replacing the composite solutions in (3.88) and (3.8) we are able to express the total free energy of the equilibrium configuration as the sum of two terms. Up to order ε it reads:

$$\mathcal{F}_{\mathrm{T}} = \mathcal{F}_c + \varepsilon \gamma_c(\theta) \ , \tag{3.97}$$

where $\mathcal{F}_c$ is the energy associated with the macroscopic part of the model (without taking into account the thickness) and $\gamma_c(\theta)$ is the effective line tension measured with respect to the reference line tension $\gamma_r = 0$, but now modified by the presence of impurities. This line tension is a quadratic function of the contact angle θ when the other parameters are fixed.

As mentioned before, if the coupling terms $\chi_{a,b}$ go to zero, then γ_c goes to γ_o, the effective line tension without the impurities. These scaled coefficients $\chi_{a,b}$, which are related to the coupling between concentration and the mean curvature of the neutral surface, will be used as control parameters. As the affinity is different in each phase, we will consider the contact angle and the line tension as functions of two variables $\theta_c(\chi_a, \chi_b)$ and $\gamma_c(\chi_a, \chi_b)$. The behaviour of these quantities will be analyzed tuning χ_a and χ_b. Analytical expressions for θ_c and γ_c are complicated and for the sake of simplicity we perform a graphical analysis.

The behavior of the line tension and the contact angle is depicted in Fig(3.7) and Fig(3.8), for different values of the coupling constants χ_a and χ_b. It is clear that γ_c and θ_c grow when the coupling constants also grow. Obviously this growing behaviour implies a growth in the line tension, because the angular dependence is quadratic. In Fig(3.8) we have supposed the case $\chi_a = \chi_b$, for simplicity. The value of the parameters are, in this case, the same as before. For the coefficients related to the concentration of
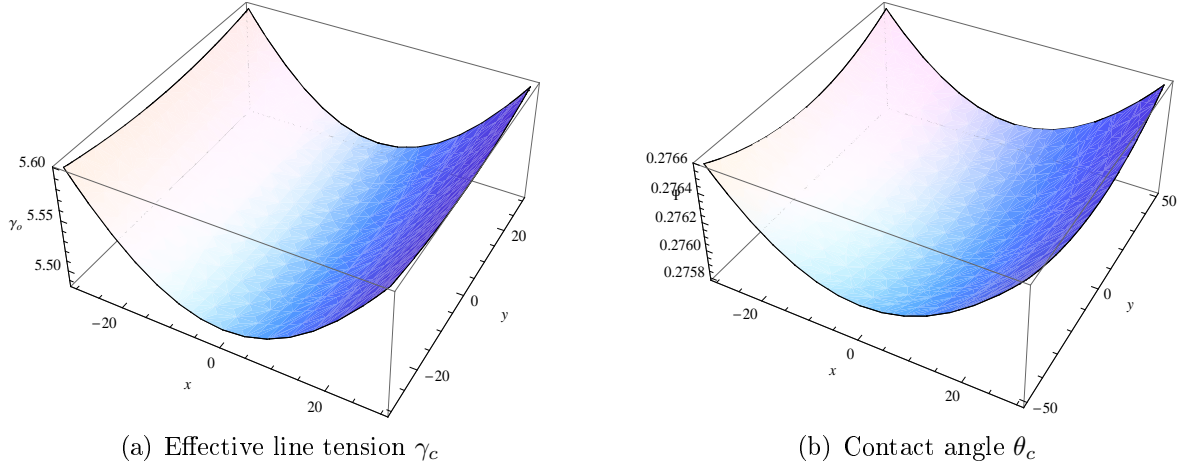
(a) Effective line tension γ_c

(b) Contact angle θ_c

Fig. 3.7: Effective line tension $\gamma_c(\chi_a, \chi_b)$ and contact angle $\theta_c(\chi_a, \chi_b)$ for the values: $\kappa_2 = 20K_BT$, $\kappa_1 = 5\kappa_2$, $H_{s1} = (50nm)^{-1}$, $H_{s2} = 0.003H_{s1}$, $\nu = 4 \times 10^{15}Jm^{-4}$, $a_1 = 7nm$, $a_2 = 5nm$, $\xi = 10^{-1}Jm^{-2}$, $\chi = 1, 2 \times 10^{-2}Jm^{-2}$, $\rho_1 = 500K_BT(\mu m)^2$, $\rho_1 = 2250K_BT(\mu m)^2$, $\beta_1 = 10^{-2}K_BT(\mu m)^4$, $\beta_2 = 0.0506K_BT(\mu m)^4$

(a) Line tension γ_c
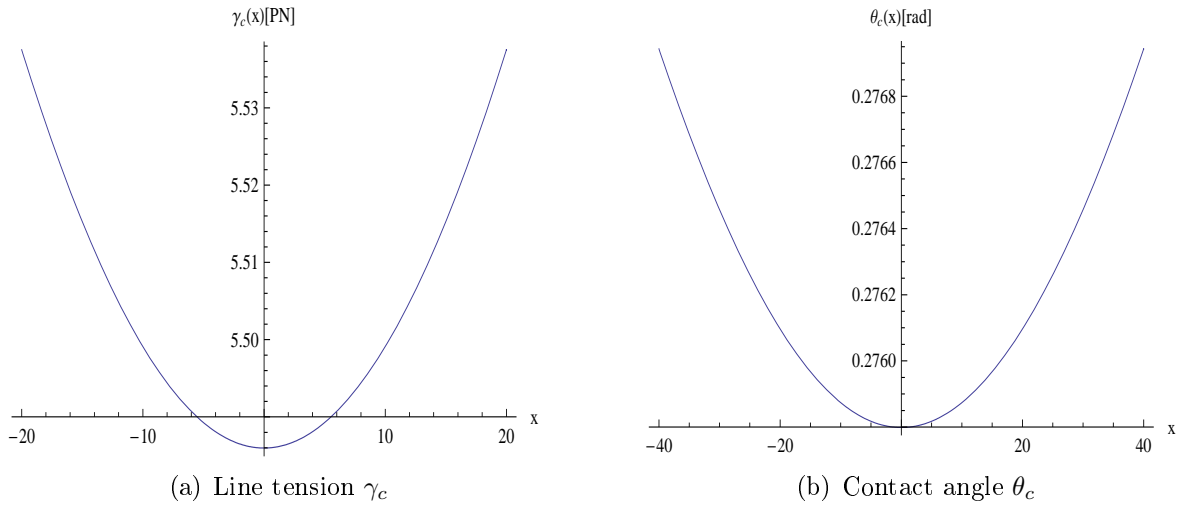

(b) Contact angle θ_c

Fig. 3.8: Effective line tension $\gamma_c(\chi_a, \chi_b)$ and contact angle $\theta_c(\chi_a, \chi_b)$ in the case $\chi_a = \chi_b$ for the values: $\kappa_2 = 20K_BT$, $\kappa_1 = 5\kappa_2$, $H_{s1} = (50nm)^{-1}$, $H_{s2} = 0.003H_{s1}$, $\nu = 4x10^{15}Jm^{-4}$, $a_1 = 7nm$, $a_2 = 5nm$, $\xi = 10^{-1}Jm^{-2}$, $\chi = 1, 2x10^{-2}Jm^{-2}$, $\rho_1 = 500K_BT(\mu m)^2$, $\rho_1 = 2250K_BT(\mu m)^2$, $\beta_1 = 10^{-2}K_BT(\mu m)^4$, $\beta_2 = 0.0506K_BT(\mu m)^4$

impurities (α_i, β_i, μ_i, etc) estimated values are given in [4, 5]. Typical values for these parameters are $\chi_a = 20K_BT\mu m$ and $\chi_b = 1.35K_BT\mu m$. It is necessary to emphasize that in this approach any parameter depends on the chemical potential m_i, or on the equilibrium optimal concentration ϕ_{oi}. The estimation of the coupling coefficients generally depends on the large scale properties of the membrane which have already

been incorporated in our description, as for instance the spontaneous curvature H_{si} of each domain.

3.9   Summary and discussion

In this chapter we have described the energetic and structural properties in the vicinity of the joint between two different domains that compose an axisymmetric deformed vesicle. In order to study these structural properties we have proposed an elastic model that takes into account the coupling between microscopic internal degrees of freedom represented by the thickness variation at the joint, and the typical macroscopic properties of vesicles, like mean and Gaussian curvatures. This model considers a *local area-difference elasticity* part in the neighborhood of the interface. As a consequence a non-homogeneous bending deformation term must be considered, that implies at the same time a thickness gradient varying through the membrane. The model also incorporates typical macroscopic properties of the membrane like spontaneous curvature, surface tension and Gaussian rigidity. In spite of the complexity of the equations we successfully calculate (by means of asymptotic methods) asymptotic solutions for the shape function and the thickness, in the entire region up to order ε.

As a direct consequence we have found a structural distortion within the joint, that is reflected in the mismatch of the thickness, that is of order ε. At the same time we find a discontinuity in the slope of the membrane shape at the interface if we consider the description at the level of Helfrich's theory. This contact angle has an influence on the macroscopic elastic description of the total energy, producing an *effective line tension*. Using typical values of parameters, the contact angle varies between 10 and 20 degrees, in agreement with a previous result obtained in [54], but when the membrane is slightly curved. We have also obtained that the presence of impurities or proteins in the membrane can modify the contact angle. As the coupling constants $\chi_{a,b}$ increase, they also increase the contact angle and the line tension. If the coupling is estimated by $\Lambda_i = K_B T R_i^2 H_{si}$ [4], the line tension grows as the spontaneous curvatures also grows. It makes sense, because the effect of the proteins is to change the local curvature of the membrane, imposing a spontaneous curvature.

Chapter 4

GROWTH AND GEOMETRY OF ELASTIC MEMBRANES OF CONSTANT GAUSSIAN CURVATURE

In this chapter we study the geometric and elastic properties of growing thin structures which are described by surfaces of constant Gaussian curvature. At first, we present a method to produce this kind of growing surfaces. A geometrical free energy, for which these surfaces are equilibrium states, is introduced and interpreted as an action. An equilibrium surface can then be generated by the evolution of a closed space curve. Because of the local symmetries of the action, the evolution is obtained using Dirac's method for constrained Hamiltonian system. This formulation leads to four first order partial differential equations, one for each canonical variable. With the appropriate choice of parametrization only one of these equations has to be solved to obtain the surface which is swept out by the evolving space curve. Finally, we illustrate the formalism by performing some evolutions from different initial conditions. Accordingly, surfaces of constant Gaussian curvature without any special symmetries can be easily produced. In particular we focus on two examples that are relevant to describe the shape adopted by growing soft tissues occurring in nature: i) the disturbance of the growth process of a pseudosphere and its energetic properties, and ii) the growth of a surface with cuspidal singularities, in which the stretching energy is concentrated.

4.1   Introduction

As mentioned in Sec. 1.2, in the case of soft thin tissues, growth processes induce residual stresses even in the absence of external loads. These residual stresses are able to change the geometrical structure of the tissue and can, for instance, induce a shape instability in the growing material [63]. The resulting shape is given by the minimization of an elastic surface energy which consists of two terms, one due to bending and one due to stretching which have been described theoretically in Sec. 2.4

Growth at this level can be interpreted as a process which fixes the distance between two points on the surface. This implies the existence of a target metric [50, 74, 96], and therefore (by the Theorema Egregium of Gauss) a prescribed Gaussian curvature K_{G} of the final surface. In general the real surface cannot adjust to the target metric in all of its points and has to stretch. However, if the thin tissue is able to assume its

(a) An Angel's Trumpet (Brugmansia).   (b) A daffodil.   (c) A morning glory

Fig. 4.1: Examples of soft tissues with nonvanishing Gaussian curvature. The flowers of type (a) and (c) exhibit a pentagonal symmetry.

target configuration, the correct shape can be found by minimizing the bending energy of the corresponding surface with prescribed metric and Gaussian curvature. Finding surfaces with a certain Gaussian curvature is thus one important and necessary step to understand such growth problems.

In this chapter we study surfaces with *constant Gaussian curvature* (c.G.c.s.). In particular, surfaces with zero Gaussian curvature are called *developable surfaces*. They have been largely discussed in the context of stresses in thin elastic sheets [8, 34, 42, 66, 100, 140]. In general, however, growth generates surfaces with fixed non-zero Gaussian curvature. Typical examples are flowers [96], plant leafs [43, 95, 103], or plastic sheets where the increase of area is induced artificially by tearing [11, 119]. But not only growth processes can generate these surfaces. Recently, it has been shown that nematic membranes can buckle into pseudospheres because of defects in their internal degree of freedom [57]. A *pseudosphere* is an axisymmetric surface with Gaussian curvature $K_G = -1$. Accordingly, surfaces of constant negative Gaussian curvature are also called *pseudospherical surfaces*. On the contrary, when this curvature is positive the surface is called a *spherical surface*.

Both types of surface have been considered from a mathematical point of view in order to study the connection between differential geometry and partial differential equations. It is, for instance, well-known that certain types of solutions of solitonic equations like the sine-Gordon or the Korteweg-de Vries equation are associated with c.G.c.s. [113, 114, 46]. Here, using some of these properties we will consider spherical and pseudospherical surfaces in order to model the geometric and elastic behaviour of thin growing tissues. Our first step is to consider a theoretical formalism that will allow us to express the growth process as the evolution of a closed curve in the space. This is the aim of the next section.

4.2 Hamiltonian formulation of surfaces with constant Gaussian curvature

The main purpose of this section is to present a formalism that will allow us to generate surfaces with *constant Gaussian curvature* (c.G.c.s.) from the evolution of a closed curve $\mathcal{C}$. In this sense we will say that the law of motion satisfied by the curve corresponds to a *geometrical evolution*.

The description of a curve in $\mathbb{R}^3$ is given by the *Frenet-Serret equations*. This structure has been considered in order to study the integrability properties of certain types of geometrical evolutions [102]. The geometrical evolution is usually expressed by an appropriate law of motion where the velocity $\dot{\boldsymbol{X}}$ of the curve is given as a function of its geometrical properties such as its curvature κ_c or its torsion τ_c. Equations of this type allow to describe different physical problems [113]. In our case the law for the evolution is expressed in terms of the acceleration of the curve and not in terms of its velocity. This is due to the fact that the curve is constrained onto a surface of constant Gaussian curvature, as we will see.

The approach that we will use here has also been used in the case of fluid membranes [26, 29]. The theoretical background has its origin in general relativity where it was proposed that the spacetime manifold $\mathcal{M}$ can be interpreted as the trajectory of an extended object (or brane) $\mathcal{B}$ embedded in a flat background spacetime $\mathcal{V}$ [25] using the ADM decomposition [9]. In our case, the manifold $\mathcal{M}$ is a two-dimensional surface Σ, the extended object is a curve $\mathcal{C}$ on the surface, and the host space is the standard three-dimensional Euclidean space $\mathbb{E}^3$. In addition, as the temporal variable is Euclidean, the ADM decomposition is the standard orthogonal decomposition of linear algebra.

For our purpose the dynamics of the curve is determined by a geometrical action that fixes the Gaussian curvature of Σ. However, as a consequence of this geometrical structure the action involves second derivatives, which implies that the phase space has to be extended: the velocity of the curve and its respective conjugate momentum have to be included as canonical variables. Furthermore, we will see that the Lagrangian function is reparametrization invariant and linear in the acceleration of the curve. This implies that the system is constrained in the phase space. In order to overcome both difficulties we will use *Dirac's method* which deals with constrained Hamiltonian systems in a systematic way [93]. In the following section we will determine a geometric free energy whose minimization produces surfaces of constant Gaussian curvature.

4.2.1 A Free Energy describing a c.G.c.s.

As seen in Chapter 2, to obtain the shape of a two-dimensional elastic object, one usually minimizes an elastic free energy which depends on the geometrical properties of the material. For instance, a fluid lipid membrane can be modeled as a two-dimensional isotropic continuum that does not resist in-plane shear. In general this fluid is assumed to be incompressible. The free energy functional $\mathcal{F}_{\mathrm{M}}$ of a closed membrane Σ whose

area and volume remain constant during its deformation can be expressed as:

$$\mathcal{F}_{\mathbf{M}}[\boldsymbol{X}] = \mathcal{F}_{\mathrm{CH}}[\boldsymbol{X}] + \mathcal{F}_{\sigma}[\boldsymbol{X}] + \mathcal{F}_{\mathrm{V}}[\boldsymbol{X}] \, , \tag{4.1}$$

where each term has been explained in Chap. 2. If we suppose that the surface tension is a constant λ, the total free energy of the closed vesicle can be recast as:

$$\mathcal{F}_{\mathbf{M}}[\boldsymbol{X}] = \frac{\kappa}{2} \int_{\Sigma} \mathrm{d}A \, K^2 + \bar{\kappa} \int_{\Sigma} \mathrm{d}A \, K_{\mathrm{G}} + B \int_{\Sigma} \mathrm{d}A \, K + \lambda \int_{\Sigma} \mathrm{d}A - P \int_{V} \mathrm{d}V \, . \tag{4.2}$$

The two first terms in Eqn. (4.2) correspond to the Willmore functional [139]. The material parameters κ and $\bar{\kappa}$ are the bending rigidity and the saddle-splay modulus, respectively. Note that the second term in (4.2) can be dropped since it is an invariant for a closed surface and thus does not contribute to the determination of the equilibrium configuration (see App. A).

The free energy Eqn. (4.2) allows us to interpret the variation of $\mathcal{F}_{\mathrm{M}}[\boldsymbol{X}]$ as the minimization of the Willmore functional subject to three global constraints that are imposed by constant Lagrange multipliers: λ is the surface tension which fixes the area, P is the pressure difference between interior and exterior that has to be maintained to keep the enclosed volume V constant. Finally we have defined B as a Lagrange multiplier fixing the total mean curvature. Note that it can be expressed as $B = -\kappa K_o$ in the notation of Chap 2.

To determine the equilibrium shape of the surface, the response of the free energy to infinitesimal variations of the embedding function $\boldsymbol{X} \to \boldsymbol{X} + \delta \boldsymbol{X}$ has to be considered. We know that it has the following structure (see Eqn. (2.22) in Chap. 2):

$$\delta \mathcal{F}_{\mathrm{M}}[\boldsymbol{X}] = \int_{\Sigma} \mathrm{d}A \, \mathcal{E}_{\mathrm{M}}(\mathcal{H})(\boldsymbol{N} \cdot \delta \boldsymbol{X}) + \int_{\Sigma} \mathrm{d}A \, \nabla_a Q_{\mathrm{M}}^a \, . \tag{4.3}$$

Note that in this case we have supposed that the closed membrane is homogeneous, and therefore the tangential part A_{M}^a of the bulk term in Eqn. (4.3) is identically zero, as mentioned in Chap. 2. The second term of this variation is a surface integral over a divergence and can thus be recast as a boundary integral. It originates from tangential variations as well as from derivatives of the normal variation and is related to the effective stresses in the surface. The bulk part of the variation is a surface integral over the Euler-Lagrange derivative $\mathcal{E}_{\mathrm{M}}$ times the normal projection of the surface variation $\delta \boldsymbol{X}$. Its vanishing determines the equilibrium shape of the interface. Hence, $\mathcal{E}_{\mathrm{M}} = 0$ is also called the shape equation which for a lipid membrane reads [24, 142]:

$$-\kappa \left[\nabla^2 K + \frac{K}{2}(K^2 - 4K_{\mathrm{G}}) \right] + 2BK_{\mathrm{G}} + \sigma K - P = 0 \, . \tag{4.4}$$

The goal of this chapter is to study surfaces of constant Gaussian curvature. A close observation of Eqn. (4.4) reveals how to construct a geometrical functional which describes a c.G.c.s.: it is sufficient to include the third and the fifth term of the free
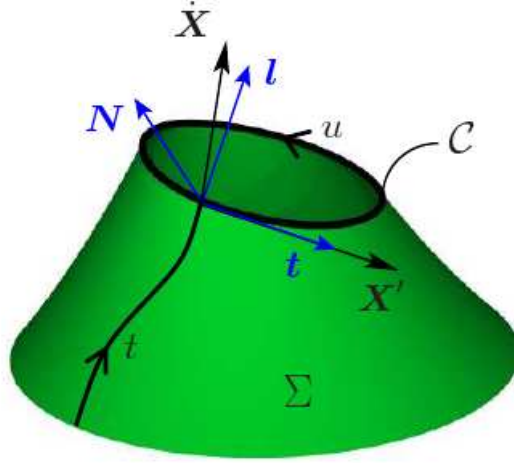
Fig. 4.2: Generation of c.G.c.s. Σ by a moving curve $\mathcal{C}$. The orthonormal vector basis $\{\boldsymbol{t}, \boldsymbol{l}, \boldsymbol{N}\}$ is the Darboux frame of the curve on the surface. The geometrical properties of Σ can be decomposed in the tangent basis $\{\boldsymbol{X}', \dot{\boldsymbol{X}}\}$ adapted to the evolution of the curve.

energy Eqn. (4.2) in the new functional:

$$\mathcal{F}_{\mathrm{G}}[\boldsymbol{X}] := \int_{\Sigma} \mathrm{d}A \, \mathcal{H}_{\mathrm{G}} = B \int_{\Sigma} \mathrm{d}A \, K - \frac{P}{3} \int_{\Sigma} \mathrm{d}A \, (\boldsymbol{N} \cdot \boldsymbol{X}) \,, \tag{4.5}$$

where B and P are constants and the integral over the volume is rewritten as a surface integral. The resulting shape equation is:

$$K_{\mathrm{G}} = \frac{P}{2B} \,, \tag{4.6}$$

which indeed fixes the Gaussian curvature of the surface locally. Note that the last term in Eqn. (4.5) is the volume term $\mathcal{F}_{\mathrm{V}}$ that has been rewritten as a surface term, as described in Sec. 2.3.1. In this case the corresponding boundary integral in (4.3) does not vanish in general since the surfaces that we will to consider here are not closed [65].

It is important to stress that $\mathcal{F}_{\mathrm{G}}$ is not a free energy obtained from elasticity theory like the free energy $\mathcal{F}_{\mathrm{M}}$ of the fluid membrane. Its equilibrium states (i.e., surfaces of constant Gaussian curvature) can nevertheless be found in analogy to the case of a fluid membrane using a Hamiltonian formulation [29]. Even though the two cases are closely related, the Hamiltonian formulation of the membrane can only be partially translated to c.G.c.s. as we will see in the following sections.

4.2.2 Projecting the surface

A c.G.c.s. will be generated by the evolution of a closed curve $\mathcal{C}$ that is parametrized by u (see Fig. 4.2). If we parametrize its evolution in time by t, the resulting surface Σ will be given by $\boldsymbol{X}(u,t)$. Since the curve stays always on the surface, the expressions for the tangential vector $\boldsymbol{X}' = \partial \boldsymbol{X}/\partial u = \partial_u \boldsymbol{X}$ and the velocity $\dot{\boldsymbol{X}} = \partial \boldsymbol{X}/\partial t = \partial_t \boldsymbol{X}$ are given by:

$$\boldsymbol{X}' = \sqrt{h}\,\boldsymbol{t}\,, \qquad \dot{\boldsymbol{X}} = \alpha \boldsymbol{X}' + \beta \boldsymbol{l}\,, \tag{4.7}$$

where $\boldsymbol{t}$ is the unit tangent vector of the curve at fixed time t, $\boldsymbol{l}$ is the unit vector normal to the curve and tangential to the surface, and $h = \boldsymbol{X}' \cdot \boldsymbol{X}'$ is the metric of the curve (see again Fig. 4.2). The functions α and β can be written in terms of the derivatives of the curve:

$$\alpha = h^{-1}(\dot{\boldsymbol{X}} \cdot \boldsymbol{X}')\,, \qquad \beta^2 = \dot{\boldsymbol{X}}^2 - h^{-1}(\dot{\boldsymbol{X}} \cdot \boldsymbol{X}')^2\,. \tag{4.8}$$

The geometrical properties of the surface Σ can be decomposed along a surface basis adapted to the curve, as in the case of the contact line variation in Chapter 2 (see also App. A.2). If we take $\boldsymbol{e}_1 = \boldsymbol{X}'$ and $\boldsymbol{e}_2 = \dot{\boldsymbol{X}}$ as the tangent vectors of the surface, the metric adopts the following form:

$$g_{ab} := \boldsymbol{e}_a \cdot \boldsymbol{e}_b = \begin{pmatrix} h & \alpha h \\ \alpha h & \alpha^2 h + \beta^2 \end{pmatrix}\,, \quad \text{where} \quad a,b \in \{1,2\}\,. \tag{4.9}$$

The determinant of this induced metric follows directly: $g = \beta^2 h$. The normal vector of Σ is given by the cross product of the tangent vectors $\boldsymbol{t}$ and $\boldsymbol{l}$: $\boldsymbol{N} = \boldsymbol{t} \times \boldsymbol{l} = \boldsymbol{e}_1 \times \boldsymbol{e}_2/(\beta\sqrt{h})$. The extrinsic curvature tensor K_{ab} can also be decomposed along $\boldsymbol{e}_1$ and $\boldsymbol{e}_2$. One obtains:

$$K_{ab} := -\boldsymbol{N} \cdot \partial_a \boldsymbol{e}_b = -\begin{pmatrix} \boldsymbol{N} \cdot \boldsymbol{X}'' & \boldsymbol{N} \cdot \dot{\boldsymbol{X}}' \\ \boldsymbol{N} \cdot \dot{\boldsymbol{X}}' & \boldsymbol{N} \cdot \ddot{\boldsymbol{X}} \end{pmatrix}. \tag{4.10}$$

Note that the curvature tensor depends on the acceleration of the curve projected along the normal direction. The curvature K and the Gaussian curvature K_{G} are the invariants of the mixed extrinsic curvature tensor $K_a^b = K_{ac}g^{cb}$. As usual, repeated indices (one up and one down) imply a summation. In this decomposition the invariants are given by

$$K = \frac{1}{\beta^2}(-\boldsymbol{N} \cdot \ddot{\boldsymbol{X}} + J_{\mathrm{K}}), \tag{4.11a}$$

$$K_{\mathrm{G}} = \frac{1}{g}[(\boldsymbol{N} \cdot \ddot{\boldsymbol{X}})(\boldsymbol{N} \cdot \boldsymbol{X}'') - J_{\mathrm{G}}]\,, \tag{4.11b}$$

where the functions $J_{\rm K}$ and $J_{\rm G}$ do not depend on the acceleration $\ddot{\boldsymbol{X}}$ of the curve:

$$J_{\rm K} \;=\; 2\alpha(\boldsymbol{N}\cdot\dot{\boldsymbol{X}}') - h^{-1}(\dot{\boldsymbol{X}})^2(\boldsymbol{N}\cdot\boldsymbol{X}'') \;, \tag{4.12a}$$

$$J_{\rm G} \;=\; (\boldsymbol{N}\cdot\dot{\boldsymbol{X}}')^2 \;. \tag{4.12b}$$

Using this decomposition in the next section we will identify the Lagrangian structure of the free energy Eqn. (4.5) and the phase space variables related to it in order to determine the dynamics of the curve $\mathcal{C}$.

4.2.3   Identification of the phase space variables

The conventional shape equation involves the metric g_{ab} and the extrinsic curvature tensor K_{ab}. Using a Hamiltonian formulation the shape equation can be rewritten in terms of the evolving curve $\boldsymbol{X}(u,t)$. This alternative structure offers a true advantage if one wants to find equilibrium solutions numerically, or if one wants to follow the evolution of the edge of a growing tissue.

To identify the appropriate phase space variables of this formulation, we express the free energy Eqn. (4.5) as an *action functional* that contains the dynamics of $\boldsymbol{X}(u,t)$ in time:

$$\mathcal{F}_{\rm G}[\boldsymbol{X}] = \int \mathrm{d}t\, L[\boldsymbol{X},\dot{\boldsymbol{X}},\ddot{\boldsymbol{X}}] \;, \qquad L[\boldsymbol{X},\dot{\boldsymbol{X}},\ddot{\boldsymbol{X}}] = \oint \mathrm{d}u\, \mathcal{L}[\boldsymbol{X},\dot{\boldsymbol{X}},\ddot{\boldsymbol{X}},\boldsymbol{X}',\boldsymbol{X}'',\dot{\boldsymbol{X}}'] \;, \tag{4.13}$$

where L is the *Lagrangian* of the system and $\mathcal{L}$ is the *Lagrangian density functional* given by:

$$\mathcal{L} = \beta\sqrt{h}\left[\frac{B}{\beta^2}\left(-\boldsymbol{N}\cdot\ddot{\boldsymbol{X}} + J_{\rm K}\right) - \frac{P}{3}\boldsymbol{N}\cdot\boldsymbol{X}\right] \;. \tag{4.14}$$

This Lagrangian density depends implicitly on the embedding function $\boldsymbol{X}$ and the normal vector $\boldsymbol{N}$. It is of second order in time derivatives of $\boldsymbol{X}$. Since $\mathcal{L}$ is linear in the acceleration $\ddot{\boldsymbol{X}}$, one could perform an integration by parts within the action to eliminate this dependence. Instead we will use the method for constrained Hamiltonian systems to proceed [93]. The strategy in this section follows directly along the lines of the fluid membrane case [29]. Differences will only become apparent later when the constraints on the system are investigated.

As a direct consequence of the acceleration dependence the phase space contains not only the position of the curve $\boldsymbol{X}(u,t)$ and its conjugate momentum $\boldsymbol{p}(u,t)$, but also the velocity of the curve $\dot{\boldsymbol{X}}(u,t)$ and its conjugate momentum $\boldsymbol{\Pi}(u,t)$. The momenta are defined by the functional derivatives:

$$\boldsymbol{\Pi} \;:=\; \frac{\delta L}{\delta \ddot{\boldsymbol{X}}}, \tag{4.15}$$

$$\boldsymbol{p} \;:=\; \frac{\delta L}{\delta \dot{\boldsymbol{X}}} - \partial_t\left(\frac{\delta L}{\delta \ddot{\boldsymbol{X}}}\right) \;. \tag{4.16}$$

The canonical momentum conjugate to the velocity can be immediately obtained from Eqn. (4.14):

$$\mathbf{\Pi} = -B\frac{\sqrt{h}}{\beta}\boldsymbol{N} \ . \tag{4.17}$$

One can show that the other canonical momentum $\boldsymbol{p}$ is related to the conserved *stress* of the surface Σ [29]. Since (4.5) does not represent the physical elastic free energy of a c.G.c.s. but is merely a geometrical functional, this *stress* does not have a physical meaning like in the case of a lipid membrane. We will nevertheless use the same terminology to make the connection with previous work [29].

For a Lagrangian which depends on the acceleration like (4.13), the first variation can be written as:

$$\delta\mathcal{F}_{\mathrm{G}}[\boldsymbol{X}] = \int_{\Sigma} \mathrm{d}A \ \mathcal{E}_{\mathrm{G}}(\boldsymbol{N} \cdot \delta\boldsymbol{X}) + \oint_{\mathcal{C}} \mathrm{d}u \ \left(\boldsymbol{p} \cdot \delta\boldsymbol{X} + \mathbf{\Pi} \cdot \delta\dot{\boldsymbol{X}}\right) \ . \tag{4.18}$$

In the case of a c.G.c.s. the Euler-Lagrange derivative is given by $\mathcal{E} = 2BK_{\mathrm{G}} - P$. On the other hand, the first variation is also given by equation (4.3):

$$\delta\mathcal{F}_{\mathrm{G}}[\boldsymbol{X}] = \int_{\Sigma} \mathrm{d}A \ \mathcal{E}_{\mathrm{G}}(\mathcal{H})(\boldsymbol{N} \cdot \delta\boldsymbol{X}) + \oint_{\mathcal{C}} \mathrm{d}u \ \sqrt{h} \, l_a Q_{\mathrm{G}}^a \ , \tag{4.19}$$

where the divergence term was rewritten as a boundary integral using Stokes theorem. The quantities l_a are the components of the vector $\boldsymbol{l} = l^a \boldsymbol{e}_a$ in the surface basis (see Fig. 4.2). The current Q_{G}^a depends on the stress-like surface tensor $\boldsymbol{f}^a$ in the form [64]:

$$Q_{\mathrm{G}}^a = -\boldsymbol{f}^a \cdot \delta\boldsymbol{X} - \left(\frac{\delta\mathcal{H}_{\mathrm{G}}}{\delta K_{ab}}\right) \boldsymbol{N} \cdot \delta\boldsymbol{e}_b \ , \tag{4.20}$$

where $\mathcal{H}_{\mathrm{G}}$ is the free energy density of (4.5). In general the tensor $\boldsymbol{f}^a$ has components tangential and normal to the surface. In the present case it is given by:

$$\boldsymbol{f}^a = \left[B(K^{ab} - Kg^{ab}) + \frac{P}{3}g^{ab}(\boldsymbol{N} \cdot \boldsymbol{X})\right] \boldsymbol{e}_b - \frac{P}{3}g^{ab}(\boldsymbol{X} \cdot \boldsymbol{e}_b)\boldsymbol{N} \ . \tag{4.21}$$

The divergence of this tensor can be used to write the shape equation (4.6) in the following form:

$$\nabla_a \boldsymbol{f}^a = \frac{1}{3}P\boldsymbol{N} \ . \tag{4.22}$$

Comparing the two versions (4.18) and (4.19) of the variation one can identify the terms proportional to $\delta\boldsymbol{X}$ and obtain the following expression for the canonical momentum conjugate to the position:

$$\begin{aligned}
\boldsymbol{p} &= -\sqrt{h} \, l_a \boldsymbol{f}^a + \partial_u(\alpha\mathbf{\Pi}) \ , &\tag{4.23}\\
&= B\sqrt{h}\left(Kg^{ab} - K^{ab}\right)l_a\boldsymbol{e}_b - \frac{P}{3}(\boldsymbol{X} \times \boldsymbol{X}') + \partial_u(\alpha\mathbf{\Pi}) \ . &\tag{4.24}
\end{aligned}$$

Note that the term proportional to P in the free energy introduces a normal component in the vector $\boldsymbol{f}^a$. We anticipate that it will also cause a source term in the Hamilton equation for the canonical momentum $\boldsymbol{p}$. Also note that we have used an alternative way to calculate $\boldsymbol{p}$. The usual way is to use the definition Eqn. (4.16) which implies calculating the functional derivatives of the Lagrangian function L.

Both $\boldsymbol{p}$ and $\boldsymbol{\Pi}$ transform as a density under reparametrizations of the surface. By using the completeness of the metric and the surface tangent vectors $g^{ab} = t^a t^b + l^a l^b$, one can demonstrate that the canonical momentum $\boldsymbol{p}$ is independent of the acceleration of the curve. Its expression as a function of the canonical variables is:

$$\boldsymbol{p} = Bh^{-1/2}\beta^{-1}\left[(\boldsymbol{N}\cdot\dot{\boldsymbol{X}}')\boldsymbol{X}' - (\boldsymbol{N}\cdot\boldsymbol{X}'')\dot{\boldsymbol{X}}\right] - \frac{P}{3}(\boldsymbol{X}\times\boldsymbol{X}') + \partial_u(\alpha\boldsymbol{\Pi})\,. \qquad (4.25)$$

Both canonical momenta are only functions of $\boldsymbol{X}$, $\dot{\boldsymbol{X}}$, and their spatial derivatives, i.e., the phase space variables are not all independent at a fixed time t. As a consequence there are constraints on the system that have to be incorporated in the Hamiltonian formulation of the problem.

4.2.4 The constrained Hamiltonian

As usual, we perform the *Legendre transformation* of the Lagrangian (4.13) with respect to the velocity $\dot{\boldsymbol{X}}$ and the acceleration $\ddot{\boldsymbol{X}}$:

$$H_{\rm c}[\boldsymbol{X},\boldsymbol{p};\dot{\boldsymbol{X}},\boldsymbol{\Pi}] := \oint {\rm d}u\,\mathcal{H}_{\rm c} = \oint {\rm d}u\,(\boldsymbol{\Pi}\cdot\ddot{\boldsymbol{X}} + \boldsymbol{p}\cdot\dot{\boldsymbol{X}}) - L[\boldsymbol{X},\dot{\boldsymbol{X}},\ddot{\boldsymbol{X}}]\,, \qquad (4.26)$$

and obtain the *canonical Hamiltonian density* of the system:

$$\mathcal{H}_{\rm c} = \left[\boldsymbol{p}\cdot\dot{\boldsymbol{X}} - \frac{\sqrt{h}}{\beta}BJ_{\rm K} + \frac{P}{3}\beta\sqrt{h}(\boldsymbol{N}\cdot\boldsymbol{X})\right]\,. \qquad (4.27)$$

Note that the dependence on $\boldsymbol{\Pi}$ is automatically eliminated. This is due to the fact that the Lagrangian is linear in the acceleration $\ddot{\boldsymbol{X}}$ and implies that the resulting Hamilton's equations are inconsistent. Following *Dirac's method* [93], one can, however, overcome this obstacle by imposing the relation (4.17) involving $\boldsymbol{\Pi}$ as a constraint on the system. The projections along the basis $\{\boldsymbol{X}',\dot{\boldsymbol{X}},\boldsymbol{N}\}$ yield a set of so-called *primary constraints*:

$$\begin{aligned} C_1 &= \boldsymbol{\Pi}\cdot\boldsymbol{X}' \approx 0\,, & (4.28\text{a}) \\ C_2 &= \boldsymbol{\Pi}\cdot\dot{\boldsymbol{X}} \approx 0\,, & (4.28\text{b}) \\ C_3 &= \boldsymbol{\Pi}\cdot\boldsymbol{N} + B\sqrt{h}\beta^{-1} \approx 0\,. & (4.28\text{c}) \end{aligned}$$

The weak equality symbol $\approx$ means that the quantities C_i are zero *on shell* (i.e., when the equations of motion are satisfied) but do not identically vanish throughout

the whole phase space. A quantity Q in phase space is thus weakly equal to a quantity W if they are only different by a linear combination of the constraints.

The *total Hamiltonian* can be obtained by generalizing the canonical Hamiltonian to:

$$H_{\mathrm{T}} = H_{\mathrm{c}} + \oint \mathrm{d}u \, (\lambda_1 C_1 + \lambda_2 C_2 + \lambda_3 C_3) , \qquad (4.29)$$

where the λ_i are Lagrange multiplier functions of the coordinates u and t enforcing the constraints (4.28). For the formalism to be consistent we require that the conservation in time of the primary constraints vanishes:

$$S_i := \partial_t C_i = \{C_i, H_{\mathrm{T}}\} \approx 0 , \qquad (4.30)$$

where the *Poisson bracket* $\{\cdot, \cdot\}$ is given by:

$$\{Q, W\} = \oint \mathrm{d}u \, \left[\left(\frac{\delta Q}{\delta \boldsymbol{X}} \cdot \frac{\delta W}{\delta \boldsymbol{p}} + \frac{\delta Q}{\delta \dot{\boldsymbol{X}}} \cdot \frac{\delta W}{\delta \boldsymbol{\Pi}} \right) - \left(\frac{\delta W}{\delta \boldsymbol{X}} \cdot \frac{\delta Q}{\delta \boldsymbol{p}} + \frac{\delta W}{\delta \dot{\boldsymbol{X}}} \cdot \frac{\delta Q}{\delta \boldsymbol{\Pi}} \right) \right] \qquad (4.31)$$

for two phase space quantities Q and W. The temporal derivative of each C_i, given in Eqn. (4.30), defines the *secondary constraints* of the system. These secondary constraints are the generators of *gauge invariances* of the system. They are expressed by:

$$S_1 = \boldsymbol{p} \cdot \boldsymbol{X}' + \boldsymbol{\Pi} \cdot \dot{\boldsymbol{X}}' \approx 0 , \qquad (4.32\text{a})$$

$$S_2 = -\mathcal{H}_{\mathrm{c}} = -\boldsymbol{p} \cdot \dot{\boldsymbol{X}} + \frac{\sqrt{h}}{\beta} B J_{\mathrm{K}} - \frac{P}{3} \beta \sqrt{h} (\boldsymbol{N} \cdot \boldsymbol{X}) \approx 0 , \qquad (4.32\text{b})$$

$$S_3 = -\boldsymbol{p} \cdot \boldsymbol{N} + \frac{P}{3} \sqrt{h} (\boldsymbol{l} \cdot \boldsymbol{X}) + \partial_u(\alpha \boldsymbol{\Pi}) \cdot \boldsymbol{N} \approx 0 . \qquad (4.32\text{c})$$

The secondary constraints (4.32a) and (4.32b) reflect the reparametrization invariance of the initial free energy $\mathcal{F}_{\mathrm{G}}$: the constraint S_1 generates the reparametrizations tangential to the curve $\mathcal{C}$ whereas S_2 generates reparametrizations out of the curve. The latter is equivalent to the vanishing of the canonical Hamiltonian density, as one would expect. With the two constraints the tangential part of the momentum $\boldsymbol{p}$ is determined completely. The secondary constraint S_3 additionally fixes its normal component.

At this point it is instructive to consider the equivalent formulation for the fluid membrane again [29]. The structure of the first two primary and secondary constraints C_1, C_2, S_1, and S_2 is the same in both cases since the free energy functional (4.2) of the fluid membrane, $\mathcal{F}_{\mathrm{M}}[\boldsymbol{X}]$, is reparametrization invariant as well. The constraints C_3 and S_3, however, are characteristic for a system with a *Lagrangian linear in the acceleration*. Another example where this occurs can be found in [30]. They do not enter in the case of the membrane since $\mathcal{F}_{\mathrm{M}}[\boldsymbol{X}]$ is nonlinear in the acceleration $\ddot{\boldsymbol{X}}$.

In fact, for a c.G.c.s. both momenta are fixed completely by the constraints. The independent degrees of freedom are the position $\boldsymbol{X}$ and the velocity $\dot{\boldsymbol{X}}$. The equations that finally determine the evolution of the curve and therefore the surface will be

two first order equations, a trivial one for the position and another one for the velocity. These equations are determined by the Hamiltonian (4.29) and its corresponding *Hamilton's equations*.

4.2.5 Hamilton's equations

In this section we obtain the equation of motions for the four phase space variables. From the constrained Hamiltonian (4.29) the following set of Hamilton's equations is obtained:

$$\partial_t \boldsymbol{X} = \frac{\delta H_{\mathrm{T}}}{\delta \boldsymbol{p}} \, , \qquad \partial_t \dot{\boldsymbol{X}} = \frac{\delta H_{\mathrm{T}}}{\delta \boldsymbol{\Pi}} \, , \qquad \partial_t \boldsymbol{\Pi} = -\frac{\delta H_{\mathrm{T}}}{\delta \dot{\boldsymbol{X}}} \, , \qquad \partial_t \boldsymbol{p} = -\frac{\delta H_{\mathrm{T}}}{\delta \boldsymbol{X}} \, . \qquad (4.33)$$

The first equation of (4.33) allows us to identify the canonical variable $\dot{\boldsymbol{X}}$ (i.e., the velocity of the curve) with the time derivative of the variable $\boldsymbol{X}$:

$$\partial_t \boldsymbol{X} = \dot{\boldsymbol{X}} \, . \qquad (4.34)$$

Since the Hamiltonian (4.29) depends on $\boldsymbol{\Pi}$ only in the terms involving the constraints, the second equation is given by:

$$\partial_t \dot{\boldsymbol{X}} = \lambda_1 \boldsymbol{X}' + \lambda_2 \dot{\boldsymbol{X}} + \lambda_3 \boldsymbol{N} \, . \qquad (4.35)$$

This is the principal equation which describes the evolution of the curve. It identifies the Lagrange multipliers; they are equivalent to the three components of the acceleration $\ddot{\boldsymbol{X}}$ of the curve in the basis $\{\boldsymbol{X}', \dot{\boldsymbol{X}}, \boldsymbol{N}\}$. The third equation in (4.33) is:

$$\partial_t \boldsymbol{\Pi} = -\boldsymbol{d} - \lambda_2 \boldsymbol{\Pi} + \lambda_3 \sqrt{h} \beta^{-2} B \boldsymbol{l} + \lambda_3 \beta^{-1} (\boldsymbol{\Pi} \cdot \boldsymbol{l}) \boldsymbol{N} \, , \qquad (4.36)$$

where $\boldsymbol{d} := \delta H_{\mathrm{c}}/\delta \dot{\boldsymbol{X}}$ is a complicate expression that just depends on the canonical variables. It is possible to show that Eqn. (4.36) coincides with the expression (4.23) of the canonical momentum $\boldsymbol{p}$. Modulo the other Hamilton equations, the fourth equation can be identified with the vectorial form (4.22) of the shape equation (4.6), which in this case is expressed in terms of the canonical variables of the problem:

$$\partial_t \boldsymbol{p} = -\sqrt{h} \beta \frac{P}{3} \boldsymbol{N} + \partial_u \left\{ \boldsymbol{m} + \partial_u [h^{-1} (\dot{\boldsymbol{X}})^2 \boldsymbol{\Pi}] + \lambda_1 \boldsymbol{\Pi} + \lambda_3 \boldsymbol{S} \right\} \, . \qquad (4.37)$$

The interested reader can find the equivalence between Eqn. (4.37) and the vectorial form Eqn. (4.22) of the shape equation (4.6) in Ref. [130] together with the definitions of the vectors $\boldsymbol{d}$, $\boldsymbol{m}$ and $\boldsymbol{S}$.

Note that Eqn. (4.37) has the form of a continuity equation with a source term given by the explicit presence of the position vector $\boldsymbol{X}$ in the Hamiltonian.

Equation (4.35) and the definition of the Gaussian curvature (4.11b) allow us to write the third Lagrange multiplier λ_3 as a function of $\boldsymbol{X}'$, $\dot{\boldsymbol{X}}$, and their spatial derivatives

$\boldsymbol{X}''$ and $\dot{\boldsymbol{X}}'$. We obtain:

$$\lambda_3 = (\boldsymbol{N} \cdot \boldsymbol{X}'')^{-1} \left[(\boldsymbol{N} \cdot \dot{\boldsymbol{X}}')^2 + g K_{\mathrm{G}} \right] , \qquad (4.38)$$

where $K_{\mathrm{G}} = P/2B$ is given by the shape equation (4.6). The two other Lagrange multipliers λ_1 and λ_2 are the tangential components of the acceleration $\ddot{\boldsymbol{X}}$. Using equation (4.35) and the expressions from section 4.2.2 one finds:

$$\lambda_1 = h^{-1} \left(\ddot{\boldsymbol{X}} \cdot \boldsymbol{X}' - \alpha h \lambda_2 \right) , \qquad (4.39)$$

$$\lambda_2 = \beta^{-2} \left[(\ddot{\boldsymbol{X}} \cdot \dot{\boldsymbol{X}}) - \alpha (\ddot{\boldsymbol{X}} \cdot \boldsymbol{X}') \right] . \qquad (4.40)$$

The projections of the acceleration onto the surface basis vectors $\{\boldsymbol{X}', \dot{\boldsymbol{X}}\}$ can be expressed in terms of derivatives of the components of the metric tensor (4.9):

$$\mathcal{A}_1 := \ddot{\boldsymbol{X}} \cdot \boldsymbol{X}' = \partial_t(\alpha h) - \frac{1}{2}\partial_u(\dot{\boldsymbol{X}}^2) = \dot{g}_{12} - \frac{1}{2}g'_{22} , \quad \text{and} \qquad (4.41)$$

$$\mathcal{A}_2 := \ddot{\boldsymbol{X}} \cdot \dot{\boldsymbol{X}} = \frac{1}{2}\partial_t(\dot{\boldsymbol{X}}^2) = \frac{1}{2}\dot{g}_{22} , \qquad (4.42)$$

yielding an alternative expression for each of the two multipliers

$$\lambda_1 = g^{1a}\mathcal{A}_a = \frac{1}{g} \left[g_{22} \left(\dot{g}_{12} - \frac{1}{2}g'_{22} \right) - \frac{1}{2}g_{12}\,\dot{g}_{22} \right] , \quad \text{and} \qquad (4.43)$$

$$\lambda_2 = g^{2a}\mathcal{A}_a = \frac{1}{g} \left[-g_{12} \left(\dot{g}_{12} - \frac{1}{2}g'_{22} \right) + \frac{1}{2}g_{11}\,\dot{g}_{22} \right] . \qquad (4.44)$$

These multipliers represent the gauge part of the evolution. Choosing values for them corresponds to fixing the parametrization of the surface. Note that this choice solely determines how the curve evolves. The underlying c.G.c.s., however, is already completely determined by the initial conditions. We will discuss this point in detail in the following section in the context of pseudospherical surfaces.

For example, if we choose an arc length parametrization for the coordinate lines of the surface (i.e., all curves of $t = \mathrm{cst.}$ and $u = \mathrm{cst.}$), the components of the metric read $g_{11} = g_{22} = 1$ and $g_{12} = \cos\theta$, where $\theta(u,t)$ is the angle between the velocity $\dot{\boldsymbol{X}}$ and the tangent $\boldsymbol{X}'$ of the curve $\mathcal{C}$. From equations (4.43) and (4.44) one then obtains $\lambda_1 = -\dot{\theta}\csc\theta$ and $\lambda_2 = \dot{\theta}\cot\theta$ for the Lagrange multiplier functions.

Since λ_1 and λ_2 are completely arbitrary they can also be chosen to vanish. In this case the equation that needs to be solved simplifies to:

$$\partial_{tt}\boldsymbol{X} = \lambda_3 \boldsymbol{N} , \qquad (4.45)$$

with λ_3 given by equation (4.38). Note that this is a nonlinear partial differential equation for $\boldsymbol{X}$ of second order in space and in time written in the form $\partial_{tt}\boldsymbol{X} =$
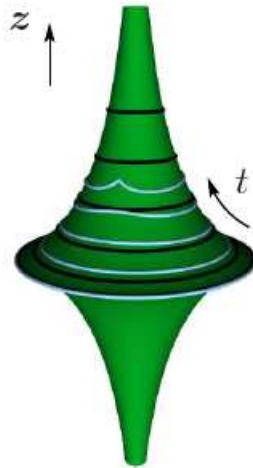
Fig. 4.3: The pseudosphere. The black curves represent the evolving circular curve at different times t ($t_\mathrm{i} = 0.2$, $t_\mathrm{f} = 2.2$, $\Delta t = 0.4$). The blue curves show a different evolution on the same surface with changed initial velocity ($\mathcal{V}_\mathrm{t} = 0.03$, $t_\mathrm{i} = 0.1$, $t_\mathrm{f} = 9.9$, $\Delta t = 2.45$).

$\boldsymbol{F}[\boldsymbol{X}', \dot{\boldsymbol{X}}, \dot{\boldsymbol{X}}', \boldsymbol{X}'']$.

The formulation discussed so far is particularly useful to determine c.G.c.s. numerically. The initial condition for equation (4.34) is a closed curve in space $\boldsymbol{X}(u, t_\mathrm{i})$ at initial time t_i. This implies that the embedding function and its first and second spatial derivatives are functions periodic in u. Additionally, the initial velocity of the curve $\dot{\boldsymbol{X}}(u, t_\mathrm{i})$ has to be specified as the initial condition for equation (4.35). The canonical momenta follow directly from the primary and secondary constraints (4.28) and (4.32). The Lagrange multipliers λ_1 and λ_2 can be chosen arbitrarily fixing the parametrization of the curve. If they are set to zero, the tangential projections $\mathcal{A}_1$ and $\mathcal{A}_2$ of $\ddot{\boldsymbol{X}}$ vanish. From equation (4.42) it follows directly that the length of $\dot{\boldsymbol{X}}$ is preserved in time for a fixed u. To ensure, for example, that the parameter t is equivalent to arc length, it is thus sufficient to choose $|\dot{\boldsymbol{X}}(u, t_\mathrm{i})| = 1$. Finally, if we now let the curve $\mathcal{C}$ evolve according to Hamilton's equations, a c.G.c.s. will be generated. However, the continuous evolution of the curve is not ensured at all and singularities may arise during the motion as we will see in the next section.

4.2.6   Singularities in the evolution

To illustrate our findings, we will specifically consider surfaces of negative Gaussian curvature $K_\mathrm{G} = -1$. A simple axisymmetric example is the *pseudosphere* (see Fig. 4.3). It is the surface of revolution of the so-called *tractrix* around its asymptote [113]. Due to the symmetry we choose to parametrize the surface in polar coordinates $\boldsymbol{X}(u, t) = (x(u, t), y(u, t), z(u, t))^\mathrm{T} = (R(t) \cos(u), R(t) \sin(u), Z(t))^\mathrm{T}$. An analytical expression

for $R(t)$ and $Z(t)$ is given by:

$$R(t) = \operatorname{sech}(t) , \tag{4.46a}$$

$$Z(t) = t - \tanh(t) . \tag{4.46b}$$

The same parametrization can be used for the generating curve if we start with a planar circle of radius $R(t_i)$ at height $Z(t_i)$ and velocity components $\mathcal{V}_R(t_i)$ and $\mathcal{V}_Z(t_i)$, where

$$\mathcal{V}_R(t) = -\operatorname{sech}(t)\tanh(t) , \quad \text{and} \tag{4.47a}$$

$$\mathcal{V}_Z(t) = \tanh^2(t) \tag{4.47b}$$

are obtained directly from equations (4.46). In this decomposition the metric is given by

$$g_{11} = \operatorname{sech}^2(t) , \quad g_{12} = 0 , \quad \text{and} \quad g_{22} = \tanh^2(t) . \tag{4.48}$$

Note that both parameters, u and t, do not directly measure the arc length of the coordinate lines. From equations (4.17) and (4.25) one easily obtains the components of the conjugate momenta:

$$\Pi_R(t) = -B\operatorname{sech}(t) , \quad \Pi_Z(t) = -2B\operatorname{csch}(2t) , \tag{4.49}$$

and

$$p_R(t) = -\frac{B}{3}\operatorname{sech}(t)\big[2t + \tanh(t)\big] , \quad p_Z(t) = \frac{B}{3}\big[3 - \operatorname{sech}^2(t)\big] . \tag{4.50}$$

Finally, the Lagrange multiplier functions of this parametrization are given by the following expressions:

$$\lambda_1(t) = 0 , \quad \lambda_2(t) = \operatorname{sech}(t)\operatorname{csch}(t) , \quad \text{and} \quad \lambda_3(t) = \operatorname{sech}(t)\tanh(t) . \tag{4.51}$$

One immediately sees that the acceleration of the evolving curve is not purely normal but has an additional tangential component in the direction of $\dot{\boldsymbol{X}}$. The black curves in Fig. 4.3 show one example of an evolution with initial time $t_i = 0.2$ and final time $t_f = 2.2$. For $t_f \to \infty$ the evolving circle converges to a point at infinity. If t_i is chosen negative, however, the evolution will always terminate at $t = 0$ since the velocity (4.47) of the curve goes to zero. This behaviour is due to a *singularity* of the surface, the circular cusp, where the curvature K diverges.

In fact, pseudospherical surfaces will *always* exhibit singularities since the hyperbolic plane cannot be immersed completely into $\mathbf{E}^3$ [69]. Typically, these singularities are *cuspidal edges* that can exhibit cusps themselves (so-called *swallowtail points*). As soon as the curve reaches a surface singularity in at least one point, the evolution terminates.

To illustrate this behaviour, we perturb the initial planar circle weakly into an ellipse
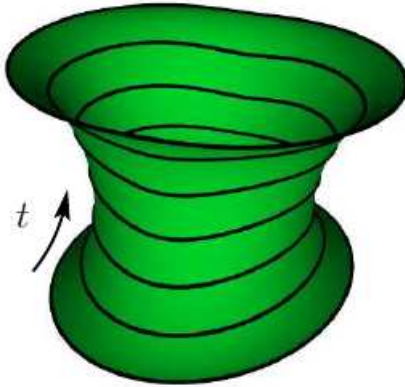
Fig. 4.4: Pseudospherical surface generated by the evolution of an ellipse. Black curves represent this evolution in time (time step $\Delta t = 1.05$). The numerical values for the initial conditions are: $a_0 = 1.1$, $b_0 = 1.4$, $\mathcal{V}_R^0 = -0.3$, and $\mathcal{V}_Z^0 = 0.1$. Initial and final time are given by $t_i = 0$ and $t_f = 6.3$, respectively.

parametrized by:

$$\boldsymbol{X}(u, t_\mathrm{i}) = (a_0 \cos(u), b_0 \sin(u), 0)^\mathrm{T} \ , \tag{4.52}$$

where a_0 and b_0 are constant and positive. Moreover, we start with an axisymmetric initial velocity given in the form:

$$\dot{\boldsymbol{X}}(u, t_\mathrm{i}) = \left(\mathcal{V}_R^0 \cos(u), \mathcal{V}_R^0 \sin(u), \mathcal{V}_Z^0\right)^\mathrm{T} \ . \tag{4.53}$$

Since no analytical solution is known, Hamilton's equations (4.33) have to be solved numerically. To simplify the numerical integration, the Lagrange multipliers λ_1 and λ_2 are chosen to vanish. In Fig. 4.4 we show one example of a surface produced by the evolution of the curve with the initial conditions (4.52) and (4.53). For increasing t the ellipse deforms and seems to turn by $90°$. At $t_f = 6.3$ the evolution stops because the curve reaches a cuspidal edge of the underlying surface. This is not evident from the figure but can be observed directly by looking at the curvature K of the surface which diverges in four points on the curve. At what point(s) the curve reaches the surface singularity first, depends on the choice of λ_1, λ_2, and the initial conditions. For instance, if we had taken other values for the Lagrange multiplier functions λ_1 and λ_2, the *same* initial conditions would have generated a *different* part of the *same* surface since the curve would have reached other points of the cuspidal singularity first.

The evolution can also terminate because the curve itself develops a singularity. This effect can be observed by looking at the pseudosphere again (see blue curves in figure 4.3). We keep the planar circle as initial curve but take a velocity which has a varying tangential component proportional to $\boldsymbol{X}'(u, t_\mathrm{i})$:

$$\dot{\boldsymbol{X}}(u, t_\mathrm{i}) = \left(\mathcal{V}_R(t_\mathrm{i}) \cos(u) - \mathcal{V}_\mathrm{t} \sin^2(u), \ \mathcal{V}_R(t_\mathrm{i}) \sin(u) + \mathcal{V}_\mathrm{t} \cos(u) \sin(u), \ \mathcal{V}_Z(t_\mathrm{i})\right)^\mathrm{T} \ , \tag{4.54}$$

where $\mathcal{V}_R(t_\mathrm{i})$ and $\mathcal{V}_Z(t_\mathrm{i})$ are given by equations (4.47). Furthermore, we set λ_1 and λ_2 to zero again. The generated surface is still the pseudosphere. However, during the course of the evolution the initially planar curve begins to deform and develops a singularity in its geodesic curvature even though the underlying pseudosphere is smooth (see figure 4.3 again).

The initial velocity must thus be carefully tuned to avoid these kinds of problem: $\dot{\boldsymbol{X}}(u, t_\mathrm{i})$ should be chosen perpendicular to the initial curve in every point. After a small time step Δt the current curve can then be used as new initial curve with an adapted initial velocity to ensure that the evolution stays perpendicular to the curve at all times. The same result can be obtained more easily if one sets $\lambda_1 = -g_{12}/\sqrt{g_{11}g_{22}}$. This adds a tangential component to $\ddot{\boldsymbol{X}}$ opposing an eventual tilt of the velocity vector out of the direction perpendicular to the curve. With this choice of λ_1 even the evolution with the initial velocity (4.54) will not develop the singularity shown in figure 4.3. The curve stays nearly planar instead and sweeps out the whole upper domain of the pseudosphere.

In the next section we will use the evolution equation (4.45) that describes c.G.c.s. to calculate the elastic properties determining the shape patterns and the preferred structures appearing in a growing thin material. In particular, we compare our findings with characteristic shapes observed in slender objects in nature.

4.3   Example 1: The pseudosphere and isometric embeddings

Having established a model for growing surfaces we can apply this formalism to biological samples like flowers commonly observed in nature. We will consider that growth imposes the Gaussian curvature of the surface, the evolving curve is the edge and we will fix the initial conditions in such a way to recover the observed shapes in nature.

As mentioned in Chap. 1, an alternative formulation of growth has been used in [42, 43] to study the evolution of a thin elastic disc. The process was decomposed into a growth step and an elastic relaxation step leading to an equilibrium configuration that contained *residual stress*. For deformations that are large compared to the thickness of the sheet (but not too large) it was proved that growth imposed the Gaussian curvature. This curvature has to vanish almost everywhere in the case of a thin elastic disc submitted to a central anisotropic homogeneous growth. The equilibrium shapes were found among the subset of surfaces with $K_\mathrm{G} = 0$ by minimization of the bending energy [42, 100].

As was stated, whereas the Gaussian curvature is zero in this special case, other objects obey different growth laws which make K_G nonvanishing. To get a handle on these processes as well, we will treat the problem of a growing sheet that evolves from a circular curve keeping K_G constant at all times t. Small perturbations from the initial conditions will show whether the state is a local energy minimum.

The resulting surfaces resemble the shape of different flowers (see Fig. 4.1) even though the actual biological processes are much more complicated. Corresponding geometries are in fact ubiquitous in nature; pseudospherical surfaces (*i. e.*, $K_\mathrm{G} < 0$)

can, for instance, be found in objects ranging from lettuce leaves [119] to various kinds of sea creatures such as sea slugs, flat worms, and nudibranchs. However, these surfaces will in general have singularities if stretching is not allowed.

4.3.1 Evolving the curve and elastic energy

We model the growth of the tissue as the motion of a closed curve $\boldsymbol{X}_t(u), u \in [0, 2\pi[$, which sweeps out a surface of constant Gaussian curvature K_{G} with increasing time $t \in [0, t_{\mathrm{f}}]$. Its evolution is described by Eqn. (4.45) which can be rewritten as:

$$\ddot{\boldsymbol{X}} = (\boldsymbol{N} \cdot \boldsymbol{X}'')^{-1} \left[(\boldsymbol{N} \cdot \dot{\boldsymbol{X}}')^2 - g(u,t)K_{\mathrm{G}} \right] \boldsymbol{N} \, , \qquad (4.55)$$

Dashes denote derivatives with respect to u and dots derivatives with respect to t. The metric determinant is then given by $g(u,t) = \dot{\boldsymbol{X}}^2 \boldsymbol{X}'^2 - (\dot{\boldsymbol{X}} \cdot \boldsymbol{X}')^2$.

At $t = 0$ the curve has some initial velocity $\boldsymbol{v}_0(u) := \dot{\boldsymbol{X}}_0(u)$. The evolution (4.55) preserves the length of $\dot{\boldsymbol{X}}$ in time for a fixed u. To ensure that the parameter t is equivalent to the arc-length, it is thus sufficient to choose $|\boldsymbol{v}_0| = 1$.

As long as the constraint on the Gaussian curvature can be fulfilled in every point, no stretching will occur in the bulk of the surface and therefore the bending energy:

$$\mathcal{F}_{\mathrm{W}}[\boldsymbol{X}] = \int \mathrm{d}u \, \mathrm{d}t \, \sqrt{g} \left(\kappa \frac{K^2}{2} + \bar{\kappa} K_{\mathrm{G}} \right) \, , \qquad (4.56)$$

is the only energy contribution. In this expression κ and $\bar{\kappa}$ denote the bending rigidity and the saddle-splay modulus, respectively, whereas K is the trace of the extrinsic curvature tensor, as we stated before. Thus, the question of determining stretching-free configurations corresponds to the problem of finding isometric embeddings of hyperbolic spaces into $\mathbb{E}^3$. Then, this geometry must minimize the Willmore functional (4.56).

At $t = t_{\mathrm{f}}$ the curve is a free edge and a *boundary layer* will exist that has to ensure that the boundary conditions of force and torque balance are fulfilled. In general this is not possible without stretching. To estimate the width Δt of this layer, the stretching energy thus has to be taken into account. The shape of the boundary layer is then determined balancing stretching and bending terms in this region. For non-Euclidean elastic plates the size of this boundary layer has been obtained in [49]. It scales with the square root of the plate thickness h, such as in the case of the width of an elastic ridge produced on a spherical shell which is subject to a punctual deformation [108].

4.3.2 Axisymmetry

For simplicity we consider an axisymmetric situation first and we assume that the curve is a planar circle of radius ρ_0 with an initial velocity parallel to the $\boldsymbol{z}$ direction. In this case $\boldsymbol{X}_t(u) = \{\rho(t) \cos u, \rho(t) \sin u, z(t)\}^{\mathrm{T}}$ and the evolution can be determined analytically. Since t measures arc-length, the condition $1 = \dot{z}^2 + \dot{\rho}^2$ holds.

The principal curvatures of an axisymmetric surface are given by $K_\perp = -\partial_\rho \dot{z}$ and $K_\parallel = -\dot{z}/\rho$. Their product is equal to the Gaussian curvature, $K_G = \partial_\rho(\dot{z}^2)/(2\rho)$. Since we want K_G to be constant throughout the growth process, it can be easily integrated yielding:

$$\dot{\rho}^2 + K_G(\rho^2 - \rho_0^2) = 0 . \tag{4.57}$$

This equation is solved by $\rho(t) = \rho_0 \cos{(\sqrt{K_G}t)}$. Consequently we have:

$$z(t) = \frac{\mathcal{E}[\![\sqrt{K_G}t, K_G\rho_0^2]\!]}{\sqrt{K_G}} , \tag{4.58}$$

where $\mathcal{E}[\![s, k]\!]$ denotes the *elliptic integral of the second kind* [1]. In the following all lengths and curvatures will be scaled with $\sqrt{|K_G|}$, *i. e.*, $\tilde{t} := t\sqrt{|K_G|}$, $\tilde{K}_\perp := K_\perp/\sqrt{|K_G|}$, etc.

If the Gaussian curvature vanishes, the sheet is a simple cylinder. For $K_G \neq 0$ singularities will occur at a finite time $\tilde{t}_s$.

For constant positive Gaussian curvature the curve will contract to a point at $\tilde{t}_s = \pi/2$. In such a case a soft tissue can only increase its circumference if axisymmetry is relaxed: in analogy to a growing flower one can, for instance, divide the surface into pieces by veins where each piece has a constant positive K_G itself (see Sec. 4.4).

Surfaces of negative Gaussian curvature will *always* exhibit singularities since the hyperbolic plane cannot be immersed completely into $\mathbb{R}^3$ [69]. Typically, these singularities are *cuspidal edges* that themselves can exhibit cusps (so-called *swallowtail points*). The axisymmetric surface has a circular cusp at $\tilde{\rho}_s := \tilde{\rho}(\tilde{t}_s) = \sqrt{1 + \tilde{\rho}_0^2}$ where $\tilde{t}_s = \text{arcsinh}\,(1/\tilde{\rho}_0)$. At that time $\tilde{K}_\parallel = -\sqrt{(\tilde{\rho}_s^2/\tilde{\rho}^2) - 1}$ vanishes and $\tilde{K}_\perp$ diverges; the surface converges towards the horizontal plane.

If the growth process stops at a time $\tilde{t}_f$ before the singularity is reached, the bending energy $\tilde{\mathcal{F}}_W := \mathcal{F}_W/(\pi\kappa)$ of the pseudospherical surface is given by:

$$\tilde{\mathcal{F}}_W = -(4 + 2m)\,\tilde{\rho}_0 \sinh\tilde{t}_f + \tilde{\rho}_s^2\left[\frac{\arctan{(\sinh\tilde{t}_f)}}{\tilde{\rho}_0} + \text{arctanh}\,(\tilde{\rho}_0 \sinh\tilde{t}_f)\right] , \tag{4.59}$$

where $m := \bar{\kappa}/\kappa$ is the ratio between the two elastic moduli associated with bending. For a thin plate it is of the order of -1 since it is given by $\nu - 1$ where ν is Poisson's ratio [83]. Note that for small $\tilde{t}_f$ the energy depends linearly on time (see Fig. 4.5):

$$\tilde{\mathcal{F}}_W \approx \frac{[(1 - \tilde{\rho}_0^2)^2 - 2\tilde{\rho}_0^2 m]\tilde{t}_f}{\tilde{\rho}_0} = \tilde{\rho}_0[(\tilde{K}|_{\tilde{t}=0})^2 - 2m]\tilde{t}_f . \tag{4.60}$$

Its minimum in this regime is thus found at $\tilde{\rho}_0^{\min} = [\sqrt{(m + 1)^2 + 3} - (m + 1)]^{-1/2}$. In the following we assume that the tissue is *incompressible* which implies that $\nu = -m = 1/2$ and $\tilde{\rho}_0^{\min} \approx 0.88$.

Close to the singularity the bending energy of the surface diverges. The real tissue will respond by relinquishing axisymmetry and the constraint on the Gaussian curva-
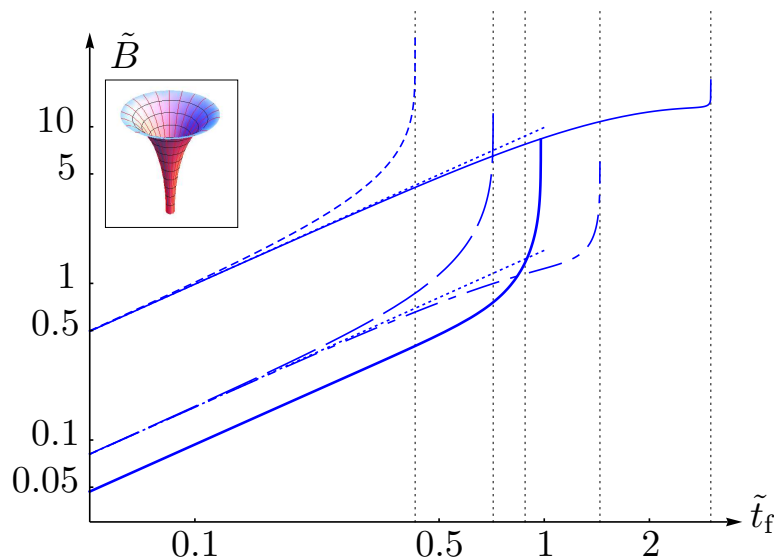
Fig. 4.5: Bending energy $\tilde{\mathcal{F}}_W$ for $m = -1/2$ and $\tilde{\rho}_0 = 0.1$ (solid line), 0.5 (dashed-dotted), 0.88 (bold solid), 1.29 (long-dashed), and 2.27 (short-dashed). Inset: axisymmetric pseudospherical surface with $\tilde{\rho}_0 = 0.1$.

ture. Stretching will then play a role as well, even *before* the singularity is reached.

4.3.3   Disturbance of the growth process

Imagine now that the initial conditions of the growth process are disturbed weakly due to external influences. For the system to stay axisymmetric the only possible change in $\boldsymbol{v}_0$ is a constant tilt in the radial direction. In this case the right-hand side of Eqn. (4.57) is equal to $\cos^2 \alpha$ where α is the tilt angle measured from the horizontal (x, y) plane. The linearity of the bending energy for small $\tilde{t}_f$ implies that it will increase for $\tilde{\rho}_0 < \tilde{\rho}_0^{\min}$ and decrease for $\tilde{\rho}_0 > \tilde{\rho}_0^{\min}$ if α is decreased slightly below $\alpha = \pi/2$.

If axisymmetry is relaxed, other scenarios are possible: the initial velocity can, for instance, have an additional component in the azimuthal direction which changes with u along the curve $\boldsymbol{X}_0(u)$. In this case the swept out pseudospherical surface is axisymmetric as well since the induced perturbation amounts just to a surface reparametrization. The evolving curve, however, will in general not stay planar any more. Moreover, singularities due to the *parametrization* can occur before the *singularity of the surface* is reached, as we have seen in Sec. 4.2.6.

If we allow small deformations from the circle, the evolution of the curve has to be determined by solving Eqn. (4.55) numerically. The new initial curve can be expanded into n modes $\boldsymbol{X}_0^n(u, \epsilon) = \rho_0^n(\epsilon)[1 + \epsilon \cos(nu)]\{\cos u, \sin u, 0\}^T$. We keep the total arc-length of this curve fixed to $L_0 = 2\pi\tilde{\rho}_0$ which implies that $\tilde{\rho}_0^n(\epsilon) = \tilde{\rho}_0/[1 + (1 + n^2)\epsilon^2/2]$.

Since the curvature of the curve has to be positive for all u to satisfy the constraint on K_G, there is a maximum $\epsilon_{\max}^n$ which decreases with increasing n. To avoid further

complications, we consider a vertical initial velocity $\boldsymbol{v}_0$ of unit length for all u. The bending energy can be calculated numerically and compared to the axisymmetric case. One finds that it increases like ϵ^2 for a fixed n and $\tilde{t}_{\mathrm{f}}$. Consequently, the system will try to stay axisymmetric during its growth.

In the following section we will study the deformations produced by a growing process on spherical surfaces. In this case stretching becomes important, concentrating in linear regions on the surface.

4.4   Example 2: A spherical surface and the stretching energy

Now we treat the case of a growing tissue with positive Gaussian curvature. Spherical and developable surfaces exhibit a common feature in reponse to deformations: the appearance of localized structures in which stretching energy is concentrated [8, 133]. In the case of spherical surfaces they are organized in intricate patterns, which transit between multiple metastable states [76, 107, 110, 133]. In this example we will use these concepts to determine the preferred shapes of an initially deformed spherical surface that grows. To achieve this in the next section we introduce the geometric and elastic properties of ridges.

4.4.1   Ridges in non-Euclidean slender structures

A ridge is a region of the surface Σ in which bending and stretching terms are of the same order. As stated, the same situation is observed in a boundary layer occurring in non-Euclidean elastic plates. We will suppose here that a regular elastic surface Σ can be deformed due to its growth process.

Ridges have been studied with the help of external loads acting locally on the surface. This classical problem has been adressed in [83, 108]. In this case a semi-spherical shell is deformed by a point-like normal force acting in its north pole. If the force is sufficiently large, a cap inversion is produced in this region. This cap minimizes the elastic energy of the configuration, since this structure preserves distances between points on Σ. In other words, the configuration is *isometric* to the spherical one and therefore the stretching energy involved is almost zero [12]. We denote Σ_n the surface produced by an isometric transformation of the original surface. Note that in the case of a growth process the original surface is not necessarily known. However, as we will see, this is not important. The surface Σ_n is not necessarily a regular configuration.

We denote Σ_r the final (and real) deformed surface. By means of a simple energetic argument we state that the final surface is very close to the isometric surface, with violation of regularity in certain lines $\mathcal{C}_n$. The neighborhood of these lines conform the ridge, where the elastic energy is concentrated. The shell is not isometric in the neighborhood to $\mathcal{C}_n$. This zone is denoted $\mathcal{C}_r$ and corresponds to the real shape.

As mentioned in Chap. 2, the elastic energy of an elastic slender body is composed by two terms. An elastic bending term accounting for the *out-plane deformations* which

is minimized by plane geometries, and a stretching term, representing the *in-plane deformations* of the body which is minimized by isometries of the reference surface (using the geometric properties of this surface, like the metric tensor or its Gaussian curvature).

A growing surface may be described by an elastic free energy of this type, where growth acts as a source of mean and Gaussian curvatures in a typical model of Föppl-von Kármán type [42]. In the previous sections we have stated that growth process can be understood as the motion of a closed curve that swept out a surface with prescribed Gaussian curvature. As a consequence of the growing process, ridges are produced to avoid singularities in the bending energy. The final surface has a discrete symmetry with respect to its center. This symmetry will be related to the number of surfaces composing Σ_n. We will determine which is the preferred symmetry that minimizes the elastic energy.

4.4.2 Constructing a piecewise c.G.c.s.

Growth processes in nature do not necessarily produce an axisymmetric final shape, as in the case of the pseudosphere. Typical examples are certain varieties of flowers and plants that present a discrete symmetry with respect to its center (see Fig. 4.1). In the case of flowers, this symmetry may be associated with a packing problem of the initial configuration that produces the final tissue [105]. Consequently, the final surfaces is composed by n identical pieces connected to each other through n *elastic ridges*. Since these ridges concentrate the stress, nature can chose to relax these stresses by *veins*, an idea suggested by Y. Couder. This idea rests on the analogy between veins in living tissues and fractures in different materials, like gel films [40].

The initial condition for the growth process is a curve composed by n circular arcs with the same radius of curvature ρ_0^n (see Fig 4.6(a)). Henceforth the superscript n indicates the dependency on the number of surface pieces.

We are interested in describing the elastic properties of a piecewise surface of constant and positive Gaussian curvature. From now on it is denoted as $\mathcal{K}_G$ to distinguish it from the pseudospherical case. At the joint between the pieces, this constraint will be relaxed and the stretching contribution will appear in order to avoid singularities.

Each piece is constructed by cutting out an axisymmetric surface Σ_s, of Gaussian curvature $\mathcal{K}_G$, with two planes P_α, which make a fixed angle $\alpha = 2\pi/n$ to each other (see Fig. 4.6(b)). The surface Σ_s is then produced by the evolution of an initial circular curve $\mathcal{C}_s^0$ of radius ρ_0^n that corresponds to the maximal equatorial circle, at $t_i = 0$.

At fixed $t > t_i$, circles on the spherical surfaces are smaller and smaller (see Fig. 4.6(b) again). The intersection between the planes P_α and the surface Σ_s is a curve on Σ_s that can be identified with the ridge. Note that for a certain $t = T_f(n)$, due to our geometrical construction, the surface leaves the vein and we will assume that the growth is stopped at this point.

However, the number n of ridges that minimizes the elastic free energy must be selected at a much earlier time $t = T_m(n)$. A parametrization of the axisymmetrical
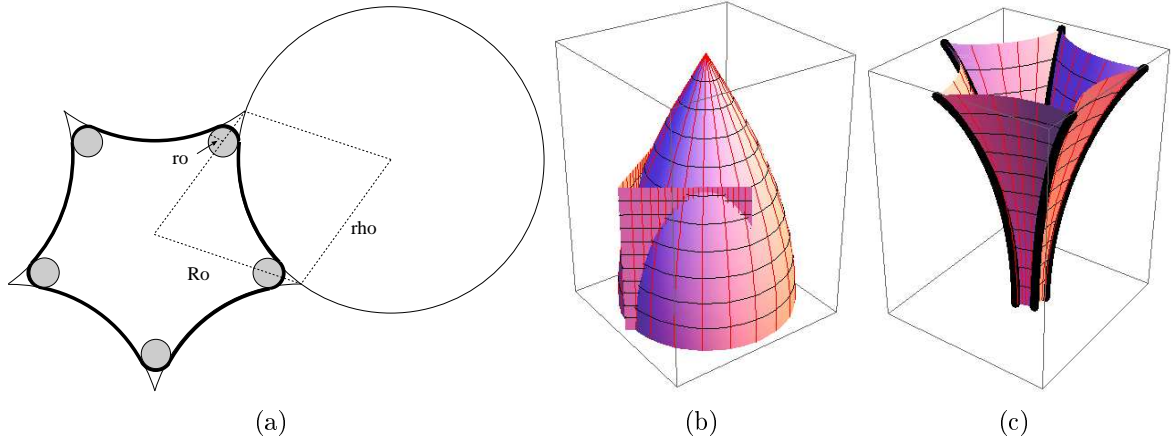
(a) (b) (c)

Fig. 4.6: (a) Constructing the initial curve $\mathcal{C}_n^0$ with $n = 5$. (b) Construction of Σ_n using a plane P_α and a spherical surface (positive and constant Gaussian curvature) Σ_s. (c) Final surface with $n = 5$.

surfaces Σ_s is given by $\boldsymbol{X}_s(\theta, t) = \{\rho(t)\cos(\theta), \rho(t)\sin(\theta), z(t)\}^T$, and we have:

$$\rho(t) \;\; = \;\; \rho_0^n \cos(t\sqrt{\mathcal{K}_G}), \tag{4.61a}$$

$$z(t) \;\; = \;\; \frac{1}{\sqrt{\mathcal{K}_G}} \mathcal{E}\left[\!\left[t\sqrt{\mathcal{K}_G}, (\rho_o^n)^2 \mathcal{K}_G \right]\!\right], \tag{4.61b}$$

where $\mathcal{E}[\![s, k]\!]$ denotes the elliptic integral of the second kind [1].

Finally the surface Σ_n is constructed by means of the union of n identical pieces of surface (see Fig. 4.6(c) for the case $n = 5$).

This surface is not regular on the ridges, since the normal vector is not well-defined. Σ_n can be interpreted as a surface that grows at the same time than Σ_s, but its initial condition is a different curve. Note that if the plane P_α is tangent to the initial curve $\mathcal{C}_s^0$ there will be no evolution and then we cannot define a surface.

Now we assume that the initial curve $\mathcal{C}_n^0$ determining Σ_n has an initial length L_0^n. There are n points on this curve describing the n starting points of the veins. These points also define a circle of radius R_0^n, centered in the z-axis of Σ_n. Using Euclidean geometry one can show that the system has to satisfy the two following equations:

$$L_0^n \;\; = \;\; 2n\delta_0^n \rho_0^n, \tag{4.62a}$$

$$R_0^n \sin\gamma(n) \;\; = \;\; \rho_0^n \sin\delta_0^n, \tag{4.62b}$$

where δ_0^n is the angle sustained by ρ_0^n, and $\gamma(n) = \pi/n$.

In order to compare the energy of surfaces with different values of n we need to fix some quantities at the initial time. We need to establish a selection process which rests on the variational property of elasticity. For this purpose we consider surfaces with different values of n, but with specific initial conditions.

Henceforth we assume that the initial length of the curve L_0^n and the initial radius of curvature ρ_0^n are independent of n. In this way we can determine the initial angle δ_0^n and the initial radius R_0^n. Defining $\epsilon = L_0/2\pi\rho_0$ we finally have:

$$\delta_0^n(\epsilon) = \epsilon\left(\frac{\pi}{n}\right) , \tag{4.63}$$

$$R_0^n(\epsilon) = \rho_0 \csc\left(\frac{\pi}{n}\right) \sin\left(\frac{\pi\epsilon}{n}\right) . \tag{4.64}$$

As mentioned, there is a maximal value for δ_0^n in which case there is no intersection between the plane P_α and the spherical surface Σ_s. We denote this maximal value as $\delta_m^n = \pi/2 - \gamma(n)$. The maximal angle implies that the possible values of ϵ are restricted: $0 < \epsilon < 0.5$.

The free energy can be minimized as a function of n or as a function of ϵ. That means, for each fixed value n the elastic free energy minimization must be performed for different values of ϵ.

Using this construction each piece of Σ_n is parametrized as:

$$\boldsymbol{X}_n(u,t) = \{r(u,t)\cos(r), r(u,t)\sin(u), z(t)\}^T , \tag{4.65a}$$

$$\begin{aligned}
r(u,t) = &-\sqrt{\rho_0^2\left(\cos^2\left(t\sqrt{\mathcal{K}_G}\right) - \csc^2\left(\frac{\pi}{n}\right)\sin^2(u)\sin^2\left(\frac{\pi(\epsilon+1)}{n}\right)\right)} \\
&+ \rho_0 \csc\left(\frac{\pi}{n}\right)\cos(u)\sin\left(\frac{\pi(\epsilon+1)}{n}\right) ,
\end{aligned} \tag{4.65b}$$

and the coordinate z is given by:

$$z(t) = \frac{1}{\sqrt{\mathcal{K}_G}}\mathcal{E}\left[\!\left[\sqrt{\mathcal{K}_G}, (\rho_o^n)^2\mathcal{K}_G\right]\!\right] , \tag{4.66}$$

where $0 \leqslant u \leqslant \pi/n$ and $0 \leqslant u \leqslant T_m$. Note that in this parametrization, the piecewise surface is symmetric with respect to the x-axis. In order to calculate the radius $r(u,t)$ it is necessary to take into account the distance $l(\epsilon,n)$ between the z-axis of the surfaces Σ_s and Σ_n. It is a constant in time, but it depends of n and ϵ. Finally the total surface can be obtained if we change $u \to (\mathrm{mod}\{nu + \pi, 2\pi\} - \pi)/n$ in the function $r(u,t)$ and $0 \leqslant u \leqslant 2\pi$, as can be seen in Fig.4.6(c).

By means of this construction the values of $R(t)$, $\rho(t)$, $\delta(t)$, and T_m can be easily obtained as function of the known parameters. The maximal possible time is given by:

$$T_m(\epsilon,n) = \frac{\gamma(n)(n - 2(\epsilon+1))}{2\sqrt{\mathcal{K}_G}} , \tag{4.67}$$

and it is possible to determine that, for certain fixed value of ϵ we have; $T_m(\epsilon,3) < T_m(\epsilon,4) < \ldots$ when n increases. Then, in order to compare the different symmetries we take $T_m(\epsilon,3)$ as the final time of growth. It is evident that the minimal case of

interest is $n = 3$. It is noteworthy that is not possible to choose any initial conditions that allow us to get an initial curve with the minimal symmetry. For example, if we consider R_0^n and L_0^n as independent parameters we cannot satisfy simultaneously the initial constraint $\delta_0^n < \delta_m^n$ for all the values of n.

We are interested in describing the geometry and the elasticity of a real deformed surface Σ_r having a discrete symmetry with respect to its center. This surface represents the mean surface of an homogeneous and isotropic elastic shell (or plate) which has a constant thickness h. In addition it is not necessarily Euclidean. This final shape is produced by the elastic deformation originated by the growth process.

We will also assume that the final shape is, in a sense, geometrically inflexible and therefore its geometry is close to the geometry of Σ_n. It can be supposed that this *virtual* surface comes from an isometric deformation of a certain initial unknown surfaces [108]. In Σ_n, violation of regularity is present for certain lines $\mathcal{C}_i$, where bending energy becomes infinite. Consequently, after the elastic relaxation, an elastic ridge of a given size ω occurs in the neighborhood of these lines. Elastic stretching energy is concentrated here.

The piecewise surface Σ_n parametrized by (4.65b) is not regular on the ridges. In order to regularize the surface we will suppose that there exist veins of a given size r_0 at each ridge. The n veins add an additional term to the total elastic energy since the surface wraps a part of each vein. Consequently the surface takes the form of the vein in this region.

In this case, the size of the ridge is known and the two principal radii of curvature can be estimated. The small one is approximately r_0 and the larger is given by the growth of the tissue in the direction of time. Note that the regularization of the surface violates the restriction of constant positive Gaussian curvature, and thus stretching will occur in this region.

In order to consider the shape of the ridge, we suppose that at each fixed time a small circle of radius r_0 is tangent to two pieces of Σ_n. As the angle ϕ between the two pieces in the ridge becomes smaller when time increases and the surface grows, the center of the small circle moves on the line with constant angle $u_f = \pi/n$. This distance $d(t)$ is a function of t. Note that the distance ω between the two tangent points at each piece is not constant in time. By means of simple geometrical relations we obtain some properties of the ridges as function of the original angle:

$$
d(t) = -\csc\left(\frac{\pi}{n}\right)\left(\rho_0 \cos\left(t\sqrt{\mathcal{K}_G}\right) + r_0\right)\sin\left(\frac{\pi}{n} - \sin^{-1}\left(\frac{\rho_0 \sin\left(\frac{\pi(\epsilon+1)}{n}\right)}{\rho_0 \cos\left(t\sqrt{\mathcal{K}_G}\right) + r_0}\right)\right),
$$
(4.68)

In our parametrization each piece of the surface is isometric to a surface of constant Gaussian curvature, except in a region given by a critical angle $U_c(t)$, which corresponds to the angle sustained by $r(u, t)$ at the tangent point between the small circle of radius r_0 and the isometric piece of surface. Then, the ridge is constrained at the intervals

$U_c(t) \leqslant u \leqslant \gamma(n)$, and $0 \leqslant t \leqslant T_m(\epsilon, 3)$, where we have:

$$U_c(t) = \frac{\pi}{n} - \arctan\theta \, , \tag{4.69}$$

and

$$\theta = \frac{r_0 \sin\left(\frac{\pi(\epsilon+1)}{n}\right)}{\left(\rho_0 \cos\left(t\sqrt{\mathcal{K}_G}\right) + r_0\right) \left(\cot\left(\frac{\pi}{n}\right) \sin\left(\frac{\pi(\epsilon+1)}{n}\right) - \cos\left(t\sqrt{\mathcal{K}_G}\right) \sqrt{1 - \frac{\rho_0^2 \sin^2\left(\frac{\pi(\epsilon+1)}{n}\right)}{\left(\rho_0 \cos\left(t\sqrt{\mathcal{K}_G}\right)+r_0\right)^2}}\right)} \, . \tag{4.70}$$

Using this, we establish a parametrization for the ridge. It is given by:

$$\boldsymbol{X}_r(u,t) = \{r_r(u,t)\cos(r), r_r(u,t)\sin(u), z(t)\}^T \tag{4.71}$$

where the radius $r_r(u,t)$ is a solution of the quadratic equation:

$$r_r(u,t)^2 - 2r_r(u,t)d(t)\cos(\gamma(n) - u) + d(t)^2 - r_0^2 = 0, \tag{4.72}$$

and the function $z(t)$ is given by the equation (4.61b). Then, using this construction, a piecewise surface can be obtained joining the n identical pieces and ridges. The parametrization of the final surface is splitted in two parts. The first one is an isometric part and the second one is the parametrization of the ridge. Note that the Gaussian curvature of the ridge is not constant. An elastic energy associated with stretching deformations must thus be calculated with respect to the isometric surface at the ridge. In the next section we will specify how the elastic free energy minimization selects certain symmetries.

4.4.3 Elastic energy of the total piecewise surface

Once the mathematical description of Σ_n has been established, we calculate its total elastic energy. This elastic energy must be composed by the stretching and bending terms. In order to compare the different configurations we will suppose that the surface, which is produced by a growth process, is an homogeneous and isotropic nonlinear elastic shell. A typical elastic theory of shells has been proposed by Koiter in 1966 [75]. A modern and formal interpretation of this theory can be found in [39] where the theory is formulated using the elements of three and two-dimensional differential geometry. The elastic theories of shells and plates are usually obtained by a dimensional reduction of the well established three-dimensional theory of finite hyperelasticity which was developed in the first years of the nineteenth century by Cauchy and Poisson. Using the fact that the thin dimension is much smaller than the other dimensions and also the standard *Kirchhoff-Love* assumption (see for example [92]) the elastic energy is written as a surface integral in terms of the middle surface of the shell. Another principal assumption is that the reference configuration is a *natural state*, i.e, there are not

mechanical stresses when the shell adopt this configuration.

Nevertheless, we know that slender elastic bodies having the ability to grow (such as plant leaves and flowers) exhibit residual stresses, and therefore in absence of external forces their natural geometry is not necessarily Euclidean. Several efforts have been made in order to incorporate this constriction in a coherent bi-dimensional elastic theory. In [43] the growth process is considered as a "plastic" deformation that changes the body from the natural unstressed configuration to some virtual one. This virtual configuration finally relaxes to a current configuration by means of an elastic processes. All this structure can be mathematically taken into account using a multiplicative decomposition of the deformation gradient elastic tensor. In this way, when the dimensionality of the elastic material is reduced and the deformations are not too large, the equations that describe the equilibrium of the plate are of Föppl-von Kármán type where growth is a source of both mean and Gaussian curvatures.

Another approach has been developed in [50]. They do not consider deformations which are not of elastic nature and therefore virtual configurations are supposed to be known. In this case the reference state is not constrained to be Euclidean and consequently residual stresses are allowed. The dimensional reduction from three dimensional theory is performed using the same assumption as in the case of Koiter's shell theory. As a result they obtain that the elastic energy of the slender body is a surface integral of the two dimensional middle surface describing this body. In this surface, stretching and bending terms are writing as functions of the geometrical properties of the surface, such as the metric and the curvature tensor. Furthermore, the reference metric is not necessarily immersible in three dimensional space and there is not a reference configuration in which stresses vanish. Their model is a Koiter's type model in which the target curvature tensor K_{ab} is set to zero.

As in the Föppl-von Kármán theory, the bending term is proportional to h^3 and the stretching term is proportional to h, where h is the thickness of the thin elastic shell:

$$E(K, g) = h \int_S \Omega_S(g) dS + h^3 \int_S \Omega_B(K) dS , \qquad (4.73)$$

where S is reference surface, $dS = \sqrt{G} d\xi^1 d\xi^2$ is the infinitesimal surface element, G is the determinant of the reference metric G_{ab}, and the stretching and bending densities are expressed as:

$$\Omega_S = \frac{1}{8} \mathcal{A}^{abcd}(g_{ab} - G_{ab})(g_{cd} - G_{cd}), \qquad (4.74)$$

$$\Omega_B = \frac{1}{24} \mathcal{A}^{abcd} k_{ab} k_{cd}, \qquad (4.75)$$

where k_{ab} is the *curvature tensor* of the current final surface and the *elasticity tensor* $\mathcal{A}^{abcd}$ is deduced supposing that the hyperelastic material is homogeneous and isotropic,

$$\mathcal{A}^{abcd} = \frac{Y}{2(1+\nu)} \left(\frac{2\nu}{1-\nu} G^{ab}G^{cd} + G^{ac}G^{bd} + G^{ad}G^{bc} \right) , \qquad (4.76)$$

where Y, ν are the Young's modulus and the Poisson ratio respectively.

In our case, the surface Σ_n can be considered as a stressed reference configuration from which the final surface is obtained by elastic relaxation. Using the symmetry of the problem, the elastic energy can be calculated in two parts. In the first part, the current deformed configuration is an isometry of the reference metric $g_{ab} = G_{ab}$, and the bending elastic energy is reduced to the Willmore functional, as stated before. Its energy density is given by:

$$\Omega_W(u,t) = \frac{h^3 K(u,t)^2}{24(1-\nu^2)} - \frac{h^3 \mathcal{K}_G(u,t)}{12(1+\nu)} , \qquad (4.77)$$

where K is the mean curvature of the surface and $\mathcal{K}_G$ its Gaussian curvature. This first part of the elastic energy is calculated in the region $0 \leqslant u \leqslant U_c(t)$ and $0 \leqslant t \leqslant T_m(3)$. Then the metric G_{ab} is given by the parametrization of the piece of surface (4.65b) in the entire limit $0 \leqslant u \leqslant \gamma(n)$ and $0 \leqslant t \leqslant T_m(3)$. If G denotes the determinant of this metric and using the obvious symmetry of the problem the isometric elastic energy of the piecewise surface is:

$$E_{iso}(n) = \int_0^{T_m(3)} \int_0^{U_c(t)} 2n\sqrt{G(n)}\Omega_W(u,t;n)\mathrm{d}u\mathrm{d}t . \qquad (4.78)$$

Almost all the functions depend on L_0, ρ_0, $\mathcal{K}_G$ and r_0. The second part of the total elastic energy is concentrated at the ridges. The reference metric is the same as in the first part, but the current final surface is approximated by the surface imposed by the vein on Σ_r. The stretching term is present to avoid singularities in the bending. We will use (4.73) to calculate the elastic energy. This time, the current metric g_{ab} is given by the parametrization (4.65b). The region of integration is given by $U_c(t) \leqslant u \leqslant \gamma(n)$ and $0 \leqslant t \leqslant T_m(3)$. The final expression is:

$$E_{rid}(n) = \int_0^{T_m(3)} \int_{U_c(t)}^{\gamma(n)} 2n\sqrt{G(n)}\Omega_R(u,t;n)\mathrm{d}u\mathrm{d}t , \qquad (4.79)$$

where the term Ω_R is the sum of stretching and bending density energies evaluated in the ridge parametrization:

$$\Omega_R(u,t;n) = h\Omega_S(u,t;n) + h^3\Omega_B(u,t;n) . \qquad (4.80)$$

The total elastic energy is the sum of (4.78) and (4.79). We find the value of n such that the total elastic energy is minimized. The energy is numerically calculated varying n and the others parameters. Some results are showed in the Figure (4.7).

We can see that the elastic energy reaches its minimum value when $n = 5$ and for

(a)
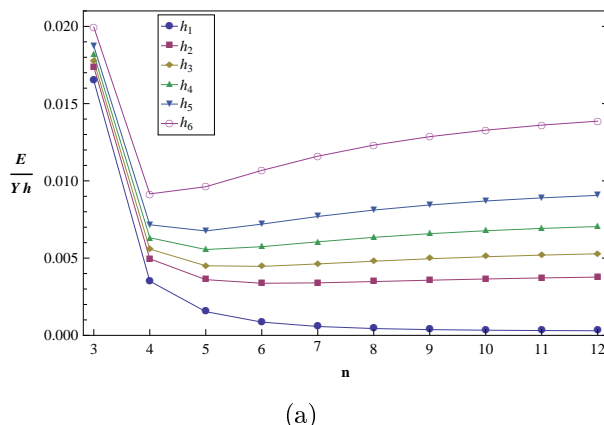
Fig. 4.7: Elastic energy of a piecewise surface as a function of n. The values of the parameters are: $r_0 = 0.02\rho_0$, $\nu = 0.5$, $\mathcal{K}_G = 1$, $L_0 = 1.5\rho_0$, $\rho_0 = 1$. Each curve represents different thickness values: $h_1 = 0.012$, $h_2 = 0.027$, $h_3 = 0.032$, $h_4 = 0.037$, $h_5 = 0.042$ and $h_6 = 0.052$. When the thickness is of the order of the ridge width ($\omega \approx 0.04$), the energy is minimized by $n = 5$ (yellow (3), green (4) and blue (5) curves, respectively). All length values are dimensionless

values of thickness that are comparable to the width of the ridge. When the thickness decreases, the minimum moves to $n = 6, 7 \ldots$, (see Fig. 4.7 again)

The minimum is not very deep and this indicates a possible dispersion which can probably be corrected considering an additional elastic term in the total elastic energy. However, our results are consistent with the symmetries presented in [105] where it is mentioned why most of the flowers have five or six petals.

It is important to note that in this approximation we have not considered the elasticity of the vein. This may be included assuming that a single vein is well described as an elastic rod. In such a case, *Kirchhoff's theory of rods* is the most appropriate mathematical framework to deal with the vein elasticity. However this increases the number of parameters that must be considered in our approach, such as the elastic bending rigidity of the vein. Then, we will not considered this assumption here.

4.5   Summary and discussion

In this Chapter we have presented a Hamiltonian formulation for the construction of constant Gaussian curvature surfaces. In the approach the geometry of the surface is reconstructed from the evolution of a closed curve in three-dimensional Euclidean space. This evolution is determined by an appropriate geometrical energy functional which is interpreted as an action. The final equation that has to be solved is of second order in the position vector. The formalism is general and allows to describe surfaces without any symmetry. It is particularly useful if one wants to construct these surfaces numerically. To this end the initial conditions and the tangential components of the acceleration have

to be properly adjusted to avoid singularities in the evolving curve. Surfaces of negative constant Gaussian curvature additionally exhibit singularities themselves which cause the evolution to stop. Tuning the conditions to find a whole cuspidal edge of the surface requires further studies but is straightforward.

The approach can, for example, be applied to a growing thin sheet where growth imposes the Gaussian curvature on the surface. As long as the sheet is able to assume its target configuration no stretching will occur. The correct shape of the surface at a certain time t can then be found by minimizing the bending energy in the subset of surfaces that obey the initial conditions. Singularities that occur during the evolution imply that the target configuration cannot be immersed completely into $\mathbb{E}^3$ any more. A combination of stretching and bending will then have to accommodate the constraints imposed by growth and elasticity. The presented formulation paves the way to treat such physical problems since it offers one tractable method to determine isometric immersions of the surface numerically.

We have focused on two examples that are relevant to describe the shape adopted by growing soft tissues in nature. First, we have shown that the *pseudosphere* is the axisymmetric surface having the minimal bending energy with respect to its perturbations during the growth process. The perturbed bending energy grows with the square of ϵ, the perturbation parameter. Determining surfaces with the same metric (and therefore the same Gaussian curvature) corresponds to finding isometric immersions in $\mathbb{E}^3$. But this problem is mathematically possible only for compact surfaces (which is our case when the perturbation takes place). Consequently, the stretching energy must not be considered and the energetic contributions are only due to bending. A pseudosphere resembles the shape of a *Daffodil* as is depicted in Fig. 4.1(b). However, the end of this flower is characterized by nice ondulations (see Fig. 4.1(b)). One may think to perform a boundary layer in which stretching energy becomes important, giving the wavy behavior.

As a second example we have treated surfaces having singularities at the beginning of the growth process. These singularities can be interpreted as ridges in the elastic theory of shells, or as veins for the case of soft tissues. In this case, a growing surface with constant Gaussian curvature has been constructed and its symmetries have been analyzed with respect to its energy minimization. We find that for values of the thickness compare with the size of the veins, the elastic energy is minimized by surfaces having $n = 5$ identical pieces. This behaviour is displayed by natural growing tissues, like flowers. *Brugmansia* and the *Morning Glory*, which are depicted in Fig. 4.1(a) and in Fig. 4.1(c) respectively, show this pentagonal symmetry. Despite its predictions, this model is nevertheless too simple to be transferred to growth process in nature. In this way, more complicated growing behavior may come, for example, from microscopic considerations [47].

Chapter 5

PACKING PROBLEM. AN EXPERIMENTAL APPROACH

In this Chapter we present an experimental approach to the packing of flexible elastic structures. Using a simple experimental setup we have characterized the geometric features of the shapes adopted by a two-dimensional elastic sheet confined to "growth" within a cylindrical fixed structure. In addition, this experimental setup has also simultaneously allowed to measure the mechanical force exerted on the container by the different configurations of the elastic sheet during the growth process. A phase diagram has then been obtained and compared with numerical simulations of the elastic theory of the rods and cylindrical sheets, showing an excellent agreement without any adjustable parameter.

5.1   Introduction

In the previous chapter we have presented a geometrical description of the growth process that occurs in biological soft tissues like flowers and plants. In all given examples, the slender structure grows without any element that confines its geometry.

In this chapter we study another aspect of the geometry of growth: the behavior of closely packed objects. In particular we focus on the packing of slender elastic sheets within a fixed container. Our approach will be experimental and our findings are compared with numerical simulations of the elastic theory of rods. The possible shapes adopted by elastic rods and their mechanical properties are determined by solving the equation of Euler's *Elastica*:

$$B \left[\frac{d^2\kappa}{ds^2} + \left(a^2 + \frac{1}{2}\kappa^2 \right) \kappa \right] = k \ , \tag{5.1}$$

where κ is the curvature of the road at arc-length s, B is the bending modulus, a is an undetermined constant of integration, and k represents the external normal forces. However, this equation does not consider the physical condition of self-avoidance, which is characteristic for the packing process.

Closely packed objects are ubiquitous in nature. Some examples include the folding of leaves in buds, the wing folding of insects in cocoons, the crumpled paper or the DNA packaging in capsids. The theoretical treatment of this class of problems sometimes becomes very complicated and numerical or experimental studies are necessary.

Fig. 5.1: (a) A schematic setup for conical packing. (b) Typical pattern at high confinement. The different curves appearing during the "growth of the elastic rod" are also depicted. (c) A typical pattern observed at lower confinement showing the emergence of complex structures [21].

A first experimental approach to the packing of elastic slender structures has been performed in conical geometry. It has been inspired by the setup used to study single developable cones [32, 35]. In this chapter we focus on the early stages of confinement in which the packing of the structure remains cylindrical. We know that conical and cylindrical geometries are described by the same equations, except for slightly different developability constraints [34]. In addition, for large confinements a thin cone is equivalent to a cylinder. In the next section we explain how to design an experimental setup that measures simultaneously the forces into the container and the shape of the configurations, when a elastic cylindrical sheet grows inside.

5.2   Experimental approach

The experimental setup designed for conical packing allows measurements of forces in the case of high confinement. It is also able to easily depict the shapes adopted by these complex configurations. However, despite the complexity we can identify the building blocks of these intricate patterns as *spiral structures* which are produced at the beginning of growth (see Fig. 5.1).

Consequently, it is necessary to study in detail the generation of an isolated spiral to understand the emergence of more complex patterns. For this purpose we have designed an experimental setup, as shown in Fig. 5.2.

Let us consider a very long elastic sheet rolled into the shape of a circular cylinder of radius R. The lateral ends of the sheet are glued to each other and the resulting long cylindrical sheet is then introduced into a cylindrical container of inner radius $b < R$, as is shown in Fig. 5.2.

A cylindrical tube serves as a container. The inner radius b of this structure is sufficiently small compared to its height H. Therefore, the complete device is axially symmetric and consequently all the cross sections of the container correspond to the

following two-dimensional packing problem: A closed elastic rod confined to growth into a two-dimensional disk of fixed radius b (see Fig. 5.3(a)). Consequently, we can say that our experimental approach is *quasi-two-dimensional*.

We are then interested in measuring the pushing force necessary to move the cylindrical sheet within the container along the direction of the axis of symmetry z. Moving slowly the sheet, we are able to measure the *tangential force* F_t acting on it. This force is related to the mean normal pressure P exerted on the container through *Coulomb's law*:

$$F_t = \mu 2\pi bHP \ , \tag{5.2}$$

where μ is the *dynamic friction coefficient* between the elastic sheet and the container. It will be determined experimentally. Note that the measurement of the force must always be almost constant, because the confinement is isotropic and there is no privileged direction on the section of the sheet that remains attached to the container.

5.2.1 Experimental setup

Below we will describe the experimental setup that has allowed us to measure the force. Note that this setup achieves the goal of simultaneous observation of configurations and measurement of pushing force. For this purpose we have used a piston-type device, which is schematically depicted in Fig. 5.2. It is principally composed by the following parts:
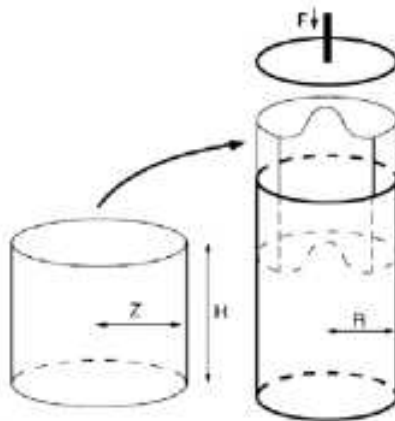
Fig. 5.2: Schematic setup for cylindrical packing. An elastic sheet is glued into a cylinder and introduced into a cylindrical container of fixed inner radius.

1. *Container*: A cylindrical Plexiglas tube of inner radius $b = 2.6[cm]$ and height $H = 38[cm]$ which has been fixed to a rectangular structure by means of a square aluminum platform ($17 \times 17[cm^2]$) with a circular hole, whose radius is exactly the same as the one of the container.
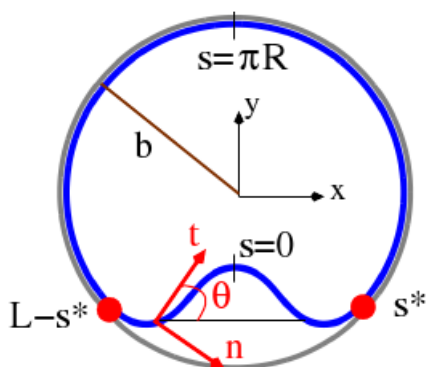
(a) Cross sectional view of the theoretical frame. Some of the typical parameters defined in [34] are depicted. From [20].
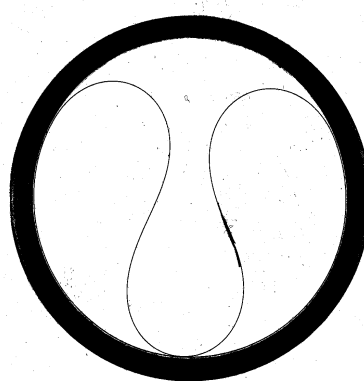
(b) Cross sectional view of a cylindrical sheet confined within the cylindrical container. The darker piece of the sheet corresponds to the overlap region.

Fig. 5.3: Cross section of the experimental setup.

2. *Motor*: The rectangular structure in which the container is mounted, supports in its upper extremity a motor. This device displaces a vertical frame (maximal displacement $h_{max} = 38[cm]$) with a constant velocity $\boldsymbol{v} = -v\widehat{z}$. The velocity and the length of displacement are controlled by a computer. We have used $v = 500[\mu m/s]$ in all our experiments. To measure the force we use a *dynamometer* which is situated at the bottom of the frame (sensitivity: $0,01[N]$, maximum supported force: $100[N]$).

3. *Aluminum disc*: At the bottom of this dynamometer we have screwed an aluminum disc (a piston-like device, see Fig. 5.2) of radius $r = 2.5[cm] < b$. This piston-like structure moves with the same velocity as the entire device (frame + dynamometer). Finally, the disc displaces the elastic sheet for each different configuration within the container.

The cylindrical elastic sheets have been obtained using a Mylar sheet of thickness $h = 0.1[mm]$ and bending modulus $B = 6.610 \times 10^{-4}[Nm]$. It has been cut in different sizes to produce multiple configurations. As mentioned, the lateral ends of the sheets are glued to each other to produce several cylindrical structures with different perimeters $L = 2\pi R$, R being the radius of the cylindrical sheet. Two different ways to glue the lateral ends have been used. They will be explained in the next section to illustrate the typical data recorded.

5.2.2   Data recorded

The typical procedure of measurement starts introducing the sheet into the cylindrical container. We produce different spiral configurations for different values of the perimeter of the sheet. All the configurations have been prepared according to the topologies observed in the conical geometry. When the sheet is introduced inside the smaller cylindrical container we let it relax to an equilibrium shape, by tapping, in order to minimize the effect of the friction at the lineic self contacts.

The bottom of the aluminum disc must almost touch the upper part of the cylindrical sheet. With the help of a computer, we start the motor at a constant velocity and thus the folded sheet is pushed along the inside of the container. The pushing force F_t is recorded when a steady state is reached by means of a software that is capable of recording a measure of the force captured by the dynamometer each $0,02[seg]$. Then, we dispose of 400 data points of the pushing force for each configuration. The same procedure is repeated for each configuration with different values of the perimeter. Finally we can obtain, using Eqn. (5.2) a phase diagram of the exerted pressure as function of the *confinement parameter*:

$$\epsilon = \frac{R - b}{b} > 0 \; . \tag{5.3}$$

Typical results of the measurement of the force are shown in Fig. 5.4 and Fig. 5.5.

5.2.3   Mechanical and elastic properties of the sheet

It will be useful to determine experimentally some elastic and mechanical quantities related to the elastic mylar sheet, such as the bending rigidity B and the dynamic friction coefficient μ between the sheet and the container. To measure μ we have disposed a strip of the mylar sheet inside the cylindrical container and we have measured the angle θ from which the elastic strip begins to move. Then, the dynamic friction coefficient is given by the simple relation $\mu = \tan\theta$. In our case we have determined $\mu \approx 0.37$.

Now, to determine B we have observed the curvature of an elastic mylar strip produced by its own weight. Thus, the shape of the strip is described by a function $z(l)$ which verifies the equation $Bz^{(4)} = \rho g h$ [83] where ρ is the density of mass, h is the sheet thickness, g is the gravity. Solving this equation we have:

$$z(l) = \frac{\rho g h}{24B} l^4 \; . \tag{5.4}$$

Using a strip without spontaneous curvature we have measured different values of the height z and the length l. Fitting these points we find $B = 0.0006566[\frac{Kgm^2}{s^2}]$. Experimental values are shown in Fig. 5.6.
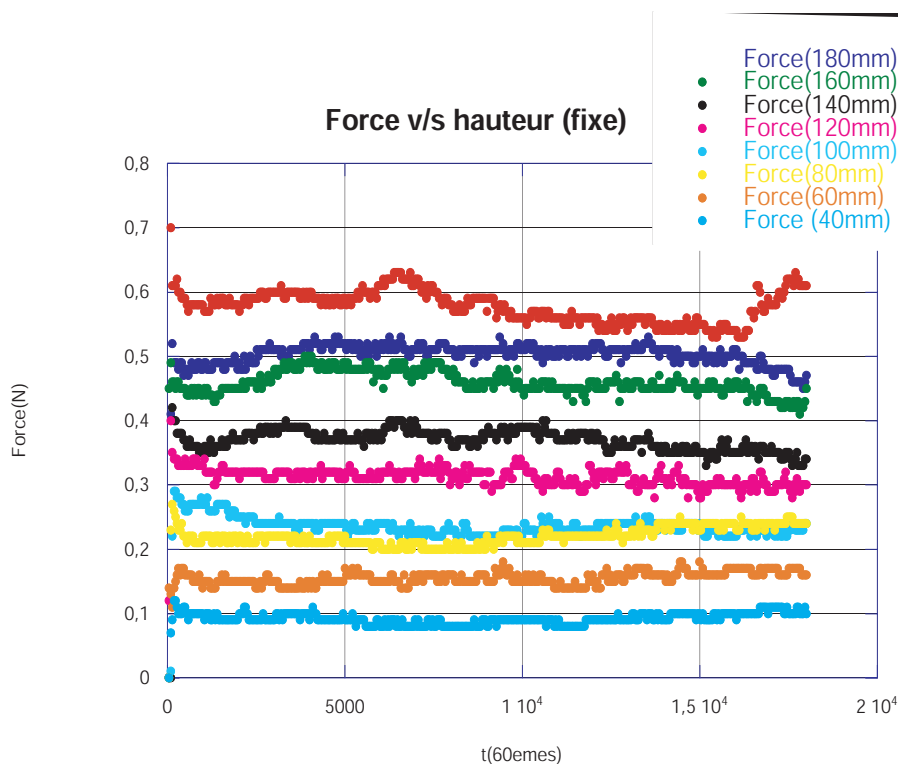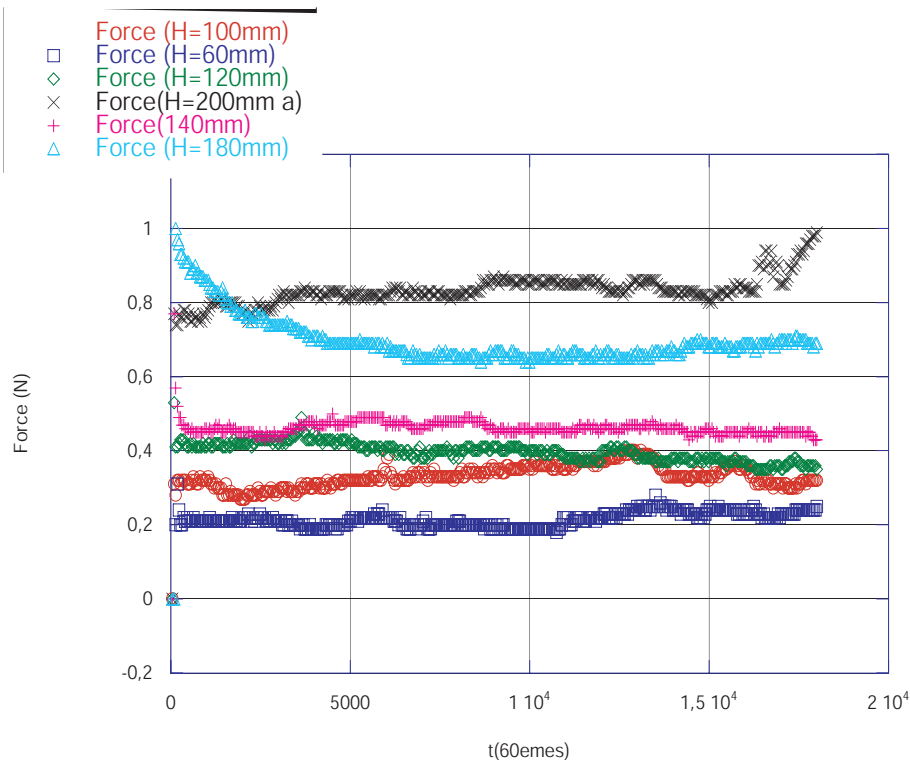
Fig. 5.4: Measures of forces for different heights of the cylindrical sheet. The value of the perimeter is $L = 200[mm]$. To glue each end of the sheet we have only put them in contact.

5.3   A phase diagram

Having defined the measurement protocol and the elastic and mechanical properties of the sheet we now show the resulting phase diagram of the pressure exerted on the container. First, we will describe the successive configurations that characterize the early stages leading to the generation of *spirals* during the packing process.

5.3.1   Towards the spiral configuration

Before analyzing the force acting on the container, it is necessary to characterize the different configurations that are allowed when the intensity of confinement increases *i. e.*, when the *packing parameter* ϵ grows. For low confinement the first configuration corresponds to a *small fold* which is symmetrical with respect to the diameter of the container. This configuration is depicted in Fig. 5.7(a).

This central fold starts to grow and its center moves inward until its extremities become diametrically opposed (see Fig. 5.7). Experimentally, the total force exerted on the container decreases as the parameter ϵ increases, as shown in Fig. 5.9. It corresponds to the measures of force for symmetrical configurations.

Fig. 5.5: Measures of force for different heights of the cylindrical sheet. The value of the perimeter is again $L = 200[mm]$. To glue the ends of the sheet to each other we have overlapped a small tip of the sheet over the other end. The size of the overlap region is $3[mm]$.

As a consequence, the bottom of the sheet, which initially was in contact with the inner wall of the container, slightly rises from it. This is very difficult to observe experimentally because this occurs a small scale (of the order of the sheet thickness) but in Fig. 5.7(b) it can be slightly appreciated. This configuration may be better perceived through numerical simulations [20, 21], where the contact between the sheet and the container is reduced to two diametrically opposed points which maintain the mechanical equilibrium of the sheet (inset 2 in Fig. 5.15). So far the sheet does no exhibit self-intersections.

Although the force decreases, the perimeter of the sheet continues to grow and consequently at $\epsilon \approx 0.25$ a first *self-contact* appears between the inward fold and the bottom of the sheet (see Fig. 5.7(c)). This type of configurations are unstable experimentally and can be only observed in a small region of the parameter ϵ.

As ϵ is increased the self-contact is driven back toward the inner wall of the container and finally reaches it, producing a particular configuration which is difficult to observe experimentally (see Fig. 5.7(d)) but, it may be again appreciated numerically (inset 4 Fig. 5.15). This configuration exhibits three points in contact with the container and it
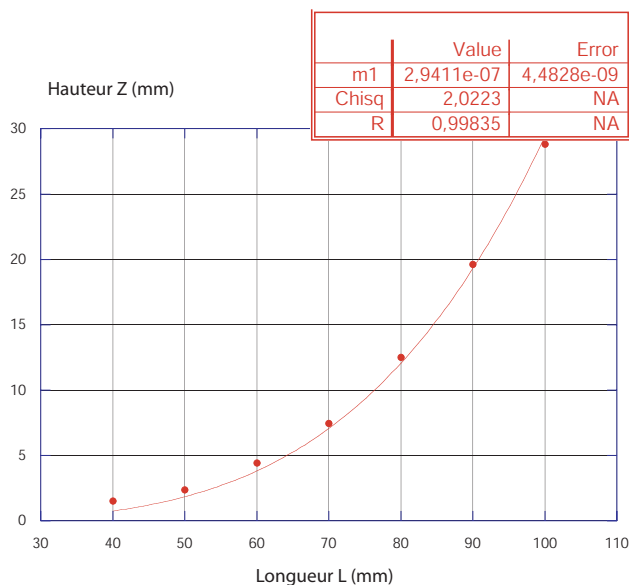
Fig. 5.6: Fit height v/s length to measure the bending rigidity B.

exists in the region: $0.31 \lesssim \epsilon \lesssim 0.39$. This additional support produces a subtle increase in the force acting on the container. The dimensionless force is shown in Fig. 5.9 and the dimensionless pressure in Fig. 5.15. As mentioned, this configuration is not easy to observe in the experiment and it exists in a small region of ϵ.

If ϵ continues to increase, the lower contact point becomes a *lineic contact* (a small curve, see Fig. 5.8(a)). This region comes back in contact with the container leaving only two symmetrical curves S connected through a contact point with the container for the region $0.39 \lesssim \epsilon \lesssim 0.62$. The top of the sheet starts to increase towards the top of the container. Consequently, a *second self contact* appears at $\epsilon \approx 0.62$ (see Fig. 5.8(b) and the inset 6 in Fig. 5.15). As the packing parameter increases, the lower contact point flattens out into an extended zone of self contact, above $\epsilon \approx 0.71$, as is depicted in Fig. 5.10 (see also inset 7 in Fig. 5.15).

The loop formed by the closed fold starts to grow to become unstable. In numerical simulations the two punctual self-contacts are maintained in configurations V and VI (bottom and top), but this is not easy to observe experimentally.

The loop stops growing when the lower self-contact becomes lineic. While symmetrical configurations disappear at $\epsilon \approx 1.04$, asymmetrical configurations may appear above $\epsilon \approx 0.85$ and there exists a *region of coexistence* between them (see Figs. 5.10(b) and 5.11(b), for example).

Then, a lower bump of one curve S composing the top loop, suddenly dives into the convex part of the second curve S forcing the lower self-contact to slide away from its symmetrical initial position (see Fig. 5.11). In the region $0.6 \lesssim \epsilon \lesssim 1.17$ asymmetrical configurations are metastable. They begin to be stable in the region $1.17 \lesssim \epsilon \lesssim 1.25$.
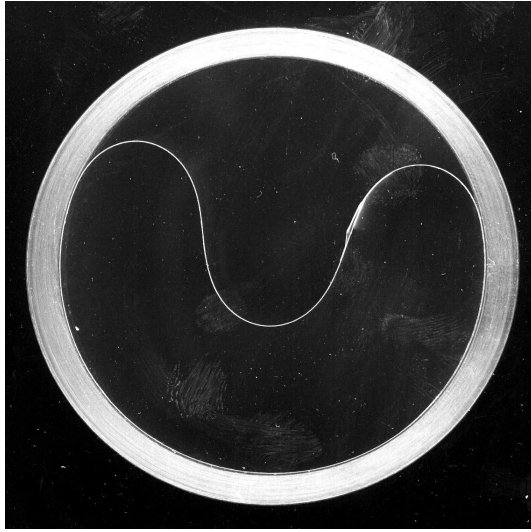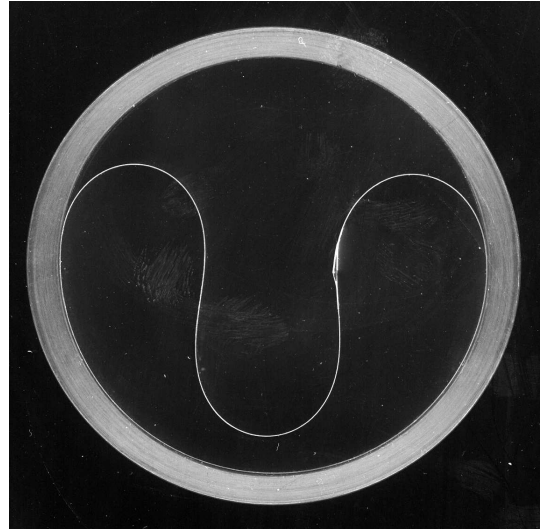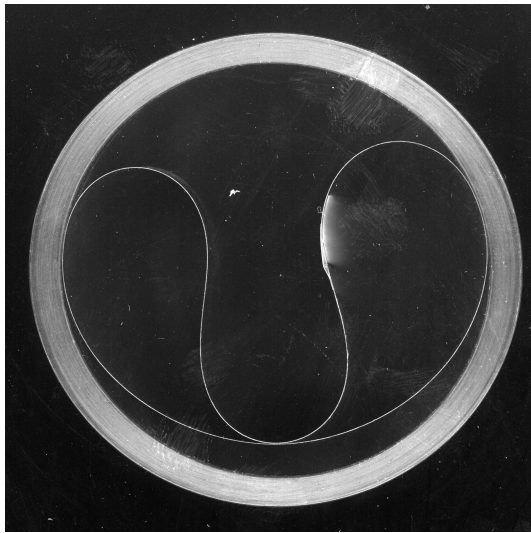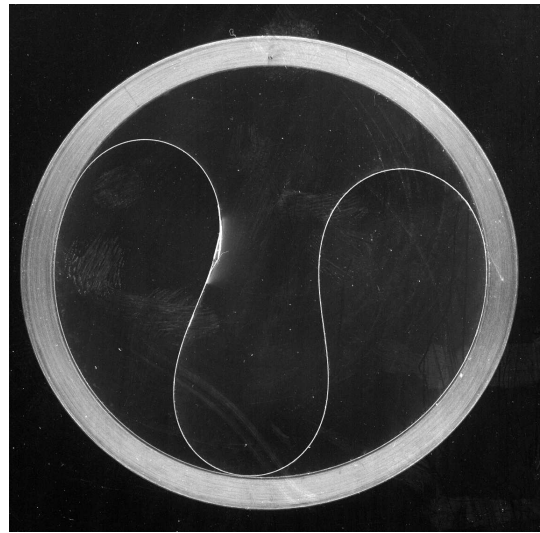
(a) Configuration I. $L = 180\ mm$, $\epsilon = 0.102$.

(b) Configuration II. $L = 202\ mm$, $\epsilon = 0.237$.

(c) Configuration III. $L = 207\ mm$, $\epsilon = 0.267$.

(d) Configuration IV. $P = 202\ mm$, $\epsilon = 0.378$.

Fig. 5.7: Cross sectional pictures of the first symmetric configurations for cylindrical packing in the low confinement regime. The height of the sheet is $H = 140\ mm$ for all the configurations. L corresponds to the perimeter of the cylindrical sheet and ϵ is the confinement parameter. The bright part of sheet corresponds to the overlap region. A first bifurcation occurs $\epsilon \approx 0.23$.

Even though the symmetrical configurations are unstable for high confinement we can observe experimentally some striking configurations in the region of coexistence (see Fig. 5.11(f) and compare the numerical values with Fig. 5.11(e)). It has two loops joined by a punctual contact. It exists experimentally between $1.25 < \epsilon < 1.9$. However, all these symmetrical configurations are unstable with respect to the asymmetrical one in this region.
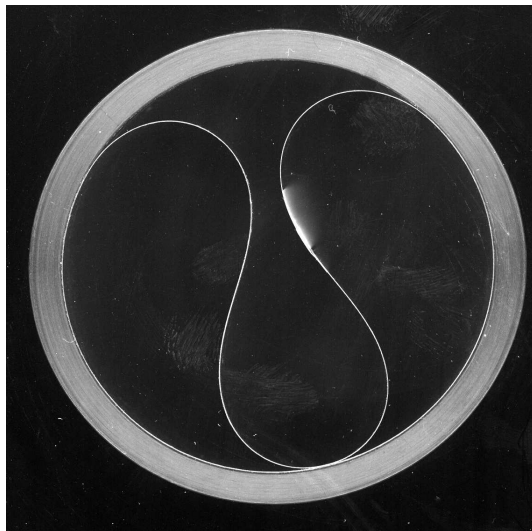
(a) Configuration V. $L = 255\ mm$, $\epsilon = 0.561$.   (b) Configuration VI. $L = 265\ mm$, $\epsilon = 0.622$.
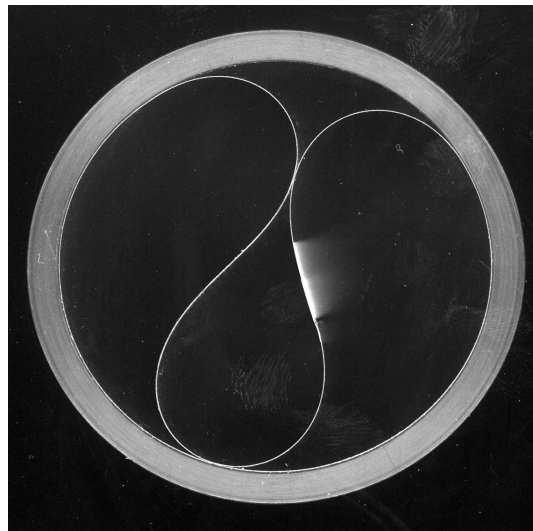
Fig. 5.8: Cross sectional pictures of the first symmetric configurations for cylindrical packing in the low confinement regime. The height of the sheet is $H = 140\ mm$ for all the configurations. L corresponds to the perimeter of the cylindrical sheet and ϵ is the confinement parameter.

In the asymmetrical stable region we observe experimentally that as ϵ increases, the inner S curve begins to rotate surrounding itself by spiral layers. Therefore, the transition between the symmetrical and asymmetrical configurations is *hysteretic*.

5.3.2   High confinement. A ying-yang-like structure

While the size of the outer loop decreases, a *ying-yang-like* shape appears. It is embedded in an effective spiral which serves as a container (see Fig. 5.12). When several turns have been completed around the spiral, the outermost layer is almost a circle (an ellipsoidal shape). The shape of the spiral curve has also been determined numerically (see right pictures in Fig. 5.15).

Finally we have performed some measures of the force acting on the container when the packing parameter ϵ is extremely high (for the perimeter $L = 935[mm]$, $L = 1250[mm]$, $L = 1550[mm]$, $L = 1700[mm]$ and $L = 1970[mm]$). The difference between these five configurations is given by the size of the outer loop (see Fig. 5.12).

In Fig. 5.13 we depict the obtained values for the dimensionless force $\tilde{F}$ as function of ϵ. In these configurations the spiral container occupies almost the whole available space within the cylindrical container. However these experimental values do not allow us to obtain conclusive results on how the force grows for high confinement.

We have observed that the value of the force is highly dependent on the size of the spiral container and on the number of turns around the spiral configurations. In almost all points, the force seems to grow.
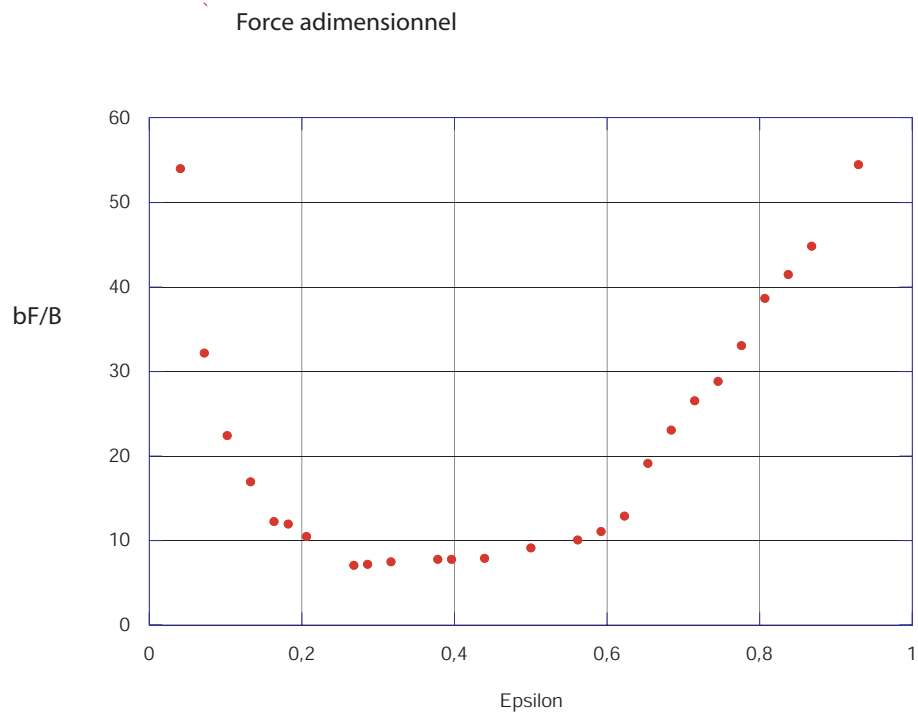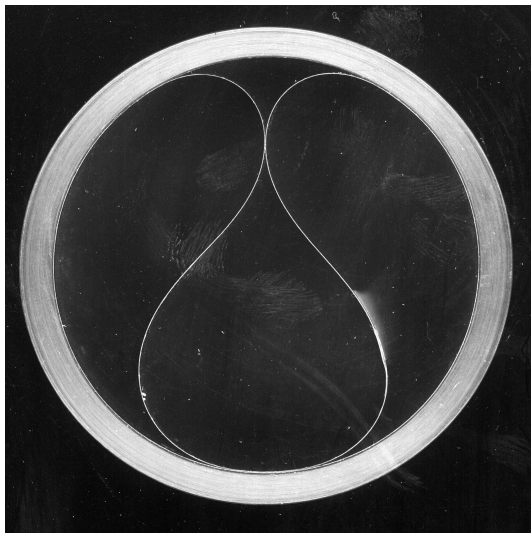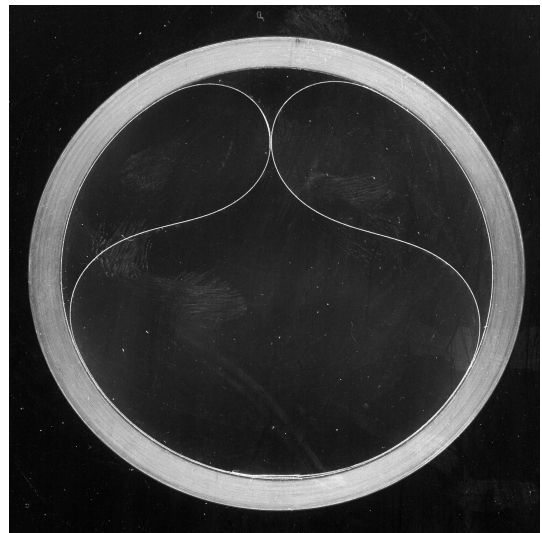
Force adimensionnel

Fig. 5.9: Experimental measurement of the dimensionless force $\tilde{F} = bF/B$ as function of the packing parameter ϵ for symmetrical configurations.
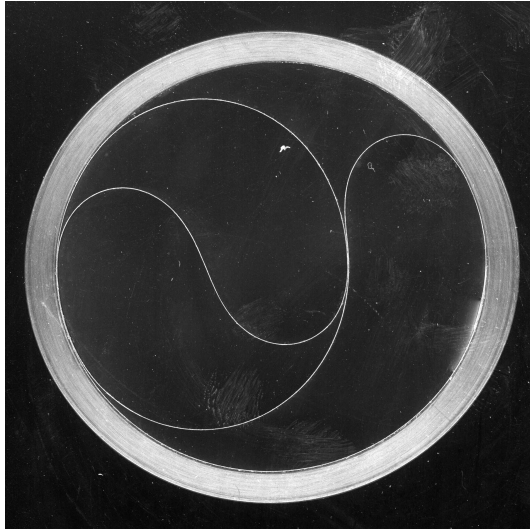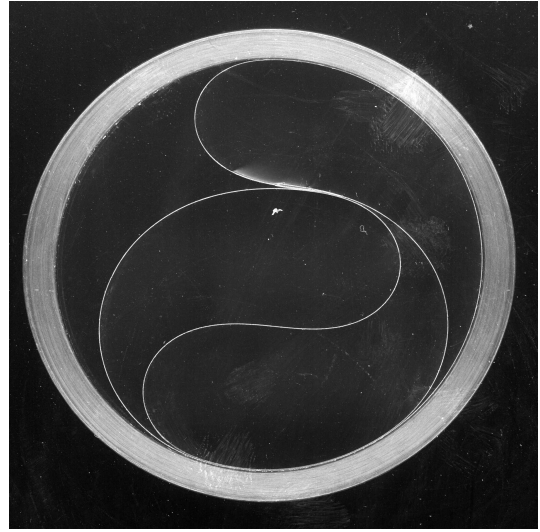

(a) Configuration VII $L = 285\ mm$, $\epsilon = 0.745$.

(b) Configuration VII $L = 315\ mm$, $\epsilon = 0.929$.

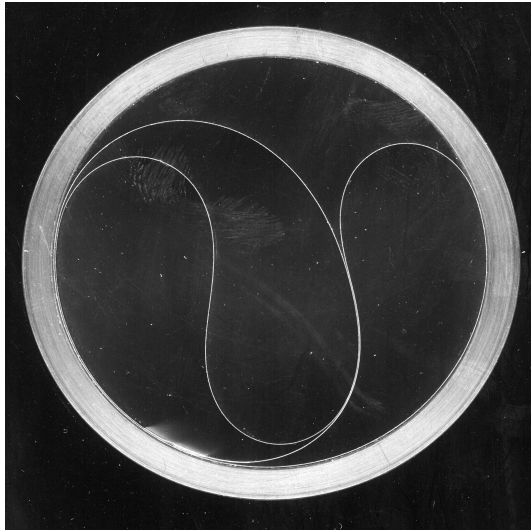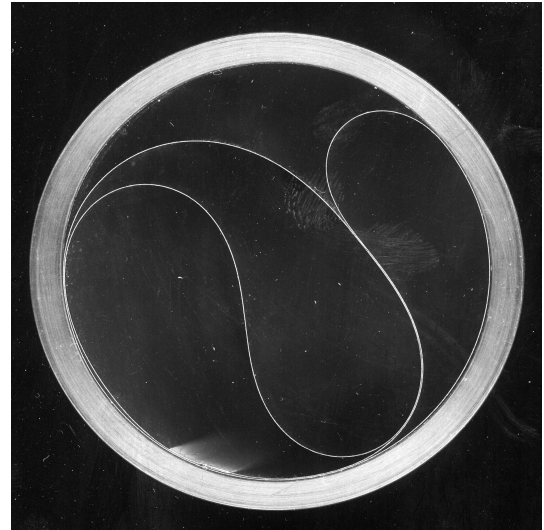*Fig. 5.10:* Symmetrical configurations. The height of the sheet is $H = 140\ mm$.

(a) Configuration VIII $L = 305$ mm, $\epsilon =$ 0.867.

(b) Configuration VIII $L = 315$ mm, $\epsilon =$ 0.929.

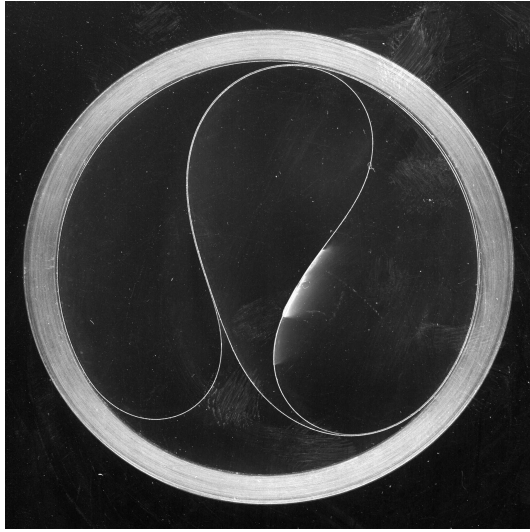(c) Configuration VIII $L = 340$ mm, $\epsilon =$ 1.082.

(d) Configuration VIII $L = 360$ mm, $\epsilon =$ 1.204.

5.3.3   Measures of the mechanical properties of the packing

The geometrical description of the configurations may be better understood characterizing the phase diagram of the dimensionless force as function of the packing parameter ϵ. They are depicted in three figures: Fig. 5.9 shows the dimensionless force for symmetrical configurations. In Fig. 5.14 the asymmetrical configurations are also depicted, showing the coexistence region. In this case we depict the values of the mean force acting on the cylindrical container. Note that the force reaches a minimum above $\epsilon = 0.29$.

In both figures (5.9 and 5.14) we can observe that the configurations II and III are

(e) Configuration VIII $L = 385$ mm, $\epsilon =$ 1.357.
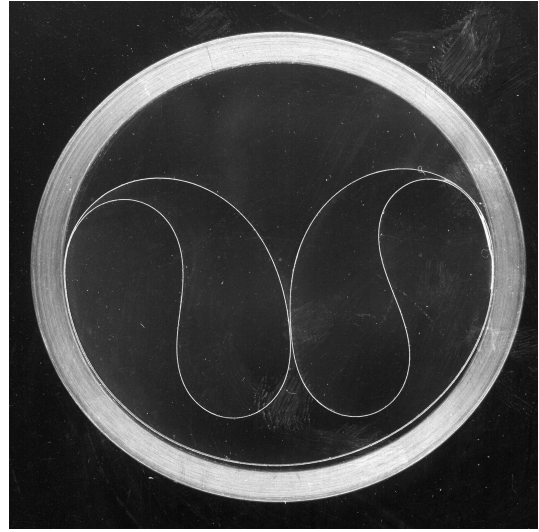
(f) Configuration VII $L = 265$ mm, $\epsilon = 1.357$.

Fig. 5.11: Evolution of the shape of the sheet when ϵ is increased. The height of the sheet is $H = 140mm$. From (a) to (e) all the configurations are asymmetrical. In (f) we depict a striking symmetrical configuration that appears for high confinement and coexists with a symmetrical configurations. However all these symmetrical configurations are unstable with respect to the asymmetrical ones in the coexistence region.

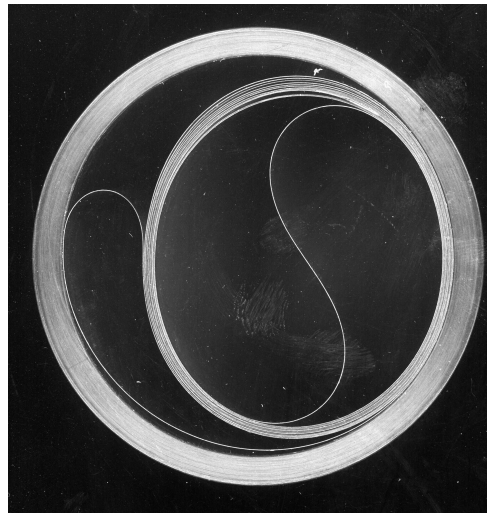*Fig. 5.12:* A ying-yang-like structure for high confinement. $L = 1700$ mm.

very difficult to measure, because their coexistence region is small. After reaching the minimum the force begins to grow weakly, and when the configuration VI is reached, it grows rapidly and the coexistence region appears. In this view, asymmetric configura-
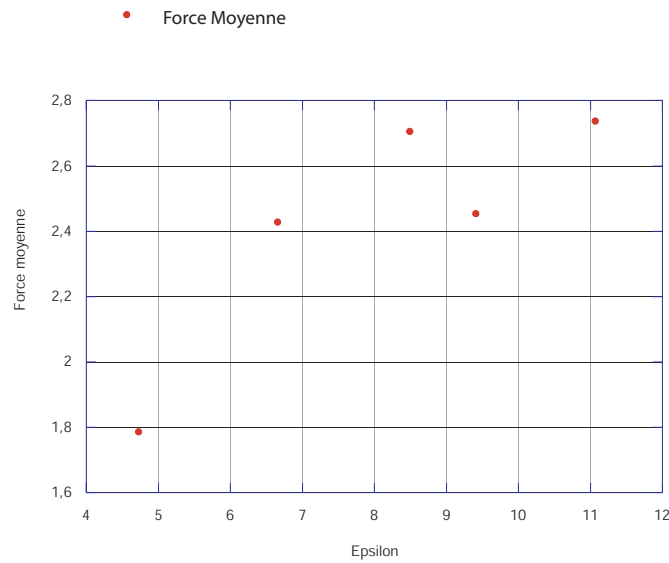
Fig. 5.13: Measures of force for high confinement.

tions are clearly more stable than the symmetric configurations for large confinements.s

5.3.4   Comparison with the numerical approach

Numerical simulations performed by L. Boué [20], based on the same experimental configurations adopted by the elastic sheets, have been developed in parallel to this experimental approach [21]. They account for both elasticity and self-avoidance, whose interplay usually yields a variety of possible self-organized patterns. Numerical simulations not only agree qualitatively with the experimental shapes, but also quantitatively with the experimental measures of the dimensionless pressure, as shown in Fig. 5.15.

In Fig. 5.15 the dimensionless pressure is depicted as a function of the confinement parameter for cylindrical packing. Diamonds correspond to the experimental values (which are related with the Fig. 5.14). Continuous lines correspond to the numerical predictions based on the theoretical approach of the problem. The dashed lines correspond to metastable asymmetrical configurations and reflect the hysteretic character of the transition. The cross in Fig. 5.14 signals a termination of the asymmetrical branch. Note that the insets represent the configurations obtained by numerical simulations. They are compared with the experimental configurations (diamonds). Both configurations and numerical values of pressure are in good agreement with our experimental approach.
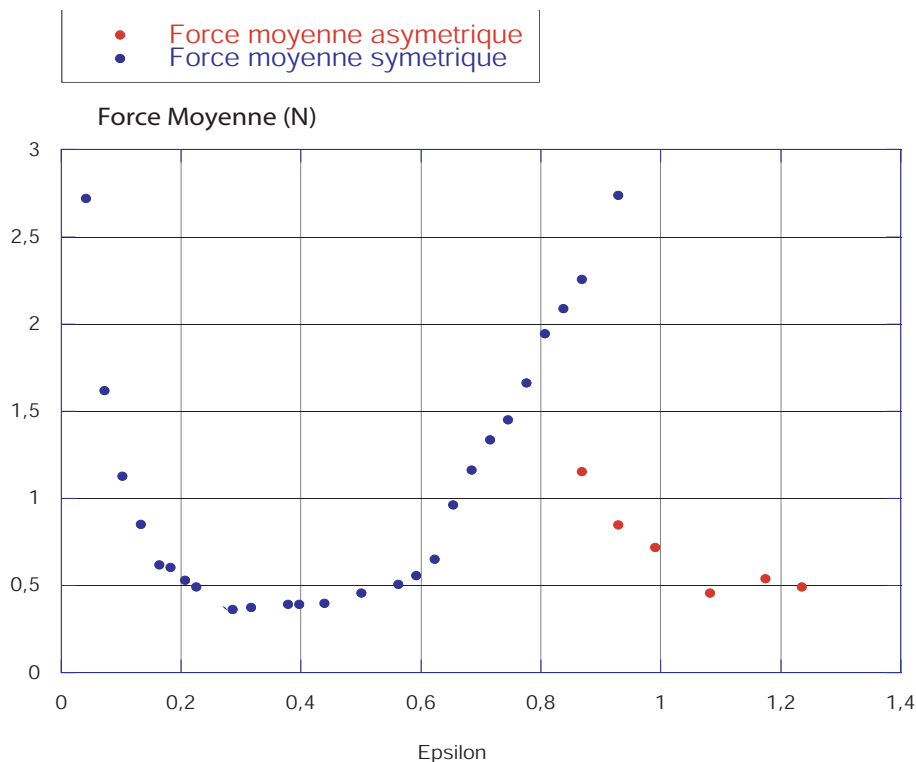
Fig. 5.14: Mean force $\tilde{F}$ as function of the packing parameter ϵ for symmetric (red points) and asymmetric (blue points) configurations. The coexistence region may be clearly appreciated.

5.4 Summary and discussion

In this Chapter we have used a simple experimental setup, to explore the successive configurations leading to the formation of a spiral during the packing process.

Our experimental setup is basically composed of a cylindrical elastic sheet (height H and perimeter $L = 2\pi R$) which is introduced within a cylindrical tube with a smaller radius $b < R$. We have measured the force F necessary to displace the sheet along the container. As there are no reconfigurations during the displacement, Coulomb's law relates the force and the mean pressure exerted by the sheet over the container: $F = \mu 2\pi b H P$, where μ stands for the friction coefficient.

We have characterized the mechanical and topological features of these bifurcations. Simultaneously, we have performed experimental measurements of the *force of confinement* acting on the container. As a consequence, we have determined that the minimum of this force is obtained for the first value of the configuration of type IV. Then, the force begins to raise slightly until the configuration of type VI is achieved. If ϵ continues to grow, the force increases sharply and the symmetrical configurations become unstable with respect to the asymmetrical ones, which appear for $\epsilon \approx 0.85$. This transition is
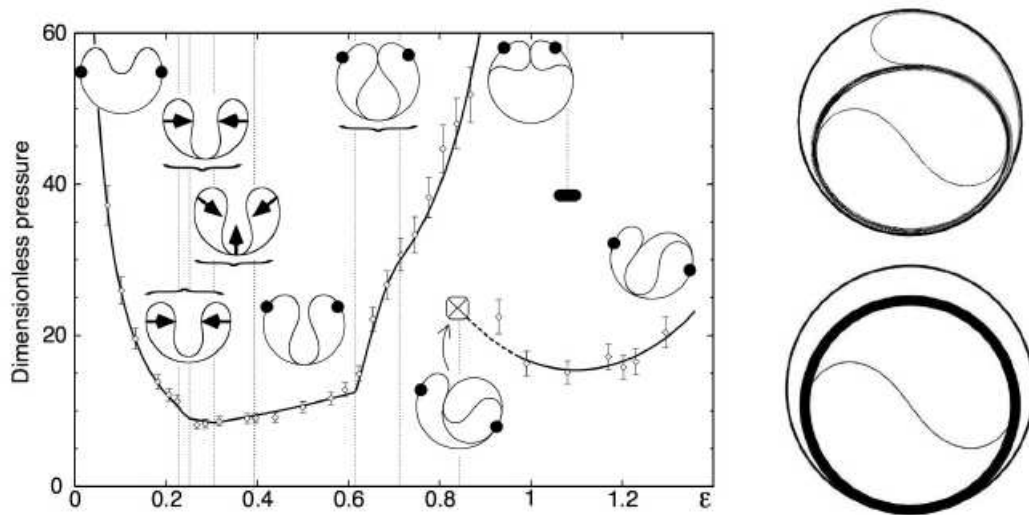
Fig. 5.15: (a) Cylindrical packing. Comparison between experimental (Diamonds) and numerical approaches (lines). Dashed line corresponds to metastable asymmetrical configurations, reflecting the hysteretic character of the transition. Vertical dashed lines correspond to separations between different types of experimental and numerical configurations. These numerical configurations are depicted as insets, numbered from 1 to 9. Vectors occurring in the insets describe the punctual contact with the container. (b) Experimental and numerical configurations for $\epsilon = 9.4$ with a S curve having a Ying-Yang-like shape at its center.

hysteretic and asymmetrical configurations are the starting point for the formation of spirals as the confinement increases.

We have compared our experimental findings with numerical simulations which have been performed in parallel to this experimental approach. The final comparison is summarized in Fig. 5.15. The shape of configurations and the values of the dimensionless pressure obtained in both, experimental and numerical approaches, are in good agreement.

Finally we mention that in an ideal system we would expect only one spiral. However, in real situations (as our experiment), friction between layers composing the sheet and the container is activated for higher confinement and tends to freeze the spiral container that surrounds the spiral configuration. This creates effective containers within which the same sequence is repeated, generating new spiral patterns, as in the case of the conical packing which is depicted in Fig. 5.1.

Chapter 6

CONCLUSIONS

In this thesis we have studied some problems involving one and two-dimensional biological objects that can be described at mesoscopic scales by its geometrical degrees of freedom. We have been able to incorporate in this formalism the microscopic properties of materials (Chap. 2) which can couple to the geometry. We have focused on two types of structures appearing in nature: lipid vesicles (Chap. 3) and growing soft tissues (Chap. 4). By means of a theoretical framework which has been outlined in Chap. 2 we have used the mechanical and geometrical properties of fluid and elastic membranes to determine the different features of these biological materials. We summarize the principal conclusions obtained in each case.

Contact angle and line tension in a biphasic vesicle

In Chap. 3 we have performed an elastic and mechanical study of the thickness variation between two phases composing an inhomogeneous lipid membrane. Lipid vesicles are the simplest systems which allow to control experimentally the properties of more complex systems, such as the plasmic membrane of cells. Inhomogeneous vesicles are composed of a mixture of three families of lipids with different physical and chemical properties, which usually triggers domain segregation. In the presence of *cholesterol* two typical phases may be observed: the liquid ordered L_o phase, which is essentially composed by cholesterol and sphingolipids and the liquid disordered L_d phase, composed by glycerolipids or phospholipids.

A phase separation is observed when the temperature is decreased or the lipid concentration is changed from the preferred values. There exists experimental and theoretical evidence showing that in a biphasic vesicle the adsorption of proteins or impurities induces the budding of a L_o domain (which in the case of cell membranes are called rafts). This process is controlled by the line tension occurring at the interface between both domains. Consequently, it is very important to reveal the physical features of this line tension, and their possible variations as a function of geometric and microscopic effects.

In the L_o phase the lipid chains are stretched to their maximum, consequently, a thickness mismatch between the two phases is produced. This effect is not considered in the usual description of elastic fluid membranes. The structural variation may be

due to internal degrees of freedom, such as the tilt of lipid molecules or the thickness difference between them, which are elastically perturbed at the joint. In this region (of order the nanometers) the elastic continuous models (the Helfrich model, for instance) is no longer valid.

We have proposed an elastic model accounting for this structural variation at the joint. It incorporates the thickness variation, the gradients of mean curvature and the variation of the concentration of proteins and impurities that are located at the contact line.

As a result, we have observed that at the joint, for each domain, we have a slope discontinuity of the large scale solution. We have also obtained a height variation between the neutral surfaces of each domain. Both features imply the existence of a finite contact angle between domains. This contact angle may be incorporated in an effective line tension, whose angular dependence is quadratic. The line tension is responsible for the stability of the budding process, because it tends to decrease the length of the contact line at the joint, favoring their separation.

Finally we have also considered an additional agent, the presence of impurities or proteins at the joint. These molecules change locally the spontaneous curvature of each domain and consequently, the values of the line tension, favoring again the instability of the budding process. This is because the coupling constant depends on the spontaneous curvature which, in turn, changes the contact angle and therefore the line tension. We have shown that the line tension always increases as a function of the spontaneous curvature.

Growth of thin elastic membranes with constant Gaussian curvature

In Chap. 4 we have presented a study of the geometrical properties of the growth of elastic membranes having a non-Euclidean geometry. Our principal motivation comes from the morphogenesis of certain types of plants and flowers occurring in nature, such as the *Brugmansia* or the *Daffodils*.

We have used some previous results on the elasticity of growing soft tissues which reveal that the growth can be interpreted as a process by which the distance between two points on the surface is fixed to a given value. Consequently, by the Gauss Theorema Egregium, the Gaussian curvature of the surface is also fixed at each instant.

In order to understand the mechanical and geometrical properties of the growing membrane, we have proposed a dynamic model that allows to obtain surfaces with constant Gaussian curvature (negative and positive) from the evolution of an initial closed curve. This theoretical model is particularly useful to calculate geometric and energetic properties of non axisymmetric surfaces in a numerical way. It can be easily generalized to surfaces with arbitrary Gaussian curvature and considers the reparametrization invariance of the surface and the Hamiltonian structure of the free energy, which can be interpreted as an action.

In particular, we have focused on two examples that are relevant to describe the shape adopted by growing soft tissues in nature. As first example we have compared the bending elastic energy of different surfaces having constant Gaussian curvature. We have considered as special case the pseudosphere, which can be generated by the evolution of a closed planar circle of fixed length. Then, we have weakly perturbed this initial condition in its wave number, so as to obtain adjacent surfaces to it, having the same geometrical properties (K_G). As a result we obtain that the pseudosphere has the minimal bending energy when compared with all the others surfaces. The energy of these surfaces increases with the square of the perturbation parameter.

As second example we have considered surfaces of positive and constant Gaussian curvature (spherical surfaces). We have constructed a piecewise surface in order to model a growing soft tissue exhibiting singularities at the beginning of the growth process. This lineic singularities can be interpreted as veins which grow following the growing surface. On these veins, the stretching energy is condensed and the bending energy becomes infinite. Stretching appears in order to avoid the singularities. We have compared surfaces with different numbers of veins and pieces. As a remarkable result we have found that the surface with $n = 5$ has the minimal elastic energy when it is compared with surfaces that grow from initial curves having the same length, and with the same final time. The case $n = 5$ corresponds indeed to most cases observed in plant morphogenesis.

Experimental approach to cylindrical packing

In Chap. 5 we have used a simple experimental setup to explore the successive configurations leading to the formation of a spiral during the packing process. Packing is a phenomenon that studies how low-dimensional objects (such as elastic rods or sheets) behave when they are constrained to grow within an object with fixed geometry.

Although this problem is very complex from a theoretical point of view, some progress can be achieved from numerical and experimental approaches. We have then studied the packing of cylindrical elastic sheets in the early stages of confinement. Using a simple experimental setup we have observed the formation of the first fold and its subsequent evolution during the packing, until the formation of the spiral. The cascade of bifurcations leading to this complex pattern has been also characterized. The appearance of the spiral is a consequence of the breakdown of symmetry presented in the early configurations. This breakdown produces asymmetrical configurations, which are more stable from the point of view of the pressure exerted on the container. Then, the spiral structure and its complicated evolution allows the reduction of pressure inside the container.

In parallel to the mechanical description of the different configurations, measurement of the confinement force as a function of the packing parameter have also been performed in order to obtain a phase diagram showing the different configurations and their evolution. Consequently, we have determined the minimum of this force and the

hysteretic region where the asymmetrical configurations appear.

Our experimental findings have been compared to numerical simulations of the elastic theory of rods. The geometry of configurations and the values of the dimensionless pressure obtained in our experiments are in good agreement with the values obtained by the numerical simulations.

In conclusion, in this thesis, we try to understand important features of fluid and elastic membranes, their shape modification under constraints and their relevance to biological processes.

Appendix A

A QUICK GLANCE TO DIFFERENTIAL GEOMETRY OF SURFACES AND CURVES

In this Appendix we give the basic concepts and formulas of the differential geometry of surfaces and curves, that have been used in the course of this thesis. Some excellent references that can be viewed as support material are [31, 39, 73, 80, 99, 131].

A.1   Surfaces

Let ω a two-dimensional open subset in $\mathbb{R}^2$. An *orientable surface* denoted by the set $\Sigma := \boldsymbol{X}(\omega)$ is defined (extrinsically) by means of an *embedding vectorial function* $\boldsymbol{X}$ which is a smooth injective immersion $\boldsymbol{X} : \omega \to \mathbb{E}^3$. Here $\mathbb{E}^3$ denotes the three-dimensional Euclidean space. Moreover, this surface may be considered as a *two dimensional manifold* endowed with a set of *curvilinear coordinates* labeling the points of ω. In this sense we require two tensors in order to define the surface Σ: *the first and second fundamental forms* denoted as g_{ab} and K_{ab}, respectively.

A.1.1   First fundamental form. The intrinsic geometry of Σ

Let us consider a two dimensional vector space (which can be identified with $\mathbb{R}^2$) in which two vectors $\boldsymbol{e}_a$, $a \in \{1, 2\}$ form a basis. Let x_a be the coordinate of a point $p \in \mathbb{R}^2$. If the mapping $\boldsymbol{X} : \omega \to \mathbb{E}^3$ is injective, each point $P \in \Sigma$ can be unambiguously written as:

$$P = \boldsymbol{X}(p) , \qquad p \in \omega , \tag{A.1}$$

and thus the two coordinates x_a of p are called the *curvilinear coordinates* of P.

If the mapping $\boldsymbol{X}$ is differentiable at p (of class $r \geq 1$) then at each point $P \in \Sigma$ we can define the two following linearly independent vectors:

$$\boldsymbol{e}_a := \partial_a \boldsymbol{X} := \frac{\partial \boldsymbol{X}}{\partial x^a} , \tag{A.2}$$

which form a *local covariant basis of the tangent plane* to the surface Σ at P.

The Euclidean metric on $\mathbb{E}^3$ induces a metric $\boldsymbol{g}$ on the surface Σ. Its covariant

components are defined as:

$$g_{ab} = \boldsymbol{e}_a \cdot \boldsymbol{e}_b \ . \tag{A.3}$$

The tangent vectors defined in (A.2) are neither orthogonal nor normalized in general. The *orientation* of Σ is defined by $\boldsymbol{N}$, the *unit normal vector* to the surface:

$$\boldsymbol{N} := \frac{\boldsymbol{e}_1 \times \boldsymbol{e}_2}{\mid \boldsymbol{e}_1 \times \boldsymbol{e}_2 \mid} \ . \tag{A.4}$$

This vector together with the two tangent vectors forms a local basis in $\mathbb{R}^3$. It is evident that $\boldsymbol{e}_a \cdot \boldsymbol{N} = 0$ and $\boldsymbol{N} \cdot \boldsymbol{N} = 1$. Both equations determine $\boldsymbol{N}$ only up to a sign. Here we assume that the surface is *orientable* and therefore a sign can be chosen consistently. Hereafter, if the surface is *closed* (as a sphere), the unit normal will be chosen pointing outward.

So far we have defined the metric tensor $\boldsymbol{g}$ using the embedding functions $\boldsymbol{X}$. This covariant second order tensor is symmetric and positive definite. It is useful to express the area and length elements at a point P on Σ. To do this, we define the contravariant components of the dual tensor of the metric:

$$g_{ab}g^{bc} := \delta_a^c \ , \qquad g^{ab} = (g_{ab})^{-1} \ , \tag{A.5}$$

where δ_a^c is the *Kronecker symbol*. The metric and its inverse can be used to raise and lower indices of other tensors. As usual, repeated indices (one up and one down) imply a summation.

To calculate the infinitesimal area element $\mathrm{d}A$ we need to use *the determinant of the metric*:

$$g := \det(g_{ab}) = g_{11}g_{22} - g_{12}g_{21} \ , \tag{A.6}$$

and it is easy to show that:

$$\mathrm{d}A = \mid \boldsymbol{e}_1 \times \boldsymbol{e}_2 \mid \mathrm{d}x^1\mathrm{d}x^2 = \sqrt{g} \ \mathrm{d}^2x \ . \tag{A.7}$$

It is also useful to define *the epsilon tensor ε_{ab}*:

$$\varepsilon_{ab} := \boldsymbol{N} \cdot (\boldsymbol{e}_a \times \boldsymbol{e}_b) \ , \tag{A.8}$$

which is antisymmetric in its two indices $\varepsilon_{ab} = -\varepsilon_{ba}$. It can also be defined as a tensor density if we use the total antisymmetric symbol ϵ_{ab}.

$$\varepsilon_{ab} = \sqrt{g}\epsilon_{ab}, \qquad \varepsilon^{ab} = \frac{\epsilon_{ab}}{\sqrt{g}} \ , \tag{A.9}$$

where $\epsilon_{12} = -\epsilon_{21} = 1$ and $\epsilon_{11} = \epsilon_{22} = 0$.

The covariant derivative and the Riemann tensor

The metric g_{ab} determines the *intrinsic geometry* of the surface Σ. It allows us to define the unique torsionless *covariant derivative* noted as ∇_a, compatible with it. This covariant derivative can be written in terms of the *Christoffel symbols*, Γ^c_{ab}. For a vector field v^a defined on Σ it reads:

$$\nabla_a v^b := \partial_a v^b + \Gamma^b_{ac} v^c \,, \tag{A.10}$$

where the Christoffel symbols of the second kind are defined by the following relation:

$$\Gamma^c_{ab} := g^{cd} \boldsymbol{e}_d \cdot \partial_a \boldsymbol{e}_b = \frac{1}{2} g^{cd} (\partial_a g_{bd} + \partial_b g_{da} - \partial_d g_{ab}) \,. \tag{A.11}$$

By acting on a tensor, the covariant derivative again yields a tensor, unlike the partial derivative. The compatibility condition of ∇_a with the metric is defined by the conditions:

$$\nabla_a g_{bc} = 0 \,, \tag{A.12a}$$

$$[\nabla_a, \nabla_b] f(x) = (\nabla_a \nabla_b - \nabla_b \nabla_a) f(x) = 0 \,, \tag{A.12b}$$

where $f(x)$ is a scalar function defined on Σ and the brackets $[\cdot, \cdot]$ express the commutation of the covariant derivative. If it is applied to a contravariant vector field v^c it produces:

$$[\nabla_a, \nabla_b] v^c := R^c{}_{dab} v^d \,, \tag{A.13}$$

where R^c_{dab} is the intrinsic *Riemann curvature tensor*. We can also define the *Ricci tensor*, which is given by the contraction of the Riemann tensor $R_{ab} := R^c{}_{acb}$. A further contraction give us the *intrinsic scalar curvature*, also know as the *Ricci scalar* $\mathcal{R} := g^{ab} R_{ab}$.

A.1.2 Second fundamental form

A two-dimensional surface cannot be defined by its metric alone. For instance, a flat surface may be deformed into a portion of a cylinder or a portion of a cone without changing the length of a curve on it. However, a cylinder and a cone are not identical surfaces. It is therefore intuitive that the missing information is provided by the *curvature* of the surface Σ. This property of a surface can be represented by a second rank symmetric tensor called the *extrinsic curvature tensor*, whose covariant components are denoted by K_{ab}.

A natural way to determine this notion consists in specifying how the curvature of a curve $\mathcal{C}$ on Σ can be computed. A moving trihedron defined in every point of the curve allows us to define its curvature $\kappa_c > 0$. This curvature can be decomposed into a part which is due to the fact that the surface is curved in $\mathbb{E}^3$ and a part which is due to the fact that the curve is itself curved. The former is called *normal curvature* and

the latter is called the *geodesic curvature*. The normal curvature is given by:

$$\kappa_n = \left(-\boldsymbol{N} \cdot \partial_a \boldsymbol{e}_b\right) \dot{x}^a \dot{x}^b , \tag{A.14}$$

where the expression in brackets is recognized as the *extrinsic curvature tensor*:

$$K_{ab} := -\boldsymbol{N} \cdot \partial_a \boldsymbol{e}_b = \boldsymbol{e}_a \cdot \partial_b \boldsymbol{N} . \tag{A.15}$$

Note that the components of this tensor form a 2×2 real matrix and therefore it can always be diagonalized. In particular the eigenvalues c_1, c_2 of the mixed matrix $K_a^b = g^{cb}K_{ac}$ are called the *principal curvatures* of the surface.

Two scalars can be defined for the tensor K_a^b. The first is the *trace of the extrinsic curvature tensor*:

$$K := \operatorname{Tr}(K_a^b) = c_1 + c_2 , \tag{A.16}$$

and the *Gaussian curvature*:

$$K_{\mathrm{G}} := \operatorname{Det}(K_a^b) = c_1 c_2 . \tag{A.17}$$

In the literature one often finds the *mean extrinsic curvature* function, which is defined by the relation $H = K/2$.

A.1.3   The Gauss and Weingarten equations

The extrinsic curvature tensor allows us to calculate the partial derivatives of the local frame vectors $\{\boldsymbol{e}_a, \boldsymbol{N}\}$ defined on Σ. To proceed note that the normal vector is a unit vector and therefore we have $\boldsymbol{N} \cdot \partial_a \boldsymbol{N} = 0$. Thus the partial derivative $\partial_a \boldsymbol{N}$ must be a tangent vector. Using the definition (A.15) we obtain the *Weingarten equations*:

$$\nabla_a \boldsymbol{N} = \partial_a \boldsymbol{N} = K_a^b \boldsymbol{e}_b . \tag{A.18}$$

Now, for the tangent vector $\boldsymbol{e}_a$ we use the equations (A.11) and (A.15) to obtain the *Gauss equations*:

$$\nabla_a \boldsymbol{e}_b = -K_{ab}\boldsymbol{N} , \tag{A.19}$$

or equivalently:

$$\partial_a \boldsymbol{e}_b = \Gamma_{ab}^c \boldsymbol{e}_c - K_{ab}\boldsymbol{N} . \tag{A.20}$$

A.1.4   Integrability conditions and Gauss' Theorema Egregium

The intrinsic and the extrinsic geometries of Σ, determined respectively by the tensors g_{ab} and K_{ab} cannot be specified independently. They are related by the integrability conditions of Eqns. (A.18) and (A.19). We assume that the embedding functions $\boldsymbol{X}$ are of class $r > 3$ and therefore we have the following commutation relations of the

second partial derivatives:

$$\partial_a \partial_b \boldsymbol{e}_c = \partial_b \partial_a \boldsymbol{e}_c \ . \tag{A.21}$$

These relations give us the *Gauss-Codazzi* and the *Codazzi-Mainardi* equations which are respectively given by:

$$R_{abcd} - K_{ac}K_{bd} + K_{ad}K_{bc} = 0 \ , \tag{A.22a}$$

$$\nabla_a K_{bc} - \nabla_b K_{ac} = 0 \ . \tag{A.22b}$$

The relations (A.22a) and (A.22b) arise from the re-writing of the conditions Eqn. (A.21) in the form of the equivalent relations $\partial_{ac}\boldsymbol{e}_b \cdot \boldsymbol{e}_d = \partial_{ab}\boldsymbol{e}_c \cdot \boldsymbol{e}_d$ and $\partial_{ac}\boldsymbol{e}_b \cdot \boldsymbol{N} = \partial_{ac}\boldsymbol{e}_b \cdot \boldsymbol{N}$, respectively.

The functions R_{abcd} constitute the *covariant components of the Riemann curvature tensor*. They can be expressed in terms of the Christoffel symbols as:

$$R^a_{\ bcd} := \partial_c \Gamma^a_{db} - \partial_d \Gamma^a_{cb} + \Gamma^a_{ce}\Gamma^e_{db} + \Gamma^a_{de}\Gamma^e_{cb} \ . \tag{A.23}$$

This relation is intrinsic, because it is defined only using the metric tensor and its derivatives and does not depend on the normal vector $\boldsymbol{N}$. A fundamental theorem for surfaces states that given the two symmetric tensor g_{ab} and K_{ab} the equations that defines them are necessary and sufficient for the existence of an embedding that define a surface with these tensors as its first and second fundamental form. This embedding is unique, up to rigid motions in $\mathbb{E}^3$.

Contraction of the equations (A.22a) and (A.22b) with the contravariant metric g^{ab} results in:

$$\mathcal{R} - K^2 + K_{ab}K^{ab} = 0 \ , \tag{A.24a}$$

$$\nabla_a K^a_b - \nabla_b K = 0 \ , \tag{A.24b}$$

which are entirely equivalents to the equations (A.22a) and (A.22b) for a two-dimensional surface.

In this deduction we have used the Ricci tensor and the intrinsic scalar curvature, both previously defined in A.1.1. Now using these definitions and the definition of the Gaussian curvature in Eq. (A.22a) we obtain:

$$R_{abcd} = K_{\mathrm{G}}(g_{ac}g_{bd} - g_{ad}g_{bc}) \ , \tag{A.25a}$$

$$\mathcal{R}_{ab} = K_{\mathrm{G}}g_{ab} \ , \tag{A.25b}$$

$$\mathcal{R} = 2K_{\mathrm{G}} \ . \tag{A.25c}$$

As a consequence we have that the definitions of the functions Γ^c_{ab} and Γ_{abc} imply that the Gauss equations and the Codazzi-Mainardi equations are reduced to one and two equations respectively. By a simple inspection we have:

$$R_{1212} = \mathrm{Det}(K_{ab}) \ , \tag{A.26}$$

and consequently the Gaussian curvature at each point of Σ can be written as:

$$K_{\mathrm{G}} = \frac{R_{1212}}{g} \ . \tag{A.27}$$

This equation is the manifestation of the *Gauss' Theorema Egregium* which states that the Gaussian curvature at each point on Σ, which is originally defined in an extrinsic way, only depends on the first fundamental form and its partial derivatives of order ≤ 2 at the same point. Thus, K_{G} is an intrinsic property of the surface.

A.1.5   The Gauss-Bonnet theorem

Another striking result involving the Gaussian curvature is the *Gauss-Bonnet theorem.* It can be stated as follows: Let Σ_o a simple connected surface patch (a two-dimensional Riemannian manifold) with boundary $\partial\Sigma_o$. Let K_{G} be the Gaussian curvature of Σ_o, and let κ_g be the geodesic curvature of $\partial\Sigma_o$. Then:

$$\int_{\Sigma_o} \mathrm{d}A \ K_{\mathrm{G}} + \int_{\partial\Sigma_o} \mathrm{d}s \ \kappa_g = 2\pi\chi(\Sigma_o) \ , \tag{A.28}$$

where K_{G} is the Gaussian curvature of Σ, κ_s is the geodesic curvature of $\partial\Sigma_o$, $\mathrm{d}A$ is the element of area of the surface, $\mathrm{d}s$ is the line element along the boundary of $\partial\Sigma_o$ and $\chi(\Sigma_o)$ is the Euler characteristic of Σ_o.

If the boundary $\partial\Sigma_o$ is piecewise smooth, then we interpret the integral over the geodesic curvature as the sum of the corresponding integrals along the smooth portions of the boundary, minus the sum of the angles α_i by which the smooth portions turn at the corners of the boundary:

$$\int_{\Sigma_o} \mathrm{d}A \ K_{\mathrm{G}} + \int_{\partial\Sigma_o} \mathrm{d}s \ \kappa_g = 2\pi\chi(\Sigma_o) - \sum_i \alpha_i \ . \tag{A.29}$$

This theorem connects the geometry of a surface in the sense of the curvature to its topology, given by the Euler characteristic which is a topological invariant. Applying this theorem particularly to compact boundaryless surface Σ, one obtains:

$$\int_{\Sigma_o} \mathrm{d}A \ K_{\mathrm{G}} = 2\pi\chi(\Sigma) = 4\pi(1 - g) \ . \tag{A.30}$$

This relation states that the total Gaussian curvature of such a closed surface Σ is equal to 2π times the Euler characteristic of the surface, a topological invariant. The second equality only works for orientable surfaces. Any orientable compact surface without boundary is topologically equivalent to a sphere with some handles attached, and the *genus g* counts the number of handles. The sphere has genus 0, the torus genus 1, etc.

A.2 Geometry of a curve on a surface

In this section we describe the geometrical properties of a curve $\mathcal{C}$ which lies on a surface Σ. These definitions are used principally in Chapters 2, 3 and 4.

A.2.1 Darboux frame

Let us consider the configuration of the Fig. 4.2. At every point of $\mathcal{C}$ we can define a natural moving frame in $\mathbb{E}^3$, composed by the vectors $\{\boldsymbol{t}, \boldsymbol{l}, \boldsymbol{N}\}$. This orthonormal trihedron is called the *Darboux frame*, where $\boldsymbol{t} = t^a \boldsymbol{e}_a$ is the unit tangent vector to $\mathcal{C}$, $\boldsymbol{N}$ is the surface unit normal and we define $\boldsymbol{l} = \boldsymbol{N} \times \boldsymbol{t}$. Note that this vector $\boldsymbol{l} = l^a \boldsymbol{e}_a$ is tangential to Σ and normal to $\mathcal{C}$. We also suppose that the curve is not singular and we can always define its curvature κ_c. If we define $\nabla_\parallel = t^a \nabla_a$ as the directional surface derivative in the direction $\boldsymbol{t}$ we can write the following three equations relating the geometrical properties of $\mathcal{C}$:

$$\nabla_\parallel \boldsymbol{t} = \kappa_g \boldsymbol{l} + \kappa_n \boldsymbol{N} , \tag{A.31a}$$

$$\nabla_\parallel \boldsymbol{l} = -\kappa_g \boldsymbol{t} + \tau_g \boldsymbol{N} , \tag{A.31b}$$

$$\nabla_\parallel \boldsymbol{N} = -\kappa_n \boldsymbol{t} - \tau_g \boldsymbol{l} , \tag{A.31c}$$

where κ_g is the *geodesic curvature*, which corresponds to the curvature κ_c of $\mathcal{C}$ projected onto the surface tangent plane. The quantity κ_n is the *normal curvature*, denoting the curvature of $\mathcal{C}$ projected onto the plane containing the vectors $\{\boldsymbol{t}, \boldsymbol{N}\}$. Finally we have τ_g, the *geodesic torsion* which corresponds to the rate of change of $\boldsymbol{N}$ around $\boldsymbol{t}$ when the trihedron moves on the curve. The geodesic curvature expresses the fact that the curve itself is curved and the normal curvature measures the effect of the surface on the curvature of the curve.

A.2.2 Projections of the extrinsic curvature onto $\mathcal{C}$

Otherwise, the geometric properties of the surfaces Σ can be decomposed on the tangent basis $\{\boldsymbol{t}, \boldsymbol{l}\}$:

$$K_\parallel = t^a t^b K_{ab} = -\boldsymbol{N} \cdot \nabla_\parallel \boldsymbol{t} , \tag{A.32a}$$

$$K_\perp = l^a l^b K_{ab} = \boldsymbol{N} \cdot \nabla_\perp \boldsymbol{l} , \tag{A.32b}$$

$$K_{\parallel\perp} = -l^a t^b K_{ab} = \boldsymbol{N} \cdot \nabla_\parallel \boldsymbol{l} = -\boldsymbol{N} \cdot \nabla_\perp \boldsymbol{t} , \tag{A.32c}$$

where we have defined $\nabla_\perp = l^a \nabla_a$ the surface derivative in the direction $\boldsymbol{l}$. As a consequence we have that $\kappa_n = -K_\parallel$ and $\tau_g = K_{\parallel\perp}$. Note that the trace of the extrinsic curvature tensor is given by:

$$K = K_\parallel + K_\perp. \tag{A.33}$$

Finally it is very useful to express the projections of the *Codazzi-Mainardi* equations

(A.24b) onto the tangent basis $\{\boldsymbol{t}, \boldsymbol{l}\}$. They read:

$$\nabla_\perp K_{\perp\parallel} = \nabla_\parallel K_\perp + (K_\parallel - K_\perp)\boldsymbol{l} \cdot \nabla_\perp \boldsymbol{t} + 2K_{\perp\parallel}\boldsymbol{t} \cdot \nabla_\parallel \boldsymbol{l} , \qquad \text{(A.34a)}$$

$$\nabla_\perp K_\parallel = \nabla_\parallel K_{\perp\parallel} + (K_\parallel - K_\perp)\boldsymbol{t} \cdot \nabla_\parallel \boldsymbol{l} - 2K_{\perp\parallel}\boldsymbol{l} \cdot \nabla_\perp \boldsymbol{t} , \qquad \text{(A.34b)}$$

Appendix B

THICKNESS VARIATIONS AND THE MODIFIED HELFRICH ELASTICITY

In this appendix we briefly outline how to derive the additional coupling terms coming from the microscopic degrees of freedom to the usual elastic description based on the Helfrich model. These additional terms involve the thickness variation induced by homogeneous and inhomogeneous bending deformations, and also by the local stretching. These contributions can be extended to the total surface, but they are excited in particular at the joint between the phases composing the vesicle.

B.1 Local elastic stretching. Area-Difference between inner and outer hydrophilic surfaces

The area of the hydrophilic outer surface $\Sigma^{(+)}$ changes in two ways. The first step is related to the extension-compression of the monolayer during an homogeneous bending deformation. The second contribution, related to the inhomogeneous bending, will be examined in the next section.

A simple way to incorporate the coupling terms between the thickness and the geometric quantities related to the neutral surface Σ is to assume that there is a local stretching term which takes into account the difference ΔA_h between the areas of both hydrophilic surfaces (inner and outer):

$$\mathcal{F}_h[\boldsymbol{X}] = \int_\Sigma \mathrm{d}A \left(\frac{f_h}{a} \right) , \tag{B.1}$$

where f_h is an homogeneous free energy density. In first approximation this term is linear in ΔA_h, because the local difference of area is a small quantity.

The stretching and bending terms that we will consider here for each phase are then expressed by:

$$\mathcal{F}_h[\boldsymbol{X}] = \oint_{\Sigma^{(+)}} dA^{(+)} f^{(+)} + \oint_{\Sigma^{(-)}} dA^{(-)} f^{(-)} , \tag{B.2a}$$

$$f^{(\mathrm{I})}(A^{(\mathrm{I})}, H^{(\mathrm{I})}, H_s^{(\mathrm{I})}) = \frac{K^{(\mathrm{I})}}{2} \left(A^{(\mathrm{I})} - A_o^{(\mathrm{I})} \right)^2 + \frac{\kappa^{(\mathrm{I})}}{2} \left(2H^{(\mathrm{I})} - H_s^{(\mathrm{I})} \right)^2 , \tag{B.2b}$$

where $A^{(I)}$ is the surface area of each side (inner and outer), $A_o^{(I)}$ is the preferred area of each monolayer, $H^{(I)}$ is the mean curvature, $\kappa^{(I)}$ is the bending stiffness and $K^{(I)}$ is the area-stretching elasticity coefficient. Note that in the expressions (3.1a) and (3.1b) we have removed the label i denoting the two phases.

As we will show in the next section, the infinitesimal area element $dA^{(I)}$ (resp. inner and outer) is related to dA, which is defined on the neutral surface, by means of an expansion to leading orders:

$$dA^{(I)} = dA \left(1 \pm 2H\eta^{(I)} + K_{\mathrm{G}}\eta^{(I)2} + \frac{1}{2}\nabla^a\eta^{(I)}\nabla_a\eta^{(I)} + \dots \right) . \tag{B.3}$$

Now we need to express the geometry of the hydrophilic areas $A^{(+)}$ and $A^{(-)}$ with respect to the neutral surface area A. We have:

$$A^{(\pm)} = A \pm \int_\Sigma \mathrm{d}A \, 2\eta^{(\pm)}H + \int_\Sigma \mathrm{d}A \, \eta^{(\pm)2}K_{\mathrm{G}} , \tag{B.4}$$

and for the mean curvature:

$$H^{(\pm)} = H \pm \eta^{(\pm)}(C_1^2 + C_2^2) , \tag{B.5}$$

where C_1 and C_2 stand for the principal curvatures on Σ. The choice of the neutral surface Σ as reference surface is convenient because the deformation of stretching and bending are independent when they are defined with respect to Σ. As a consequence the area of the neutral surface does not change during the deformation of bending. In this case this choice provide us the following relation between $\eta^{(+)}$ and $\eta^{(-)}$:

$$\frac{K^{(+)}\eta^{(+)}(x)}{A_o^{(+)}} - \frac{K^{(-)}\eta^{(-)}(x)}{A_o^{(-)}} = 0 , \tag{B.6}$$

and now if we replace the equations (B.4) and (B.5) in (B.2a) after a long but trivial calculation we obtain:

$$\frac{f_h}{a} = \frac{1}{2}\kappa(2H - H_s)^2 + \overline{\kappa}K_{\mathrm{G}} + 2\Lambda Hu + u^2 K_{\mathrm{G}}\delta + \lambda , \tag{B.7}$$

where the coefficients are complicated functions of the physical parameters. For instance we have:

$$\kappa = \kappa^{(+)} + \kappa^{(-)} , \tag{B.8}$$

$$\overline{\kappa} = \overline{\kappa}^{(+)} + \overline{\kappa}^{(-)} , \tag{B.9}$$

$$H_s = \frac{\kappa^{(+)}H_s^{(+)} + \kappa^{(-)}H_s^{(-)}}{\kappa^{(+)} + \kappa^{(-)}} , \tag{B.10}$$

$$\Lambda = \frac{K^{(+)}K^{(-)}(A_o^{(+)} - A_o^{(-)})}{K^{(+)}A_o^{(-)} + K^{(-)}A_o^{(+)}} , \tag{B.11}$$

$$\delta = \frac{K^{(+)}K^{(-)}(K^{(+)}A_o^{(-)} - K^{(-)}A_o^{(+)})(A_o^{(+)} - A_o^{(-)})}{(K^{(+)}A_o^{(-)} + K^{(-)}A_o^{(+)})^2} \, , \tag{B.12}$$

All these expressions are valid for each domain. Note that we have omitted the label $i \in \{1, 2\}$ denoting each phase composing the vesicle.

B.2   Thickness gradients and inhomogeneous bending

As mentioned earlier in Sec. 3.3.1 the inhomogeneous bending contribution can be isolated considering the following free energy:

$$f_{nh}^{(I)} = \xi^{(I)} \Delta A_{nh}^{(I)} \, , \tag{B.13}$$

which represents the change of energy per lipid molecule arising from the extension of the hydrophilic surface. From now on we will perform the calculations using the outer monolayer. As shown in Fig. (3.4) an inhomogeneous bending deformation is reflected in the appearance of an non-zero angle ω between the outer unit normal $\boldsymbol{N}^{(+)}$ and the unit normal to the neutral surface $\boldsymbol{N}$. In this case the hydrophilic surface is not parallel to the neutral one.

The additional extension is accounted for by the term:

$$\Delta A_{nh}^{(+)} = \frac{a^{(+)}}{cos\omega} - a^{(+)} \, , \tag{B.14}$$

where $a^{(+)}$ is the area per lipid molecule on the hydrophilic surface. Now we need to express Eqn. (B.14) as a term depending on the thickness gradient. To do this note that the hydrophilic surface of each monolayer is determined by a radius vector:

$$\boldsymbol{X}^{(\pm)} = \boldsymbol{X} \pm \eta^{(\pm)}(x)\boldsymbol{N} \, . \tag{B.15}$$

With this expression and the definitions introduced in the App. A we can relate the geometrical characteristic of $\Sigma^{(+)}$ through the geometrical properties of Σ. These quantities will be given as expansions in series up to order two on the distance $\eta^{(+)}$. For instance, the determinant of the metric $g^{(+)} = \mathrm{Det}(g_{ab}^{(+)})$ can be expressed as:

$$g^{(+)} = \left(1 + 4H\eta^{(+)} + 4H^2\eta^{(+)2} + 2K_{\mathrm{G}}\eta^{(+)2} + \ldots\right) \, , \tag{B.16}$$

where we have used an identity valid for any tensor M_{ab} in two-dimensions:

$$\mathrm{Det}(g_{ab} + M_{ab}) = \left(1 + M_a^a + \frac{\mathrm{Det}(M_{ab})}{\mathrm{Det}(g_{ab})}\right)\mathrm{Det}(g_{ab}) \, , \tag{B.17}$$

where g_{ab} is the metric tensor and $M_a^a = g^{ab}M_{ab}$ is the trace of the tensor M_{ab}. As a consequence the area per molecule on the hydrophilic surface (inner and outer)

corresponding to an homogeneous bending at the dominant order is given by:

$$a^{(I)} = a \left(1 \pm 2H\eta^{(I)} + K_G\eta^{(I)2} + \ldots\right) , \tag{B.18}$$

where a is the area per molecule measured on the neutral surface. To calculate $\cos(\omega)$ we need the expression for the the hydrophilic unit vector. It reads:

$$\boldsymbol{N}^{(+)} = \frac{\theta_1 \boldsymbol{N} - \left[(1 + 2H)\nabla_c\eta^{(+)} + \eta^{(+)}\nabla_a\eta^{(+)}K_c^a\right]\boldsymbol{e}^c}{\sqrt{\theta_1^2 + \theta_2(\nabla\eta)^2 + 2\eta(1 + H\eta)(\nabla_a\eta)(\nabla_b\eta)K^{ab}}} \tag{B.19}$$

where the functions $\theta_1 = a^{(+)}/a$ and $\theta_2 = g^{(+)}/g$ are defined by:

$$\theta_1 = 1 + 2H\eta^{(+)} + K_G\eta^{(+)2} + \ldots , \tag{B.20a}$$
$$\theta_2 = 1 + 4H\eta^{(+)} + 4H^2\eta^{(+)2} + 2K_G\eta^{(+)2} + \ldots . \tag{B.20b}$$

Henceforth by simplicity we drop the symbol $(+)$. From Eqn. (B.19) we calculate directly $\cos\omega = \boldsymbol{N} \cdot \boldsymbol{N}^{(+)}$. It reads:

$$\cos\omega = \frac{\theta_1}{\sqrt{\theta_1^2 + \theta_2(\nabla\eta)^2 + 2\eta(1 + H\eta)(\nabla_a\eta)(\nabla_b\eta)K^{ab}}}, \tag{B.21}$$

where K^{ab} is the curvature tensor of the neutral surface Σ. The third term in Eqn. (B.21) is of order three in η and therefore it can be neglected. Then, expanding the terms in the root, the value of $\sec\omega$ is given by:

$$\sec\omega = 1 + \frac{1\theta_2}{2\theta_1^2}(\nabla\eta)^2 \tag{B.22}$$

Using Eqn. (3.4) and Eqn. (B.22) the energy of the inhomogeneous bending is:

$$f_{nh} = \xi[a(1 + 2H\eta + \eta^2 K_G)(1 + \frac{1\theta_2}{2\theta_1^2}(\nabla\eta)^2) - a(1 + 2H\eta + \eta^2 K_G)];$$

$$f_{nh} = \xi\frac{1}{2}a\frac{\theta_2}{\theta_1}(\nabla\eta)^2 . \tag{B.23}$$

Finally at the leading order in η it is given by:

$$f_{nh} = \frac{1}{2}a\xi(1 - 2H\eta - K_G\eta^2 - \ldots)(\nabla\eta)^2$$

$$f_{nh} = \frac{1}{2}\xi a(\nabla\eta)^2 , \tag{B.24}$$

The calculation for the inner layer $(-)$ is similar. It is only necessary to change the coefficient $\xi^{(-)}$, the normal distance η which in this case is $\eta^{(-)}$ and take the minus sign in Eqn. (B.18). The total energy is finally given by the sum of both contributions

(inner and outer) . It can be easily obtained using the relation between $\eta^{(+)}$, $\eta^{(-)}$ and u expressed in the definition of the neutral surface Σ as was mentioned before. Finally, the total energy over the neutral surface is obtained integrating the density of energy per molecule area f_{nh}:

$$\mathcal{F}_{nh}[\boldsymbol{X}] = \int_{\Sigma} \mathrm{d}A \left(\frac{f_{nh}}{a} \right) \tag{B.25}$$

Appendix C

PUBLISHED AND SUBMITTED PAPERS

In this tesis the following papers has been published and submitted

BIBLIOGRAPHY

[1] M. Abramowitz and I. A. Stegun. *Handbook of Mathematical Functions*. Dover, New York, 1970, 1970.

[2] S. Akimov, P. Kuzmin, J. Zimmerberg, and F. Cohen. Lateral tension increases the line tension between two domains in a lipid bilayer membrane. *Phys. Rev. E.*, **75**:011919–011926, (2007).

[3] J. M. Allain. *Instabilités des membranes lipidiques inhomogènes. Implications biologiques*. PhD thesis, Université Paris VII -Denis Diderot, 2005.

[4] J. M. Allain and M. Ben Amar. Biphasic vesicle: instability induced by adsorption of proteins. *Physica A*, **337**:531–545, (2004).

[5] J. M. Allain and M. Ben Amar. Budding and fission of a multiphase vesicle. *Eur. Phys. J. E*, **20**:409–420, (2006).

[6] J. M. Allain, C. Storm, A. Roux, M. Ben Amar, and J. F. Joanny. Fission of a multiphase membrane tube. *Phys. Rev. Lett*, **93**:158104–158108, (2004).

[7] M. Ben Amar and A. Goriely. Growth and instability in elastic tissues. *J. Mech. Phys. Solids*, **53**:2284–2319, (2005).

[8] M. Ben Amar and Y. Pomeau. Crumpled paper. *Proc. R. Soc. Lond. A*, **453**:729–755, (1997).

[9] R. Arnowitt, S. Deser, and W. Misner. The dynamics of general relativity. *http://arxiv.org/pdf/gr-qc/0405109v1*, , (2004).

[10] E. Atilgan and S. X. Sun. Shape transitions in lipid membranes and protein mediated vesicle fusion and fission. *J. Chem. Phys*, **126**:095102–095111, (2007).

[11] B. Audoly and A. Boudaoud. Self-similar structures near boundaries in strained systems. *Phys. Rev. Lett.*, **91**:086105–086108, (2003).

[12] B. Audoly and Y. Pomeau. *Elasticity and Geometry*. Oxford University Press, To appear 2009.

[13] K. Bacia, P. Schwille, and T. Kurzchalia. Sterol structure determines the separation of phases and the curvature of the liquid-ordered phase in model membranes. *Proc. Natl. Acad. Sci. USA*, **102**:3272–3277, (2005).

[14] T. Baumgart, S. Das, W. W. Webb, and J. T. Jenkins. Membrane elasticity in giant vesicles with fluid phase coexistence. *Biophys. J.*, **89**:1067–1080, (2005).

[15] T. Baumgart, S. T. Hess, and W. W. Webb. Imaging coexisting fluid domains in biomembrane models coupling curvature and line tension. *Nature*, **425**:421–424, (2003).

[16] C. M. Bender and S. A. Orzag. *Advanced mathematical methods for scientists and engineers*. Springer, New York, 1999.

[17] P. Biscari and G. Napoli. Inclusion-induced boundary layers in lipid vesicles. *Biomechan Model Mechanobiol*, **6**:297–301, (2006).

[18] M. Bloor and M. Wilson. Method for efficient shape parametrization of fluid membranes and vesicles. *Phys. Rev. E.*, **61**:4218–4229, (2000).

[19] A. A. Boulbitch. Equations of heterophase equilibrium of a biomembrane. *Arch. Appl. Mech.*, **69**:83–93, (1999).

[20] L. Boué. *Vers une physique statistique du pliage et du froissage de structures élastiques*. PhD thesis, Université Paris VI -Pierre et Marie Curie, 2008.

[21] L. Boué, M. Adda-Bedia, A. Boudaoud, D. Cassani, Y. Couder, A. Eddi, and M. Trejo. Spiral patterns in the packing of flexible structures. *Phys. Rev. Lett.*, **97**:166104–166107, (2006).

[22] P. Canham. Minimum energy of bending as a possible explanation of biconcave shape human red blood cell. *J. Theor. Biol*, **26**:61–81, (2001).

[23] R. Capovilla and J. Guven. Geometry of lipid vesicle adhesion. *Phys. Rev. E*, **66**:041604–041608, (2002).

[24] R. Capovilla and J. Guven. Stresses in lipid membranes. *J. Phys. A: Math. Gen.*, **365**:6233–6247, (2002).

[25] R. Capovilla, J. Guven, and E. Rojas. Hamiltonian dynamics of extended objects. *Class. Quantum Grav.*, **21**:5563–5585, (2005).

[26] R. Capovilla, J. Guven, and E. Rojas. Hamilton's equations for a fluid membrane: axial symmetry. *J. Phys A: Math. Gen.*, **38**:8201–, (2005).

[27] R. Capovilla, J. Guven, and J. A. Santiago. Lipid membranes with an edge. *Phys. Rev. E.*, **66**:021607–021613, (2002).

[28] R. Capovilla, J. Guven, and J. A. Santiago. Deformations of the geometry of lipid vesicles. *J. Phys. A: Math. Gen.*, **36**:6281–6295, (2003).

[29] R. Capovilla, J. Guven, and J. A. Santiago. Deformations of the geometry of lipid vesicles. *J. Phys. A: Math. Gen.*, **36**:6281–6295, (2003).

[30] Guven J. Capovilla R., Escalante A. and Rojas E. Hamiltonian dynamics of extended objects: Regge-teielboim model. *arXiv:gr-qc/0603126*, , (2006).

[31] M. Do Carmo. *Differential Geometry of Curves and Surfaces*. Prentice-Hall, Englewood Cliffs, NJ, 1976.

[32] E Cerda, S. Chaïeb, F. Melo, and L. Mahadevan. Conical dislocation in crumpling. *Nature*, **401**:46–49, (1999).

[33] E. Cerda and L. Mahadevan. Conical surfaces and crescent singularities in crumpled sheets. *Phys. Rev. Lett.*, **80**:2358–2361, (1998).

[34] E. Cerda and L. Mahadevan. Confined developable elastic surfaces: cylinders, cones and the *elastica. Proc. R. Soc. A*, **461**:671–700, (2005).

[35] S. Chaïeb, F. Melo, and J-C. Géminard. Experimental study of developable cones. *Phys. Rev. Lett.*, **80**:2354–2357, (1998).

[36] S. Chaïeb, F. Melo, and J-C. Géminard. Crescent singularities and stress focusing in a buckled thin sheet: Mechanics of developable cones. *Phys. Rev. E*, **60**:6091–6103, (1999).

[37] C-M. Chen, P. G. Higgs, and F. C. MacKintosh. Theory of fission for two-component lipid vesicles. *Phys. Rev. Lett.*, **79**:1579–1582, (1997).

[38] P. G. Ciarlet. A justification of the von kármán equations. *Arch. Rat. Mech. Analysis*, **73**:349–389, (1980).

[39] P. G. Ciarlet. *An introduction to Differential Geometry with applications to Elasticity*. Springer, 2005.

[40] Y. Couder, L. Pauchard, C. Allain, M. Adda-Bedia, and S. Douady. The leaf venation as formed in a tensorial field. *Eur. Phys. J. B*, **28**:135–138, (2002).

[41] S. L. Das and J. T. Jenkins. A higher-order boundary layer analysis for lipid vesicles with two fluid domains. *J. Fluid Mech.*, **597**:429–448, (2008).

[42] J. Dervaux and M. Ben Amar. Morphogenesis of growing soft tissues. *Phys. Rev. Lett.*, **101**:068101–068104, (2008).

[43] J. Dervaux, P. Ciarletta, and M. Ben Amar. Morphogenesis of thin hyperelastic plates: A constitutive theory of biological growth in the föppl-von kármán limit. *J. Mech. Phys. Solids*, **57**:458–471, (2009).

[44] M. Deserno, M. M. Müller, and J. Guven. Contact lines for fluid surface adhesion. *Phys. Rev. E.*, **76**:11605–011613, (2007).

[45] C. Dietrich, L. A. Bagatolli, Z. N. Volovyk, N. L. Thompson, M. Levi, K. Jacobson, and E. Gratton. Lipid rafts reconstituted in model membranes. *Biophys. J*, **80**:1417–1428, (2001).

[46] Q. Ding and K. Tenenblat. On differential systems describing surfaces of constant curvature. *Journal of Differential Equations*, **184**:185–214, (2002).

[47] D. Drasdo. Buckling instabilities of one-layered growing tissues. *Phys. Rev. Lett.*, **84**:4244–4247, (2000).

[48] H. G. Döbereiner, J. Käs, D. Noppl, I. Sprenger, and E. Sackmann. Budding and fission of vesicles. *Biophys. J.*, **65**:1396–1403, (1993).

[49] E. Efrati, E. Sharon, and R. Kupferman. Buckling transition and boundary layer in non-euclidean plates. *Phys. Rev. E*, **80**:016602–016619, (2009).

[50] E. Efrati, E. Sharon, and R. Kupferman. Elastic theory of unconstrained non-euclidean plates. *J. Mech. Phys. Solids*, **57**:762–775, (2009).

[51] E. Evans and D. Needham. Physical properties of surfactant bilayer membranes: thermal transitions, elasticity, rigidity, cohesion, and colloidal intercations. *J. Phys. Chem.*, **91**:4219–4228, (1987).

[52] E. Evans and R. Skalak. *Mechanics and Thermodynamics of Biomembranes*. Boca Raton: CRC Press, 1980.

[53] L. Foret. A simple mechanism of raft formation in two-component fluid membranes. *Eurphys. Lett.*, **71(3)**:508–514, (2005).

[54] J. B. Fournier and M. Ben Amar. Effective creases and contact angles between membrane domains with high spontaneous curvature. *Eur. Phys. J. E*, **21**:11–17, (2006).

[55] J. B. Fournier and C. Barbetta. Direct calculation from the stress tensor of lateral surface tension of fluctuating fluid membranes. *Phys. Rev. Lett*, **100**:078103–078107, (2008).

[56] J. B. Fournier and P. Galatola. Tubular vesicles and effective fourth-order membrane elastic theories. *Europhys. Lett.*, **39**:225–230, (1997).

[57] J. Frank and M. Kardar. Defects in nematic membranes can buckle into pseudo-spheres. *Phys. Rev. E*, **77**:041705–041713, (2008).

[58] Y. C. Fung. *Biomechanics: material properties of living tissues*. Springer, New York.

[59] Y. C. Fung. *Biomechanics: motion, flow, stress, and growth.* Springer, New York, 1990.

[60] A. Föppl. *Vorlesungen über technische Mechanik.* Leipzig, (1907).

[61] M. Gandhavadi, D. Allende, A. Vidal, S. A. Simon, and T. J. McIntosh. Structure, composition, and peptide binding properties of detergent soluble bilayers and detergent resistant rafts. *Biophys. J.*, **82**:1469–1482, (2002).

[62] R. Goetz and W. Helfrich. The egg carton: Theory of a periodic superstructure of some lipid membranes. *J. Phys. II France*, **6**:215–223, (1996).

[63] A. Goriely and M. Ben Amar. Differential growth and instability in elastic shells. *Phys. Rev. Lett.*, **94**:198103–198106, (2005).

[64] J. Guven. Membrane geometry with auxiliary variables and quadratic constraints. *J. Phys. A: Math. Gen.*, **37**:L313–L319, (2004).

[65] J. Guven. Laplace pressure as a surface stress in fluid vesicles. *J. Phys. A: Math. Gen.*, **39**:3771–3785, (2006).

[66] J. Guven and M. M. Müller. How paper folds: bending with local constraints. *J. Phys. A: Math. Theor.*, **41**:055203–055217, (2008).

[67] M. Hamm and M. M. Kozlov. Elastic energy of tilt and bending of fluid membranes. *Eur. Phys. J. E*, **3**:323–335, (2000).

[68] W. Helfrich. Elastic properties of lipid bilayers: Theory and possible experiments. *Z. Naturforsch A.*, **33**:305–315, (1973).

[69] D. Hilbert. über flächen von konstanter gaussscher krümmung. *Trans. Amer. Math. Society*, **2**:87–, (1901).

[70] Y. Jiang, T. Lookman, and A. Saxena. Phase separation and shape deformation of two-phase membranes. *Phys. Rev. E*, **61**:R57–R61, (1999).

[71] F. Jülicher and R. Lipowsky. Domain-induced budding of vesicles. *Phys. Rev. Lett.*, **70**:2964–2967, (1993).

[72] F. Jülicher and R. Lipowsky. Shape transformation of vesicles with intramembrane domains. *Phys. Rev. E.*, **53**:2670–2682, (1996).

[73] R. Kamien. The geometry of soft materials: a primer. *Rev. Mod. Phys.*, **74**:953–971, (2002).

[74] Y. Klein, E. Efrati, and E. Sharon. Shaping of elastic sheets by prescription of non-euclidean metrics. *Science*, **135**:1116–1120, (2007).

[75] W. T. Koiter. On the nonlinear theory of thin elastic shells. *Proc. Kon. Ned. Akad. Wetensch.*, **B69**:1–54, (1966).

[76] S. Komura, K. Tamura, and T. Kato. Buckling of spherical shells adhering onto a rigid substrate. *Eur. Phys. J. E*, **18**:343–358, (2005).

[77] M. M. Kozlov. Energy of nonhomogeneous bending of surfactant monolayer. persistence length. *Langmuir*, **80**:1541–1547, (1992).

[78] M. M. Kozlov. Membrane shape equations. *J. Phys.: Condens. Matter*, **18**:S1177–S1190, (2006).

[79] P. A. Kralchevsky, J. C. Eriksson, and S. Ljunggren. Theory of curved interfaces and membranes: mechanical and thermodynamical approaches. *Adv. Colloid Interface Sci.*, **48**:19–59, (1994).

[80] E. Kreyszig. *Differential geometry*. Dover, Mineola, NY, 1991.

[81] P. B. Sunil Kumar, G. Gompper, and R. Lipowsky. Budding dynamics of multi-component membranes. *Phys. Rev. Lett.*, **86**:3914–3917, (2001).

[82] P. Kuzmin, S. Akimov, Y. Chizmadzhev, J. Zimmerberg, and F. Cohen. Line tension and interaction energies of membrane rafts calculated from lipid splay and tilt. *Biophis. J*, **88**:1120–1133, (2005).

[83] L. D. Landau and E. M. Lifshitz. *Theory of elasticity*. Butterworth-Heinmann, London, 1997.

[84] M. Laradji and P. B. Sunil Kumar. Dynamics of domain growth in self-assembled fluid vesicles. *Phys. Rev. Lett.*, **93**:198105–198108, (2004).

[85] J. C. Lawrence, D. E. Saslowsky, J. M. Edwardson, and R. M. Henderson. Real-time analysis of the effects of cholesterol on lipid raft behavior using atomic force microscopy. *Biophys. J.*, **84**:1827–1832, (2003).

[86] S. Leibler. Curvature instability in membranes. *J. Phys. (France)*, **47**:507–516, (1986).

[87] R. Lipowsky. Budding of membranes induced by intramembrane domains. *J. Phys. II.*, **2**:1825–1830, (1992).

[88] R. Lipowsky. Domain-induced budding of fluid membranes. *Biophys. J.*, **64**:1133–1138, (1993).

[89] R. Lipowsky and E. Sackmann. Eds. *Structure and Dynamics of Membranes, Handbook of Biological Physics, volume 1*. Elsevier, North Holland, 1995.

[90] S. Ljunggren, J. C. Eriksson, and P. A. Kralchevsky. Minimization of the free energy of arbitrarily curved interfaces. *Journal of Colloid and Interface Science*, **191**:424–441, (1997).

[91] M. A. Lomholt and L. Miao. Description of membrane mechanics from microscopic and effective two-dimensional perspectives. *J. Phys. A: Math. Gen.*, **39**:10323–10354, (2006).

[92] A. E. H. Love. *The Mathematical Theory of Elasticity.* Cambridge University Press, Cambridge, 1906.

[93] Henneaux M. and Teitelboim C. *Quantization of Gauge Systems.* Princeton University Press, Princeton, N. J., 1992.

[94] F. C MacKintosh and T. C. Lubensky. Orientational order, topology and vesicle shapes. *Phys. Rev. Lett.*, **67**:1169–1172, (1991).

[95] M. Marder. The shape of the edge of a leaf. *Foundations of physics*, **33**:1743–1768, (2003).

[96] M. Marder and N. Papanicolaou. Geometry and elasticity of strips and flowers. *J. Stat. Phys.*, **125**:1069–1096, (2006).

[97] L. Miao, U. Seifert, M. Wortis, and H-G. Döbereiner. Budding transitions of fluid-bilayer vesicles: The effect of area-difference elasticity. *Phys. Rev. E.*, **49**:5389–5407, (1993).

[98] N. Mohandas and E. Evans. Mechanical properties of the red cell membrane in relation to molecular structure and genetic defects. *Annu. Rev. Biphys. Biomol. Struct*, **23**:787–818, (1994).

[99] M. M. Müller. *Theoretical studied of fluid membranes mechanics.* PhD thesis, Mainz, 2007.

[100] M. M. Müller, M. Ben Amar, and J. Guven. Conical defects in growing sheets. *Phys. Rev. Lett.*, **101**:156104–156107, (2008).

[101] M. M. Müller, M. Deserno, and J. Guven. Interface-mediated interactions between particles: A geometrical approach. *Phys. Rev. E.*, **72**:061407–061423, (2005).

[102] K. Nakayama, H. Segur, and M. Wadati. Integrability and the motion of curves. *Phys. Rev. Lett.*, **69**:2603–2606, (1992).

[103] S. Nechaev and R. Voituriez. On the plant leaf's boundary, 'jupe à godets' and conformal embeddings. *J. Phys. A: Math. Gen.*, **34**:11069–11082, (2001).

[104] P. Nelson and T. Powers. Rigid chiral membranes. *Phys. Rev. Lett.*, **69**:3409–3412, (1992).

[105] Y. Nishiyama. Why is a flower five-petaled. *Journal of Science Education and Technology*, **13**:107–114, (2004).

[106] R. W. Ogden. *Non-Linear Elastic Deformations*. Dover, New York, 1997.

[107] L. Pauchard and S. Rica. Contact and compression of elastic sphericall shells: the physics of a ping-pong ball. *Phil. Mag. B*, **78**:225–233, (1998).

[108] A. V. Pogorelov. *Bendings of surfaces and stability of shells. Number* 72 *in Translation of mathematical monographs*. American Mathematical Society, Providence, RI, 1988.

[109] T. R. Powers, G. Huber, and R. E. Goldstein. Fluid-membrane tethers: Minimal surfaces and elastic boundary layers. *Phys. Rev. E*, **65**:041901–041911, (2002).

[110] C. Quilliet. Depressions at the surface of an elastic spherical shell submitted to external pressure. *Phys. Rev. E*, **74**:046608–046613, (2006).

[111] G. Richardson, L. J. Cummings, H. J. Harris, and P. O'Shea. Toward a mathematical model of the assembly and disassembly of membrane microdomains: Comparison with experimental models. *Biophys. J.*, **92**:4145–4156, (2007).

[112] E. K. Rodriguez, A. Hoger, and A. D. McCulloch. Stress-dependent finite growth in soft elastic tissues. *J. Biomech.*, **27**:455–467, (1994).

[113] C. Rogers and W. K. Schief. *Bäcklund and Darboux Transformations-Geometry and Modern Applications in Soliton Theory*. Cambridge University Press, Cambridge, U. K., 2002.

[114] R. Sasaki. Soliton equations and pseudospherical surfaces. *Nucl. Phys. B*, **154**:343–357, (1979).

[115] U. Seifert. Configurations of fluid membranes and vesicles. *Adv. Phys.*, **46**:13–137, (1997).

[116] U. Seifert, K. Berndl, and R. Lipowsky. Shape transformations of vesicles: Phase diagram for spontaneous- curvature and bilayer-coupling models. *Phys. Rev. A.*, **44**:1182–1202, (1991).

[117] S. Semrau, T. Idema, L. Holtzer, T. Schmidt, and C. Storm. Accurate determination of elastic parameters for multicomponent membranes. *Phys. Rev. Lett*, **100**:088101–088104, (2008).

[118] S. Semrau, T. Idema, T. Schmidt, and C. Storm. Membrane-mediated interactions measured using membrane domains. *Biophys. J.*, **96**:4906–4915, (2009).

[119] E. Sharon, B. Roman, and H. Swinney. Geometrically driven wrinkling in free plastic sheets and leaves. *Phys. Rev. E*, **75**:046211–046217, (2007).

[120] Q. Shi and G. A. Voth. Multi-scale modeling of phase separation in mixed lipid bilayer. *Biophys. J.*, **89**:2385–2394, (2005).

[121] K. Simons and E. Ikonen. Functional rafts in cell membranes. *Nature*, **387**:569–572, (1997).

[122] R. Skalak, A. Tozeren, R. P. Zarda, and S. Chien. Strain energy function of red blood cell membranes. *Biophys. J.*, **51**:245–264, (1973).

[123] R. Skalak, S. Zargaryan, R. K. Jain, P. A. Netti, and A. Hoger. Compatibility and the genesis of residual stress by volumetric growth. *J. Math. Biol.*, **34**:889–914, (1996).

[124] G. Staneva, M. Angelova, and K. Koumanov. Phospholipase a2 promotes raft budding and fission from giant liposomes. *Chem. Phys. Lipids*, **129(1)**:53–62, (2004).

[125] G. Staneva, M. Seigneuret, K. Koumanov, G. Trugnan, and M. I. Angelova. Detergents induce raft-like domains budding and fission from giant unilamellar heterogeneous vesicles: A direct microscopy observation. *Chem. Phys. Lipids*, **136**:55–66, (2005).

[126] S. Svetina, M. Brumen, and B. Žekš. Lipid bilayer elasticity and the bilayer couple interpretation of red cell shape transformations analysis. *Stud. Biophys.*, **110**:177–184, (1985).

[127] S. Svetina and B. Žekš. Bilayer couple hypothesis of red-cell shape transformation and osmotic hemolysis. *Biomed. Biochim. Acta.*, **42**:S86–S90, (1983).

[128] S. Svetina and B. Žekš. Membrane bending energy and shape determination of phospholipid-vesicles and red blood-cells. *Eur. Biophys. J*, **17**:101–111, (1989).

[129] T. Taniguchi. Shape deformation and phase separation dynamics of two components vesicles. *Phys. Rev. Lett.*, **76**:4444–4447, (1996).

[130] M. Trejo, M. Ben Amar, and M. M. Müller. Hamiltonian formulation of surfaces with constant gaussian curvature. *J. Phys. A: Math. Theor.*, **42**:425204–425219, (2009).

[131] Z. C. Tu and Z. C. Ou-Yang. Elastic theory of low-dimensional continua and its applications in bio- and nano-structures. *J. Comput. Theor. Nanosci.*, **5**:422–447, (2008).

[132] M. S. Turner, P. Sens, and N. D. Socci. Nonequilibrium raftlike membrane domains under continuous recycling. *Phys. Rev. Lett.*, **95**:168301–168304, (2005).

[133] A. Vaziri and L. Mahadevan. Localized and extended deformations of elastic shells. *Proc. Natl. Acad. Sci. USA*, **105**:7913–7918, (2007).

[134] B. Božič, S. Svetina, S. Žekš, and R. Waugh. Role of lamellar membrane-structure in tether formation from bilayer vesicles. *Biophys. J.*, **61**:963–973, (1992).

[135] S. Veatch and S. L. Keller. Organization in lipid membranes containing cholesterol. *Phys. Rev. Lett.*, **89**:268101–268104, (2002).

[136] T. von Kármán. *Enzyclopädie der mathematischen Wissenschaften, Forschungsarbeiten.* Berlin, (1910).

[137] X. Wang and Q. Du. Modelling and simulations of multi-component lipid membranes and open membranes via diffuse interface approaches. *J. Math. Biol.*, **56**:347–371, (2008).

[138] W. Wiese, W. Harbich, and W. Helfrich. Budding of lipid bilayer vesicle and flat membranes. *J. Phys.: Condens. matter.*, **4**:1467–1657, (1992).

[139] T. J. Willmore. *Total curvature in Riemannian Geometry.* John Wiley & Sons, New York, NY, 1982.

[140] T. Witten. Stress focusing in elastic sheets. *Rev. Mod. Phys.*, **79**:643–675, (2007).

[141] M. Yanagisawa, M. Imai, T. Masui, S. Komura, and T. Otha. Growth dynamics of domains in ternary vesicles. *Biophys. J.*, **92**:115–125, (2007).

[142] O. Zhong-can and W. Helfrich. Bending energy of vesicle membranes: General expressions for the first, second, and third variation of the shape energy and applications to spheres and cylinders. *Phys. Rev. A.*, **39**:5280–5288, (1989).

Résumé:

Cette thèse est consacrée à l'étude théorique des membranes fluides, comme les vésicules lipidiques, et des membranes élastiques comme les tissus vivants. Nous avons utilisé des méthodes alliant calcul variationnel et géométrie différentielle des surfaces pour décrire les divers aspects mécaniques et topologiques de ces objets et leur influence sur leur comportement physique et biologique.

Dans une première partie nous avons abordé le problème de la tension de ligne entre deux domaines qui composent une vésicule inhomogène. A partir d'un modèle modifiant la description habituelle de ces membranes, nous avons montré que les variations structurelles de l'épaisseur de la membrane au raccord impliquent l'existence d'un angle de contact effectif et, par conséquent, une augmentation de la tension de ligne. Nous avons aussi discuté le rôle des impuretés qui se localisent autour de cette ligne de contact.

Dans une deuxième partie nous avons étudié la croissance des tissus vivants. Pour les objets minces, elle contribue à fixer la géométrie intrinsèque, c'est-à-dire la courbure de Gauss. Nous avons proposé un modèle dynamique permettant de générer des surfaces à courbure de Gauss constante. Ces surfaces ont été comparées à la forme de certaines fleurs.

La dernière partie à été consacrée à l'étude expérimentale du confinement d'une feuille élastique cylindrique à l'intérieur d'un objet de géométrie fixée. Nous avons caractérisé les patrons et le diagramme de phase de la force exercée par ces configurations au début de la croissance.

Mots-clés: Élasticité - Membranes Lipidiques - Tension de Ligne - Croissance des Tissus Vivants - Calcul Variationnel - Géométrie Différentielle

Abstract:

This thesis is devoted to the theoretical study of fluid membranes, such as lipid vesicles, and elastic membranes like living tissues. We have used the methods of differential geometry of surfaces and variational calculus to describe the topological and mechanical aspects of these objects and their influence on their physical and biological characteristics.

In the first part, we have discussed the problem of the line tension between two domains composing an inhomogeneous lipid vesicle. Using a model that modifies the usual description of fluid membranes we have shown that the structural variations of the thickness at the joint imply the existence of a contact angle and, consequently, an increase of the line tension. We have also discussed the role of impurities which adhere at the contact line.

In the second part, we have studied the growth of living tissues. For slender objects this process contributes to fix the intrinsic geometry *i.e.*, the Gaussian curvature. We have proposed a dynamic model allowing the production of surfaces with constant Gaussian curvature. These surfaces have been compared with the shape of certain flowers.

The last part is devoted to the experimental study of cylindrical packing of an elastic sheet within an object of fixed geometry. We have characterized the patterns and the phase diagram of the force exerted by these configurations in the early stages of the growth.

Keywords: Elasticity - Lipid Membranes - Line Tension - Growth of Living Tissues - Variational Calculus - Differential Geometry